UNIVERSITY OF OKLAHOMA

GRADUATE COLLEGE

EXPERIMENTAL MEASUREMENT AND MODELING OF THERMAL CONDUCTIVITIES OF CARBON FIBERS AND THEIR COMPOSITES MODIFIED WITH CARBON NANOFIBERS

A DISSERTATION

SUBMITTED TO THE GRADUATE FACULTY

in partial fulfillment of the requirements for the

Degree of

DOCTOR OF PHILOSOPHY

By

JUNFENG LIANG
Norman, Oklahoma
2014

EXPERIMENTAL MEASUREMENT AND MODELING OF THERMAL CONDUCTIVITIES OF CARBON FIBERS AND THEIR COMPOSITES MODIFIED WITH CARBON NANOFIBERS

A DISSERTATION APPROVED FOR THE
SCHOOL OF AEROSPACE AND MECHANICAL ENGINEERING

BY

Dr. Mrinal C. Saha Chair

Dr. M. Cengiz Altan

Dr. David Baldwin

Dr. Feng C. Lai

Dr. Shivakumar Raman

Acknowledgements

I would like to thank my graduate advisor, Dr. Mrinal C. Saha, for his guidance and support. As a graduate advisor, he secured my involvement in research projects and inspired me to continue my education. It has been a privilege to learn the characteristics of a productive researcher and professional from an excellent mentor.

I would also like to thank my committee members Dr. M. Cengiz Altan, Dr. David Baldwin, Dr. Feng C. Lai and Dr. Shivakumar Raman for taking the time to be a part of my PhD research and education.

Much appreciation goes to the AFOSR for funding this research through the grant number FA 9550-10-1-0031.

I would like to extend my gratitude to Dr. Anandh Balakrishnan for helping me learn 3ω technique at the initiate stage of my research, Daniel Smith and Marcus Hart for preparing some materials and composites, and Dr. Steven P. Crossley and his graduate student Nicholas M. Briggs for their help for growing CNF on carbon fiber tows

I would also like to thank Billy Mays and Greg Williams for all of their help in the machine shop. With their guidance and help, all the components necessary in my experimental setup to complete my research were manufactured.

Finally, I want to thank my parents Yueqiang and Yunxian Zhang for always supporting me and instilling the motivation to always put forth my best work helping me grow as a person.

Table of Contents

List of Tables

List of Figures

Abstract

Carbon fiber reinforced composites (CFRCs) show superior thermal performance along the fiber direction due to high thermal conductivity of carbon fiber in the fiber direction. However, these composites suffer from poor through-thickness thermal performance due to (i) low thermal conductivity of carbon fiber in its transverse direction (radial direction), (ii) low thermal conductivity of polymer matrix, and (iii) high thermal resistance at the fiber-matrix interface. One of the contemporary ways to enhance the through-thickness thermal conductivity of the composite is to incorporate carbon based nano materials such as carbon nanofibers (CNFs) through matrix and/or fiber. This work provides a systematic characterization of thermal conductivities of carbon fibers and their composites modified with CNFs using experimental measurement and theoretical modeling.

We choose 3ω method as the measurement technique is very fast, accurate, non-sensitive to convection and radiation heat loss, and its potential to measure different types of materials including carbon fibers. Therefore this research leads to the development of a number of instrumentation and procedures for measuring thermal conductivities of carbon fibers and their composites using 3ω method:

- Wire-based 3ω method was implemented to measure thermal conductivity of carbon fiber reinforced epoxy composites, with its procedure and sample preparation improved.
- Longitudinal thermal conductivity of individual carbon fibers was measured using specially designed 3ω setup with vacuum environment. Lu's one-

dimensional heat conduction model was incorporated to determine the longitudinal thermal conductivities of individual carbon fibers.

- Radial or transverse thermal conductivity of individual carbon fiber filament was developed for 3ω method by submerging the fiber into deionized water. Accordingly a two-phase heat conduction model was developed for determining the transverse thermal conductivities of individual carbon fibers.

With the development of the aforementioned experimental setups and techniques, thermal conductivities of hierarchical carbon fibers and hierarchical carbon fiber composites were then studied. Different amount of CNFs were grown in the range of 5% to 38% by weight directly on carbon fiber tows and fabrics using chemical vapor deposition (CVD) method to produce hierarchical fibers and hierarchical composites, respectively. A consistent increase of thermal conductivities was observed with the increase amount of CNFs on the carbon fibers and their composites. Both SEM and the mass increase confirm that the enhancement of thermal conductivities stems from the increase of CNFs growth. It is also found that enhancement of thermal conductivities for carbon fibers is significantly higher than that for their composites, which indicates that defects in the composites level compromise the enhancement of thermal conductivities from the hierarchical carbon fibers.

Thermal conductivities of carbon fibers and their hierarchical composites at different temperatures from 20 ℃ to 60 ℃ (up to 100 ℃ for composites) were also measured. It was found that the thermal conductivities of carbon fibers moderately increase with the temperature, while the thermal conductivities of carbon fiber composites significantly increase as the temperature increase. Therefore, it is believed that the thermal

conductivity of epoxy matrix and the thermal interfacial resistance between the carbon fibers and the matrix determine the temperature dependency of thermal conductivity of the composites.

Finally, a theoretical model for hierarchical carbon fiber composites was developed using effective medium theory to predict the through-thickness thermal conductivities of carbon fiber laminated composites. Parametric study has been done addressing thickness and length of the growth as well as growth pattern. Two types of growth patterns such as surface growth and full growth were investigated. It was found that the surface growth is more effective in enhancing the through-thickness thermal conductivity of carbon fiber reinforced composites.

Chapter 1 Introduction

1.1 Application of Carbon Composites in Thermal Management

Carbon fibers were first commercially produced in the late 1950s and since then have been employed as reinforcement in composites for many applications. With an average of six times the tensile strength of high-strength alloy steel and two thirds the weight of aluminum, carbon fiber composites with an epoxy matrix (CFRCs) are considered as replacements for metals in situations where excellent specific strength properties are needed [1]. They have become a dominant material for high performance components in aircraft radiators, directed energy mirror structures, satellites, missiles and other aerospace structure. For example, the Lockheed-Martin F-22 Raptor's airframe is made up of mostly CFRCs panels and titanium. The new Boeing 787 Dreamliner contains approximately 23 tons of carbon fibers, which is over 50% of its overall weight [2].

In many of these applications, due to the requirement of the dissipating the rapid increased thermal load, thermal conductivity is another important material property beside specific strength for designing an optimum product. For instance, due to the limited aircraft idling time, the heating of the fuel by electronics, increased engine performance and increase flight speed, the thermal load imposed on a military aircraft engine can be as high as 10,000 kW [3]. For safe operation of such vehicles, using extensive CFRCs work, a high thermal conductivity is needed to conduct away the accumulated heat. Similar challenge is also encountered in the composite missile structures, where heat generated by sensor and guidance electronics must be removed to prevent overheating and malfunction. Designers in the Aviation and Missile Research

Development and Engineering Center are looking for solution for fast dissipation of heat load in the composites missiles without bringing in additional weight and bulk to the system.

1.2 Anisotropy of Thermal Conductivity of the CFRCs

The thermal conductivities of CFRCs used in the structural purpose are anisotropic depending on the fiber orientation. In practice, the in-plane direction of CFRCs often aligns with the along-fiber direction, where the thermal conductivity is very high; through-thickness direction is often the perpendicular-to-fiber direction, where the thermal conductivity can be much lower than the other direction. For example, for unidirectional carbon fiber composites, thermal conductivity in the fiber direction can be 60 times higher than thermal conductivity of transverse direction [3]. Likewise, for woven carbon fabric composites, in-plane thermal conductivity can be about seven times of the value of thermal conductivity in through-thickness direction [4].

The anisotropy of thermal conductivity of CFRC stems from the structure of the composite and the characteristics of the constituent materials. Usually, carbon fibers used in the structural purpose are arranged as lamellar reinforcement in the composites in the form of a fabric with woven continuous fibers. Because a carbon fiber is itself very anisotropic, with the thermal conductivity much higher in the axial direction than the transverse direction, the thermal conductivity of a lamella is much higher in the fiber direction of the lamellae than in the transverse direction or through thickness direction. In the composite, these lamellae with anisotropic thermal performance are bonded together with matrix material, which has even lower thermal conductivity compared to the transverse direction of carbon fiber lamellae. Furthermore, interfacial thermal resistance

on the boundary between the carbon lamellae and the matrix can hinder the heat transfer between them. Due to the absence of fibers in the through-thickness direction and the fact that the interface between lamellae is relatively rich in the matrix polymer, the heat conduct in through-thickness direction has to pass through the transverse direction of the carbon fibers, the fiber-matrix interface and the low conductive matrix, which contributes to the poor through-thickness thermal conductivities of CFRCs. Therefore, the main problem in the thermal conductivity of the composite lies in the through-thickness direction.

In many applications, both in-plane heat spreading and through-thickness heat removal are important for effective heat dissipation. The effective thermal conductivities of CFRCs are of great importance in the effective design and application of composite materials. Further improvement of thermal conductivity over the existing highly-oriented carbon fiber while retaining the desired mechanical property has proven to be very challenging due to the structure of the CFRCs. Therefore, while many approaches have been applied to develop CFRCs with better thermal conductivities in the through-thickness direction, they can be mainly classified into two categories: (1) arrange a higher percentage of carbon fibers in the transverse direction to the carbon fabric reinforcement; (2) add inclusions with high thermal conductivity into the carbon fiber composites. The first approach results in the 3 dimensional weaving of the carbon fiber laminate. It leads to not only to a more isotropic thermal response of the composites, but also to a lower fiber volume fraction in the in-plane directions that in turn reduces the in-plane mechanical properties [5].

For the second approach, carbon nanoparticles such as carbon nanotubes (CNT) and carbon nanofibers (CNF) are mainly selected as the inclusion due to their low weights and high thermal conductivities. There are two main methods to include carbon nanoparticles in CFRCs: substituting the matrix with polymer nanocomposites matrix to make hybrid carbon fiber composites and graft carbon nanoparticles on carbon fiber to fabricate hierarchical carbon fiber composites.

1.2.1 Hybrid Carbon Fiber Composites

To fabricate hybrid carbon fiber composite, the matrix is substituted by a polymer nanocompsites matrix, followed by a conventional infusion/impregnation of the carbon nanoparticles modified matrix into the primary fiber assembly.

It has been reported that, carbon nanoparticles such as CNF and CNT has superior thermal conductivities. For instance, multi-walled carbon nanotube (MWCNT) has thermal conductivity as high as 3000 W/m-K which is as high as that of diamond [6]; while thermal conductivity of single walled carbon nanotube can be even high [7]. CNF, as another type of carbon reinforcement, also exhibits high thermal performance: vapor grown CNF has been reported to have thermal conductivity as high as 1900 W/m-K [8].

Many studies have showed that thermal conductivities of matrices can be greatly augmented by incorporating CNFs and CNTs to manufacture carbon polymer composites. After the invention of vapor grown carbon nanofiber [9] and CNTs [10], there were many studies on using CNTs to improve the thermal performance of polymer matrix due to their extremely high thermal conductivities. These studies show that by incorporating CNFs and CNTs, thermal conductivities of the composites can be much higher than their

corresponding neat matrices [8, 11-13]. The enhancement of thermal conductivity with carbon nanofillers varies from 50% [14] to as high as 800% [15] depending on the type of the fillers, quantity of the fillers added, the surface treatment of the fillers and the level of dispersion. This approach generally also has the advantages of simplicity and compatibility with standard industrial techniques.

However, one of the main issues stems from the viscosity of the epoxy-nanoparticle mixture. Viscosity of the carbon nanoparticle modified polymer matrix increases dramatically with increasing of nanoparticle content, which can lead to difficulty in many impregnation methods such as vacuum assisted resin transfer molding (VARTM) due to the incomplete matrix infusion [16]. Therefore the inclusion of carbon nanoparticles is limit to relative small weight percent.

1.2.2 Hierarchical Carbon Fiber Composites

The second approach is to improve the heat transport in fiber-matrix interface by modifying the structure of surface of carbon fiber with carbon nanoparticles growth. The modified carbon fiber exhibits a hierarchical structure forming conductive pathways interlock between the carbon fiber and the matrix; thus is expected to improve the thermal conductivity in the transverse direction [17]. Recently, there have been increasing reports on growing nanoparticles on carbon fiber to fabricate multifunctional hierarchical CFRCs.

Hierarchical carbon fiber structure was developed as early as 1991. By using cooper-nickel catalyst precursor, Downs and Baker successfully generated vapor-grown carbon microfibers on the sides of parent carbon fibers, which brought in a novel concept to

improve the transverse properties of carbon fabrics [18]. After discoveries of carbon nanotubes, interest has been moved on to development of hierarchical composites, in which a nano scale carbon nanotube reinforcement is utilized alongside traditional micro scale reinforcing fibers. Thostenson *et al*. first modified the surface of pitch-based carbon fiber by growing carbon nanotubes directly on carbon fibers using chemical vapor deposition [19]. Later on, many attempts have been made to improve mechanical properties by growing carbon nanotubes on different types of conventional carbon fibers [20-23]. Despite the consistent increase of research on developing hierarchical CFRCs, literatures that report the improvement of thermal conductivity in transverse direction are scarce. The only existed data as the author knows is from Veedu *et al*. They have examined the through-thickness thermal conductivity versus temperature of a high-temperature epoxy/SiC woven cloth composite with well- aligned CNT forest growth on the fiber bundle surface. The 3D composites demonstrate about 50% improvement of transverse thermal conductivity compared to base composite [24].

The result of Veedu's pioneer work shows a promising enhancement of thermal conductivities for the carbon fiber composites through growing CNTs. However, systematic work on studying the effect of the growth of carbon nanoparticles on thermal conductivity of the carbon fiber composites, so far, has not yet been seen. Majority of the following work were focused on mechanical properties of the hierarchical composites. This gives motivation of this research: to develop method to systematically characterize the effect of the growth of nanoparticles on enhancing thermal conductivities of carbon fiber composites first through experimental measurement and second through modeling. In next section, different thermal conductivity measurement techniques will be reviewed.

Pros and cons of each technique are discussed to determine the best method for the study on hierarchical carbon fiber and it's composite.

1.3 Review of Thermal Conductivity Measurement

In physics, heat transfer problem is described using a heat wave model similar to the ideas for shear waves in liquids. In the linearized theory, the heat flux (q) is determined by an integral over the history of the temperature gradient weighted against a relaxation function called the heat flux kernel (Q_k), as shown in equation (1.1). The area under the curve giving the monotonic relaxation of the heat-flux kernel is the thermal conductivity (equation (1.2)) [25].

$$q = -\int_{-\infty}^{t} Q_k(t-t')\nabla T(x,t')\mathrm{d}t' \tag{1.1}$$

$$k = \int_{-\infty}^{t} Q_k(t-t')\mathrm{d}t' = \int_{0}^{\infty} Q_k(s)\mathrm{d}s \tag{1.2}$$

Substitute (1.2) into (1.1), we have

$$q = -k\nabla T \tag{1.3}$$

where T is temperature. This is so called Fourier's law, popularly used for calculating heat conduction in thermal engineering. Equation (1.3) shows that thermal conductivity reflects the capability of a material to conduct heat over time.

While the theory behind thermal conductivity measurements is relatively simple, accurate measurements are often difficult to carry out. As a consequence, there are almost as many ways to measure thermal conductivity as there have been experimentalists seeking to determine thermal conductivity. The methods fall into two broad categories: steady state and non-steady state measurements [26].

1.3.1 Steady State Measurements

There are five basic types of steady state measurements: axial rod, guarded hot plate, comparative, radial flow, and photometer. Each of these methods depends simply on the definition of heat flux in equation (1.3). For isotropic materials in which neither longitudinal heat flow nor the temperature gradient vary with time, (1.3) can be rearranged to yield

$$k_{mean} = \frac{Q(x_2 - x_1)}{A(T_2 - T_1)} \tag{1.4}$$

where Q is the heat flow rate, A is the area of cross section and x_2 and x_1 are points at temperatures T_2 and T_1 respectively.

1.3.1.1 Axial rod method

In Axial rod method, the electrical power applied to the heater is directly determined. This method yields useful results only for highly conductivity materials and, as such, is not at all suitable for thermal conductivity measurements of particulate materials.

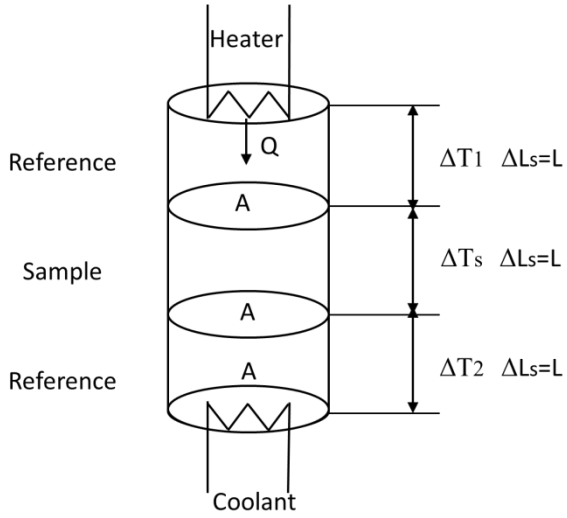

Figure 1 Schematic of axial rod method: Sample is sandwiched between two reference materials.

1.3.1.2 Guarded hot pate method (ASTM C 177)

Guarded hot plate is a widely used and versatile method for measuring the thermal conductivity of insulations. A flat, electrically heated metering section surrounded on all lateral sides by a guard heater section controlled through differential thermocouples, supplies the planar heat source over the hot face of the specimens. The most common measurement configuration is the conventional, symmetrically arranged guarded hot plate where the heater assembly is sandwiched between two specimens. In the single sided configuration, the heat flow is passing through one specimen and the back of the main heater acts as a guard plane creating an adiabatic environment.

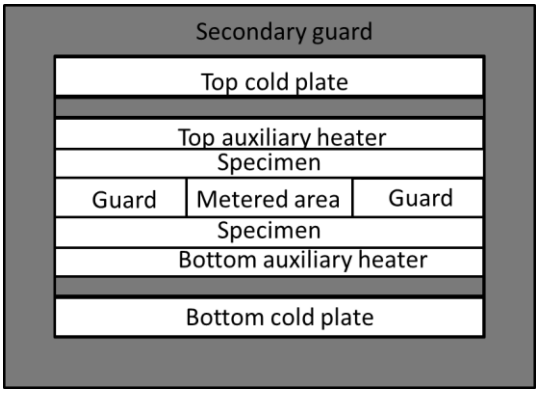

(a)

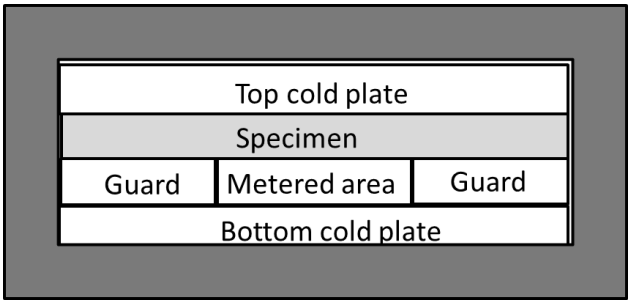

(b)

Figure 2 Schematics of Guarded hot plate method: (a) double sided configuration (b) single sided configuration.

Inaccuracies in this method can occur from radial heat loss, thermal imbalance between the hot plate and the guard, and heat flow distortion due to the gap between the hot plate and the guard. Radial temperature gradients can be minimized by using sufficiently wide guard heaters, insulating the edges, and using an outer guard heater matched the vertical gradient.

1.3.1.3 Comparative method

The comparative method is based upon the comparison of the heat flux through the sample to the heat flux through a standard with a known thermal conductivity. The sample is normally sandwiched between two cylinders of the standard. This set, in turn, is placed between a heat source and a heat sink that determine the vertical temperature gradient.

If the cross section of the sample matches that of the two standards, then at equilibrium

$$k_S \left(\frac{\Delta T}{\Delta x}\right)_S = k_{TS} \left(\frac{\Delta T}{\Delta x}\right)_{TS} = k_{BS} \left(\frac{\Delta T}{\Delta x}\right)_{BS} \qquad (1.5)$$

where k_S, k_{TS}, and k_{BS} are the thermal conductivities of the sample, the top standard, and the bottom standard, respectively; Δx is the thickness of each of the specimens; and ΔT is the temperature difference across each specimen. If the thermal conductivity of the standard is comparable to the thermal conductivity of the sample, the temperature gradient across the stack is more uniform and therefore easier to measure and maintain at equilibrium.

Inaccuracies in this method can occur from heat channeling, radial heat loss, heat shunting, and inadequate thermal contact between sample and standard.

1.3.1.4 Radial flow

The radial flow apparatus typically consists of a cylindrical central heater core surrounded by an outer heater, which is set at a lower temperature than the inner heat. The sample resides in the annulus between the heaters. Solid materials must be prepared

as a series of stacked disks, whereas particulate materials may simply be poured in. Guard heaters are placed at each end and used to match the temperature gradient of the radial cross section, to ensure radial heat flow with no end heat loss.

For radial heat flow the one-dimensional heat diffusion equation is solved for a cylindrical coordinate system, which yields

$$k = \frac{Q}{2\pi L}\frac{\ln r_2/r_1}{\Delta T} \qquad (1.6)$$

where r_1 is thermocouple position near the core heater and r_2 is the thermocouple position near the outer heater.

Inaccuracies in this method can occur from longitudinal heat loss, convection currents, radiation losses, thermal expansion of the sample or core heater, perturbation of the heat flow by the thermocouples, and unsymmetrical heat flow.

1.3.1.5 Photometry

Photometry was developed as a way to measure thermal conductivities of particulate materials under vacuum and low temperatures. The base of the sample is heated by a temperature bath, and the top of the sample radiates into a vacuum cavity maintained at liquid nitrogen temperature, 77 ℃.

The emitted flux Q per surface area of the sample A is computed by measuring the brightness temperature of the surface of the sample and assuming that

$$Q = \sigma T_{top\ of\ sample}^{-4} - \sigma T_{chamber\ walls}^{-4} \quad (1.7)$$

where $\sigma = 5.67051 \times 10^{-8}$ W/m^2 K^4 is the Stefan-Boltzmann constant. This assumption implies that the flux emitted follows Planck's law and originates from the surface of the sample; that the heat flow is one-dimensional; that the emissivity of the sample is equal to unity; and that the brightness temperature, effective temperature, and kinetic temperature are all equal. The conductivity then can be determined with (1.4). $T_2 - T_1$ is equal to the surface temperature of the sample, as measured with the photometer, minus the bath temperature, and $x_2 - x_1$ is the sample thickness.

Inaccuracies in this method can occur from radial heat loss, deviations of the experimental conditions from those assumed, and measurement error.

1.3.2 Nonsteady State Measurements

There are four types of nonsteady state measurements, all variations of the line-heat source method first proposed by Stalhane and Pyk [27]: the probe, the transient hot wire, the differentiated line-heat source, and a 3ω method developed by Cahill et al [28] for the specific purpose of measuring the thermal conductivity of thin film material.

Each of these methods is based on the assumption of radial diffusion of heat from a line source:

$$\frac{\partial T}{\partial t} = \frac{\alpha}{r}\frac{\partial}{\partial r}\left(r\frac{\partial T}{\partial r}\right) \tag{1.8}$$

where α is the thermal diffusivity of the sample, t is time, and r is the radial distance from the heat source. For the first three line-heat methods the boundary conditions are as follows: for $t = 0$ and $r \geq 0$, $T = 0$ (thermal equilibrium); for $t > 0$ and $r \to \infty$, $T = 0$ (no heat flow far from the source); and for $t > 0$ and $r \to 0$, $-2\pi rk(\partial T/\partial t) = q$, where q is the power per unit length of the heat source after time zero.

1.3.2.1 Thermal conductivity probe

The thermal conductivity probe consists of a thin strand of wire as a heat source, a thermocouple to measure the change in temperature, a tube or sheath around the two wires to hold them in place and protect them from corrosion, and a thermally conductive epoxy, resin, or cement to hold the wires in place within the sheath.

Error in the probe method stems from the inaccuracy of the series approximation for the thermal problem, the deviation of the probe from a perfect line-heat source, the finite dimensions of the sample, contact resistance between the probe and the sample, a varying power input due to both drift in the instrument and the resistance change of the wire with change in temperature, uncertainty in the measurement of the power input, a drift of thermal equilibrium, and thermal instability within the sample.

1.3.2.2 Transient hot wire

The transient hot wire technique is essentially the same as the probe, except the wires are not encased in a protective sheath. For low conductivity materials, however, a two-wire system is impractical. In order to satisfy the assumption, the thermocouple would

have to be placed very close to the heating wire, or the duration of the measurements would have to be very long. At close proximity to the heating wire the thermocouple would behave as a heat sink compared to the surrounding sample through absorption of the heat wave, and may reflect some of the heat wave as well. The errors expected from the transient hot wire technique are the same as those expected from the probe.

1.3.2.3 Differentiated line-heat source

The differentiated line-heat source technique was originally developed by Merrill for use with particulate materials under a high vacuum. The setup is similar to that used for a two-wire line-heat source. A thermocouple is placed parallel to the heating wire at a distance of 2 mm. At this range the thermocouple is not expected to be a serious heat sink problem but is close enough for the boundary conditions to still apply.

1.3.2.4 3ω method

As in the closely related hot-wire and hot-strip techniques, the 3ω method uses a radial flow of heat from a single element that is used both as a heater and thermometer. The major difference is use of the frequency dependence of temperature oscillations instead of the time-domain response.

In 3ω method an AC heating current across a small line heater is used to heat up the surface of the sample and a lock-in amplifier is used to measure the response for extracting thermal conductivity and the heat capacity of the sample. The small line heater is deposited on the sample surface by sputtering the patterned using photolithography. It acts as both heater and thermometer [29]. It can be demonstrated that the heat loss due to convection and radiation is negligible.

3ω method has many advantages when measuring the thermal properties. The main advantages of this method are

1. Errors due to heat loss from convection and radiation are minimized
2. The sample preparation time is relatively low compared to other thermal measurement techniques.
3. The cost incurred in testing a given sample is much lower compared to other techniques.
4. Thermal conductivities can be measured in both through-thickness and in-plane direction simultaneously.
5. The most important advantage is that configuration can be modified to measure wide ranges of materials including liquid, bulk solid, thin film, fiber filament or even nano materials.

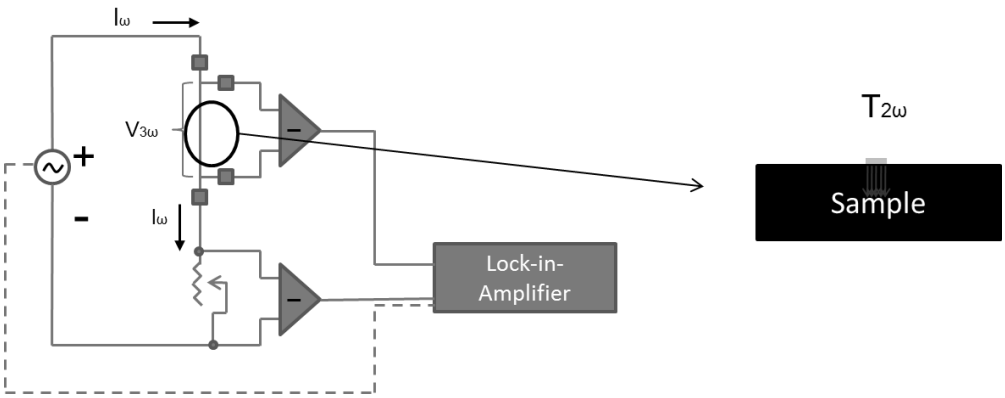

Figure 3 Illustration of a typical 3ω thermal conductivity measurement circuit (left) and the sample with metal heater/sensor (right), showing temperature fluctuating at 2ω frequency

There are different ways of utilizing 3ω method according to the geometry of the specimens. For bulk material or thin film material, metal strip pattern [29] or metal wire [30] is placed across the sample serving as the heating element and sensing element. For electrical conductive wire or fiber, the specimen itself is utilized as the heater and senor, i.e., the AC current is applied directly across the specimen [31, 32].

While many techniques for measuring thermal conductivity are available, not all of them are feasible for measuring thermal conductivity for carbon fiber and CFRC. Guarded hot plate and comparative methods are suitable for measuring thermal conductivity of CFRC and in fact they are two of most popular ways that has been used to measure thermal conductivity of CFRCs in through-thickness direction. However, due to the anisotropy and the generally planar geometry of CFRCs, it is difficult to accurately measure in-plane thermal conductivity of CFRCs with these two methods. Meanwhile, due to the configuration of the measurement setup, all the methods listed in this section are unable to measure thermal conductivities of individual carbon fibers except 3ω method. As discussed in section 1.3.4, 3ω method is superior to the other methods in accuracy and versatility. Therefore 3ω method was chosen as the experimental technique to measure thermal conductivities of CNFs modified carbon fibers and their composites. In next section, we will have a historical review of 3ω method; consequently, problems to used 3ω method for measuring thermal conductivities of carbon fibers and CFRCs will be discussed.

1.4 Historical Review of 3ω Method

The 3ω method has been used as a valuable, narrow-band detection technique to measure the thermal properties of materials, mainly in small structures, where the

dimensions of a thermocouple would seriously perturb the system. The prototype of 3ω technique is attributed to Corbino in 1910s who discovered the small third-harmonic voltage component while applying an alternating current through a heater [33, 34]. He noticed that the temperature fluctuation of an AC heated wire gives useful information about the thermal properties of the constituent material.

However, the practical application of this fluctuating signal at 3ω did not appear until in 1961, when Korostoff published a paper on a method for studying vacancies in solids. In this work, he determined the dependence of the approach of vacancy concentration to equilibrium in a specimen subjected to a periodic temperature variation [35]. In the same year, Rosethal presented the thermal equations for a bridge-wire of an equivalent electroexplosive device. In his work, sinusoidal current passed through a thermally sensitive resistance and generated a third harmonic voltage. By measuring the variation of this third harmonic with frequency, he determined the thermal time constant including specific heat [36].

The next significant advance came from Lowenthal in 1962, who obtained the data from measurements from light emission instead of thermionic emission and hence extend the ranges of temperature for the measurement of specific heat of metals [37]. Holland *et al.* in 1963 further developed this technique to measure specific heat of metal filament with alternating current using narrow band techniques and a synchronous detector, which is relatively insensitive to thermal noise [38]. In addition, Gerlich, *et al*. independently developed a so-called temperature-modulation technique to measure the specific heats of Ge, Si and Ge-Si Alloys [39]. This technique shared the same principle with narrow band 3ω method.

In 1986, Birge introduced a novel application of the 3ω phenomenon, which, instead of measuring the filament specimen, measured the specific heat of liquid using the metal filament as heater and sensor [40]. In his work, he also obtained the temperature-dependent relaxation time comparable to other techniques. In the next year, he published another paper on extending the measurement technique to measure frequency-dependent specific heat of a liquid over a frequency range exceeding five decades [41].

In the same year Cahill and Pohl developed an AC technique using a single element simultaneously as heater and thermometer [29]. In their experiment, metal films with a width small compared to the wavelength of the diffusive thermal wave was used, to generate a cylindrical heat flow pattern with which they directly determined the thermal conductivity of bulk materials. In his paper, the name, "3ω method" was first time referred. This remarkable paper became probably the most well-known origin of 3ω method for thermal conductivity measurement, and resulted in extension of 3ω method to many other materials. In 1989 and 1990, Cahill *et al*. continually published two papers on measuring thermal conductivity for thin film materials [28, 42]. In their study, they successfully measured the thermal conductivity of films with thickness in ten micron scale on the substrate with 3ω method. It is found that, by increasing the frequency ω, or more precisely decreasing the wavelength, the penetration depth can be deduced to smaller than the thickness of the film and hence measurement can be confined to the film.

Models and scheme for analysis data were greatly developed after Cahill's contribution. In 2001, Borca-Tasciuc *et al.* presented a detailed analysis and mathematical modeling of the 3ω method applied for different experimental conditions to determine the thermal conductivity of the films [43]. Based on their work, Olson *et al*

(2005) used an improved data reduction method to extend the popular 3ω method to general layered geometries [44]. Consequently, a simplified experimental technique and supporting analytical model were developed to implement the 3ω method with commercial wire test elements by Olsen and Garikapati in 2007 [30]. This technique is referred as "wire-based 3ω method" in the present study and will be discussed in more details in the coming sections.

Along with the development of data analysis scheme, the range of objects of the measurement has also been broadened during this decade by different group of researchers. In 1999, Kim *et al.* introduced interfacial thermal resistance when measuring thermal conductivity of thin films [6]. Instead of using the popular assumption of infinite substrate thickness, they considered the finite thickness of the substrate and applied multilayer models to analyze data to obtain the thickness-dependent thermal conductivity and interfacial thermal resistance. Yi in 1999 measured the thermal conductivities and specific heat on MWNT arrays by using a self-heat 3ω method [45]. This is the first time 3ω method is applied to measure thermal conductivity of material of sub-micron scale. In 2005, Choi *et al.* successfully obtained the thermal conductivities of individual multiwalled carbon nanotubes [46]. In their work, a microfabricated device was used for the placement of individual nanotubes to suspend between the metal electrodes. By using the same principle presented by Yi, 3ω method was employed to measure thermal conductivity of material in nano scale. In 2007 Bourgeois *et al*. also performed thermal conductance measurements on individual suspended nanowires by the 3ω method [47].

Lu *et al.* in 2001 presented a 3ω method for simultaneously measuring the specific heat and the thermal conductivity of a rod or filament like specimen using a way similar

to a four-probe resistance [31]. In their paper, the high and low frequency limit for the applied 1D heat conduction equation were provided. This work has become one of the most important references for measuring thermal conductivity of individual filament type material including carbon fibers. Four years later, Demas *et al.* gave a general analysis on the thermal voltage response for both suspended wire and narrow planar heater. The difference between the current and voltage-driven setups was also discussed. After them, Hou *et al*. in 2006 developed a complete solution for the thermal transport in single-wire based 3ω experiment and studied the effect of radiation on the experiment [48]. Recently, Wang *et al*. in 2007 also presented a 3ω method for simultaneously measuring thermal conductivity, thermal diffusivity and heat capacity of an individually suspended wire. Their method is similar to that of Lu *et al.* but with different closed form solution for the heat conduction problem [32].

The aforementioned 3ω methods to measure individual nanotubes, nanowire, rod-like filament, and fiber filament provide foundation for measuring thermal conductivity of CNFs modified carbon fibers in the present study.

There are many other researches on application of 3ω method, but they are outside the scope of this work, which is why they are not included here despite their importance as thermal conductivity measurement method.

1.5 Statement of the Problem

From previous sections, it can be seen that carbon nanoparticle modified CFRC is a promising multi-functional composite material in thermal management application. To systematically the thermal conductivity of hierarchal CFRC and its reinforcement, carbon

fiber, is the key to understand and to develop this new type of composite material. In this study, CNF is selected as the nanoparticle reinforcement, and laminated carbon fabric epoxy composite is chosen as the neat carbon composite. In the on-going discussion, CFRC is referred to laminated carbon fabric reinforced epoxy composites if it is not specified.

In this study, 3ω method is selected as a general method to measure thermal conductivity for carbon fiber and its composites. Before practically applying 3ω method for the study of thermal conductivities of CNF modified carbon fibers and their composites, there are some technical problems to be considered.

1) Wire-based Heating Pattern Preparation for 3ω Method

The main disadvantage of traditional 3ω is the expense required in the preparation of the metal pattern on the specimen. This is normally done by photolithography or sputtering whose equipment generally costs between $50 and $200k [30]. Meanwhile, the process of lithography includes chemical etch, which limits the range of materials that can be tested. The matrix material in this study epoxy resin is a thermal set polymer whose properties can degrade under the effect of the etching chemicals.

It has been described in the literature that using fine metal wire and more complicated conduction model, one can remove the photolithography process in the sample preparation [30]. This is so-called wire-based 3ω method. However, this kind of substitution also brings in two issues: 1. the requirement of great effort and high skill to precisely mount the fine wire on the surface of the specimen; 2. the difficulty of ensuring contact between the specimen and the wire due to the complexity. A scheme must be

designed to perfectly attach the fine wire on the surface of the specimen without disturbing the wire itself.

2) Electrical Conductivity of the Specimen

Carbon fibers are electrical conductive material. When embedded inside the polymer matrix, the carbon fibers are insulated inside the composites. However, in order to have good contact between the wire and the specimen in wired-based 3ω measurement, the surface of the composites need to be cut and polished into a flat and smooth plane. In such a case, the fibers will be exposed, making electrical bridging between the heating wire and the carbon fibers. Insulation need to be introduced to cut off such electrical bridging.

3) Thermal conductivities of Individual Carbon Fibers

In this study, carbon fiber is the object that the CNFs directly modified. Therefore it is critical to measure the thermal conductivity of CNFs modified carbon fiber. Investigation of the effect of CNFs on thermal conductivity carbon fiber will provide a better understanding on the effect of CNFs on the fiber composites. Techniques and setup of 3ω method to measure thermal conductivities of individual fiber filaments need to be implemented.

4) Modeling for Hierarchical Carbon Fiber Composites

Since development of hierarchical carbon fiber composites is still in its infancy, modeling work with the preliminary experimental data of thermal conductivity of hierarchical fiber is an efficient way to further the study and will provide a guiding for

the design of the hierarchical composites. However, although there are some literatures reporting the experimental data on thermal conductivities of hierarchical carbon fiber composites, so far modeling for thermal conductivities of hierarchical composites does not exist. There is need to develop either theoretical model or numerical simulation to take advantage of the measured data for understanding and design of the material structure.

6) Anisotropy of Carbon Fiber

When using 3ω method to measure the thermal conductivities of individual fiber filaments, one significant assumption is that the carbon fiber is isotropic. Thus, a one dimensional governing equation can be applied to describe the heat flux conduct across the carbon fiber. However, it has been well known that carbon fiber is an anisotropic material, whose thermal properties in radius direction can be significant different from that in longitudinal direction. For example, by solving an inverse problem from carbon fiber-epoxy composite, Hind and Robitaille has found that longitudinal thermal conductivity of PAN-based carbon fiber, HexPly T300, was ten times of its transverse thermal conductivity [4]. In the work of Nozawa *et al.*, longitudinal thermal conductivity of Pitch-based carbon fiber, P120s, has been reported to be 250 times higher than its transverse thermal conductivity; however the detail of measurement is absence [49].

Modeling CFRCs requires defining the thermal conductivity of carbon fiber in radial direction. This is often achieved by assuming certain lower value than its counterpart in longitudinal direction (for example, 1/10 of longitudinal thermal conductivity). For CNFs modified carbon fiber, such assumption will not hold. It is important to established

experimental approach to directly measure the transverse thermal conductivities of individual carbon fibers.

1.6 Objectives

According to the problems listed in section 1.5, there are following objectives for this study:

- To develop the tools and procedures required for the preparation of specimen for wire-based 3ω method, with simplicity and robustness. This method must able to be applied to measure CFRCs.
- To established setup to systematically measure the longitudinal thermal conductivities of individual carbon fiber filaments.
- To develop technique, experimental setup and procedure to measure thermal conductivities of individual carbon fibers in transverse direction.
- Experimentally investigate the relation between CNF growth and the thermal conductivities of the hierarchical carbon fiber and hierarchical CFRCs especially in transverse direction.
- To build up multiscale modeling of hierarchical CFRCs to investigate the effect of the growth of CNFs on thermal conductivities of CFRCs.

1.7 Dissertation Outline

This dissertation includes both experimental work and modeling work. It is divided into six chapters. Chapter 1 is the introduction. Chapter 2 presents the basic principles of using 3ω method to measure the thermal conductivities of carbon fiber composites, individual carbon fibers in longitudinal direction and individual carbon fibers in radial

direction. Theory to extract thermal conductivities from the experimental data is also discussed in detail. In Chapter 3, the experimental setup and the procedure of 3ω method for all the measurements are described. Some technical issues and their solutions are discussed. Chapter 5 presents the results for the measurement of thermal conductivities of hierarchal carbon fibers and their composites. Validation for each method is also given in this chapter. Finally, chapter 6 summarizes the whole present work and gives some possible future directions.

Chapter 2 Experimental Principle and Theory of 3ω Method

2.1 Introduction

This chapter presents an overview of the basic experimental principle of measuring thermal conductivity with 3ω method and the theory to determine the thermal properties from the 3ω experiment. The detail of the measurement techniques and the theories to analyze the data are different as respect to material types and as respect to direction of the thermal conductivity. Here, three major techniques are presented for measuring the thermal conductivity for bulk material, longitudinal thermal conductivities for individual fibers, and transverse thermal conductivities for individual fibers. These three techniques are either adapted from existed techniques or developed recently to satisfy the need to study the thermal conductivity of hierarchical carbon fiber and its composite.

Section 2.2 presents the basic experimental principles and a brief theory for measuring thermal conductivity of bulk material such as carbon fiber composites. The theory for origin of the 3ω harmonic response on narrow metal strip under a ω AC voltage is presented in detail. Consequently, the way to determine thermal properties of bulk material using a metal strip as heater and sensor is presented. After that, a simplified 3ω method, so-called wire-based 3ω method is introduced and the corresponding theory is also explained. Since we used this technique to measure the thermal conductivity of the carbon epoxy composites, the protocol of this method will be discussed in more detail.

In section 2.3 wire-based 3ω is extended to measure the longitudinal thermal conductivities of individual fibers. In this technique, the general experimental principle is similar to the wire-based 3ω presented in section 2.2, but with some modification

according to the material geometry. Unlike measuring bulk material with metal wire, the specimen itself in this section is used as heater and sensor. The theory behind is consequently different: the heat flux across an individual fiber specimen is assumed to be a one dimensional along the fiber longitudinal direction. Therefore, Lu's model is used to set up the mathematic relation between the 3ω signal and the thermal properties.

Section 2.4 presents a recent developed technique for measuring the transverse thermal conductivity of an individual fiber by 3ω method. In this technique, a piece of fiber filament is submerged into deionized water and AC voltage of frequency ω is applied on it to create a transverse heat flow. Analytical solution for such a two phase heat conduction problem is presented in this section. The corresponding theoretical 3ω response is further derived in term of thermal properties of the individual fiber.

2.2 Measuring Thermal Conductivity of Bulk Material with 3ω Method

2.2.1 Metal Strip on Bulk Materials

2.2.1.1 Experimental principle

The general concepts and nomenclature common to all the 3ω method for measuring bulk materials will be introduced in this section for the most intuitive case of 3ω method. As already mentioned, 3ω signal is formed by supplying a metal strip with AC voltage or current in the frequency of ω.

The most common way to generate the ω supply is by using a function generator or oscillator, which provides a voltage source in the range frequency from sub Hz to more than thousand Hz. Although an operational amplifier circuit may be used to convert this voltage source to a current source, it is more common to use the voltage source directly

while analyzing the data as if a current source has been used. This simplification is valid if the sample resistance is small compared to the total resistance of the circuit and gives a correction factor to use when the sample resistance is larger.

Platinum, silver or gold, is usually chosen to make the metal strip because they have relatively high thermal conductivities but low electrical conductivities. The narrow metal strip is produced on the sample by photolithography or by evaporation. For most samples that are not soluble in water, photolithography is commonly used to produce the metal strip that is from 5 to 35 μm wide. For other samples the strip can be evaporated through a mask, which produces the pattern with larger width.

In order to obtain the output of the third harmonic response, the voltage across the specimen is usually first balanced with an impedance bridge circuit to filter out the fundamental and the noise. This impedance bridge can be Kelvin double bridge, variable RC network, Wheatstone Bridge, or tripling circuit. Lock-in amplifier, synchronous detector, or oscilloscope, typically, is then applied to measure the third harmonic voltage across the specimen.

2.2.1.2 Theory for determining thermal conductivity from 3ω response

As discussed in the previous section, in the conventional sample preparation the heating element is created using chemical vapor deposition followed by photolithography. The cross section of the heating element is rectangular. The height of the element is very small compared to the width of the element. This reduction in height helps in reducing the heat loss due to convection and radiation (effects due to black body radiation).

To derive the equation relating the thermal conductivity to the temperature oscillations of the narrow strip heater-sensor, we begin with the exact solution for the amplitude of the temperature oscillations at a distance r from a line source of heat with period $2\pi/\omega$ containing a time-factor $e^{i\omega t}$, which will be understood to multiply all temperatures and fluxes and will be omitted through. Before that, we consider a circular cylinder with infinite diameter whose axis coincides with the axis of z is heated, and the initial and boundary conditions are independent of the coordinates θ and z. The temperature will be a function of r and t only (Figure 4), and this equation is:

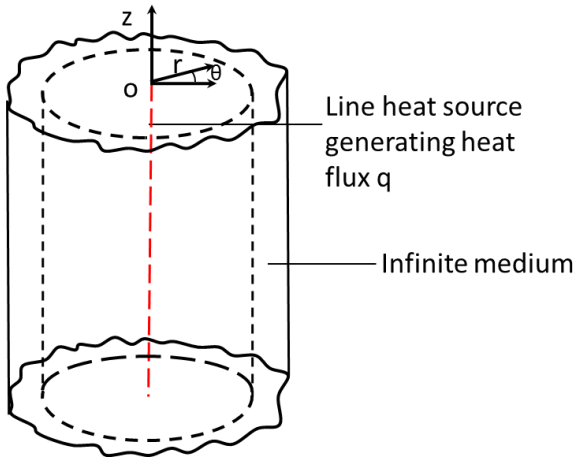

Figure 4 A line heat source in the center of a cylinder with infinite length and diameter.

$$\rho C \frac{\partial \Delta \boldsymbol{T}}{\partial t} = k\left(\frac{\partial^2 \Delta \boldsymbol{T}}{\partial r^2} + \frac{1}{r}\frac{\partial \Delta \boldsymbol{T}}{\partial r}\right) \tag{2.1}$$

Substitute $\Delta \boldsymbol{T}$ with $\Delta T e^{i\omega t}$, (2.1) becomes

$$\frac{d^2\Delta T}{dr^2} + \frac{1}{r}\frac{d\Delta T}{dt} - \frac{i\omega}{\alpha}\Delta T = 0 \tag{2.2}$$

where $\alpha = k/\rho C$ is the thermal diffusivity. The general solution of (2.2) is

$$\Delta T = NI_0(\varphi r) + MK_0(\varphi r) \tag{2.3}$$

$$\varphi = \left(\frac{i\omega}{\alpha}\right)^{\frac{1}{2}} \tag{2.4}$$

where N and M are constant determined by the boundary condition. The flux q is given by

$$q = -k\frac{\partial \Delta T}{\partial r} = -k\varphi\, NI_1(\varphi r) + k\varphi\, MK_1(\varphi r) \tag{2.5}$$

Now we consider the boundary conditions. At the location infinite far away from the heat source ($r = \infty$), the temperature should be finite, therefore N=0, (2.5) becomes:

$$q = k\varphi\, MK_1(\varphi r) \tag{2.6}$$

Meanwhile, at r=0, the amplitude of heat flux satisfies:

$$q = \frac{P}{area} = \frac{P}{2\pi L} \tag{2.7}$$

Combine (2.6) and (2.7), with r=0, we can obtain

$$M = \frac{P}{2\pi Lk} \tag{2.8}$$

So the solution of (2.2) is

$$\Delta T = \frac{P}{2\pi Lk} K_0(\varphi r) \tag{2.9}$$

If we have half space along z axis as its surface and if the surface is insulated against heat flux (Figure 5), except at the axis where there is a flux of q, then the temperature distribution is the same as that for an infinite space but with a heat flux $2q$, i.e.,

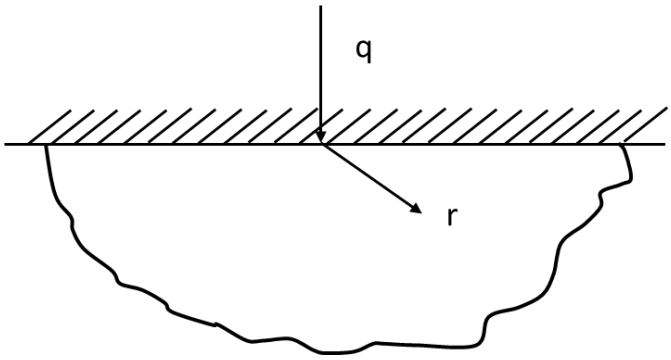

Figure 5 Cross section of a line heat source on the surface of a semi-infinite medium with heat flux q. The top surface of the medium is insulated.

$$\Delta T = \frac{P}{\pi L k} K_0(\varphi r) \tag{2.10}$$

If $|\varphi r| \ll 1$, (2.10) can be approximately written as [50]

$$\Delta T = \frac{-P}{\pi L k}\left(\ln\left(\frac{\varphi r}{2}\right) + \gamma\right) \tag{2.11}$$

or

$$\Delta T = \frac{P}{\pi L k}\left(\frac{1}{2}\ln\frac{\alpha}{r^2} + \ln 2 - \gamma - \frac{1}{2}\ln(2\omega) - \frac{i\pi}{4}\right) \tag{2.12}$$

where γ is Euler-Mascheroni constant approximately equaling to 0.5722. The result has been written to separate the frequency-dependent and the imaginary contributions to the solution. A complete solution for the temperature oscillations in a line source of finite width involves a convolution of this result across the width of the line and then an average across the line, but since we are only interested in determining the thermal conductivity, and not the thermal diffusivity, a complete solution is unnecessary. As long as the thermal penetration depth is much larger than the width of the line, i.e.,$|\varphi r| \ll 1$, the slope of the ΔT versus ln(ω) curve is independent of the width of the line and of the averaging procedure.

Equation (2.12) can now be used to calculate the periodic change in the resistance of the heating element.

$$\Delta R = \Delta T \frac{\partial R}{\partial T} \tag{2.13}$$

Since the temperature fluctuates at a frequency of 2ω, the resistive change will also fluctuate at 2ω. The current flowing through the heater is exactly in phase with the driving voltage at ω, thus the periodic change in the resistance will produce a small fluctuation in voltage across the test section.

$$V_{\Delta R \cdot \Delta T} = \frac{V}{R}\cos(\omega t) \cdot |\Delta \bar{T}| \cos(2\omega t + \emptyset_{\Delta \bar{T}}) \frac{\partial R}{\partial T} \tag{2.14}$$

where $\emptyset_{\Delta\bar{T}}$ denotes the phrase difference between the current and the temperature and the bar accent denotes the average. Using trigonometric relations, this can be rewritten:

$$V_{\Delta R\cdot\Delta T} = \frac{1}{2}\frac{V}{R}|\Delta\bar{T}|\frac{\partial R}{\partial T}[\cos(3\omega t + \emptyset_{\Delta\bar{T}}) + \cos(\omega t + \emptyset_{\Delta\bar{T}})] \tag{2.15}$$

Thus there is a component of the response which oscillates at 3ω and a portion which oscillates at ω. Both of these signals are of equal magnitude and both are in phase with the temperature oscillation.

$$\Delta V_{3\omega} = \Delta V_{\omega} = \frac{V^3}{2\pi R^2 Lk}\frac{\partial R}{\partial T}\left[\frac{1}{2}\ln\frac{\alpha}{r^2} + \ln 2 - \gamma - \frac{1}{2}\ln(2\omega) - \frac{i\pi}{4}\right] \tag{2.16}$$

Equation (2.16) can also be recast to utilize commonly used RMS voltages and frequency values, rather than peak values and angular frequencies:

$$\Delta V_{3\omega\_rms} = \frac{V_{rms}^3}{4\pi R^2 Lk}\frac{\partial R}{\partial T}\left[\ln\left(\frac{\alpha}{4\pi f r^2}\right) - \frac{i\pi}{2} + 2c_1\right] \quad c_1 \approx 0.924 \tag{2.17}$$

where f is the ordinary frequency. If two 3ω voltages are measured at two separate frequencies, the constant terms in equation (2.17) can be canceled out

$$k = \frac{V_{rms}^3}{4\pi R^2 L}\frac{\partial R}{\partial T}\frac{\ln\left(\frac{f_1}{f_2}\right)}{\left(\Delta V_{3\omega\_rms}\right)_2 - \left(\Delta V_{3\omega\_rms}\right)_1} \tag{2.18}$$

Equation (2.18) uses only two points to determine the value of the material thermal conductivity. A more robust approach is to use a composite of several points to reduce the effect of the error associated with any two particular values. Equation (2.17) can be modified to into the following form in preparation for this approach.

$$\Delta V_{3\omega} = \frac{V^3}{4\pi R^2 L k}\frac{\partial R}{\partial T}\left[\ln\left(\frac{\alpha}{4\pi f_0 r^2}\right) - \ln\left(\frac{f}{f_0}\right) - \frac{i\pi}{2} + 2c_1\right] \tag{2.19}$$

The constant f_0 is an arbitrary reference frequency which is used to maintain dimensional uniformity. Since the 3ω voltage is linear with respect to the natural log of *f*, linear regression can be applied over N experimental measurements in the following manner.

$$\Delta V_{3\omega\_rms} \approx c_2\left[-\ln\left(\frac{f}{f_0}\right)\right] + c_3 \tag{2.20}$$

$$c_2$$

$$= \frac{N\sum_{j=1}^{N}\left(-V_{3\omega\_rms_j}\cdot\ln\left(\frac{f_j}{f_o}\right)\right)-\sum_{j=1}^{N}V_{3\omega\_rms_j}\cdot\sum_{j=1}^{N}\left(-\ln\left(\frac{f_j}{f_o}\right)\right)}{N\cdot\sum_{j=1}^{N}\left(-\ln\left(\frac{f_j}{f_o}\right)\right)^2-\left[\sum_{j=1}^{N}\left(-\ln\left(\frac{f_j}{f_o}\right)\right)\right]^2} \quad (2.21)$$

c_3

$$= \frac{\sum_{j=1}^{N}\left(-\ln\left(\frac{f_j}{f_o}\right)\right)^2\cdot\sum_{j=1}^{N}V_{3\omega\_rms_j}-\sum_{j=1}^{N}\left(-\ln\left(\frac{f_j}{f_o}\right)\right)\cdot\sum_{j=1}^{N}\left(-V_{3\omega\_rms_j}\cdot\ln\left(\frac{f_j}{f_o}\right)\right)}{N\cdot\sum_{j=1}^{N}\left(-\ln\left(\frac{f_j}{f_o}\right)\right)^2-\left[\sum_{j=1}^{N}\left(-\ln\left(\frac{f_j}{f_o}\right)\right)\right]^2} \quad (2.22)$$

Terms in equation (2.19) and (2.20) can now be directly equated.

$$k = \frac{{V_{rms}}^3}{4\pi R^2 L c_2}\frac{\partial R}{\partial T} \quad (2.23)$$

$$\alpha = 4\pi f_o r^2 \exp\left(\frac{c_3}{c_2} - 2c_1\right) \quad (2.24)$$

The thermal conductivity can also be directly calculated from the imaginary, or out of phase, component of the 3ω voltage. Meanwhile, in equation (2.15) we can see that, 1ω component might be also used to determine thermal conductivity of the sample. However, since this component has the same frequency as the driven voltage, it is very

sensitive to noises. Therefore in practical application, 3ω is normally used for measuring thermal conductivity.

2.2.2 Metal Wire on Bulk Materials

2.2.2.1 Experimental principle

In the early days, the 3ω method was developed for measuring dielectric thin film materials [42]. Due to the use of the photolithographic pattern, such technique was limited by the cost effectiveness. To simply the sample preparation and make the measurement more cost-effective, a wire-based 3ω that developed by Garikapati and Olson can be used [30]. For point of view of apparatus, there is no different between using lithographic metal strip and using commercial metal wire. The main difference is in the way of preparation of the specimen and the theory to extract the thermal properties.

Wires of platinum are chosen typically with diameter smaller than 10μm so that the temperature over the cross-section of the wire can be considered as uniform. The length of the wire used should be at least 100 times of its diameter so that the end effect of the wire can be neglected.

In order to ensure good contact between the wire and the surface of the specimen, the surface of the specimen must not only be smooth (the arithmetic average of the absolute values of the surface at least 10 times smaller than the diameter of the wire), but also be flat. This is usually achieved by using sand paper with different level of grit in sequence until a flat and smooth surface can be observed under microscope. Similar to hot plate method, contact agent is also required to secure the wire on the surface and reduce the contact resistant.

Lead wires can be connected to the heater wire with conductive epoxy, soldering or simple clamping. Since commercial wire normally has larger dimension than lithographic metal pattern and the geometry of the wire limit its contact with the specimen surface, in order to reduce the heat loss in convection and black body radiation, it is preferable to keep the specimen and with the wire in the vacuum environment.

2.2.2.2 Theory for determining thermal conductivity from 3ω response

The objective of this derivation is to develop an expression for the impedance at the surface of a structure like the one shown in Figure 6. The assumed periodic temperature profile can be substituted into the appropriate partial differential equation for two-dimensional conduction. A factor of 2 is introduced to account for the frequency doubling which results from sinusoidally driven Joule heating

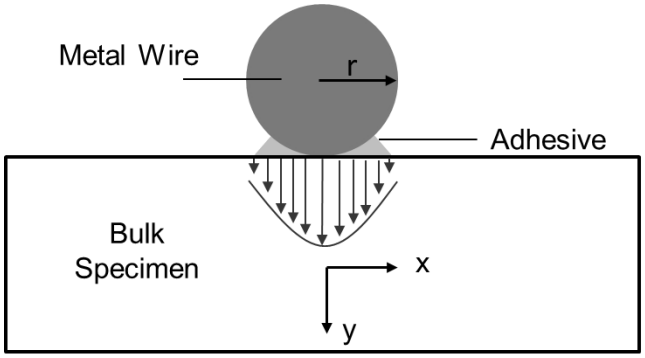

Figure 6 Cross-section of the modified heating element for wire-based 3ω method. The drawing is not to the scale.

$$T = \boldsymbol{T}\exp(i2\omega t) \tag{2.25}$$

$$i2\omega\boldsymbol{T} = \alpha_x \frac{\partial^2 T}{\partial x^2} + \alpha_y \frac{\partial^2 T}{\partial y^2} \tag{2.26}$$

It is now useful to employ a Fourier transform to simplify this differential equation. Equations (2.27) and (2.28) show the forward and reverse transforms respectively

$$\hat{f}(\lambda) = \int_{-\infty}^{\infty} f(x)\exp(-i\,\lambda x)\mathrm{d}x \tag{2.27}$$

$$f(x) = \frac{1}{2\pi}\int_{-\infty}^{\infty} \hat{f}(\lambda)\exp(i\,\lambda x)\mathrm{d}\lambda \tag{2.28}$$

Applying the forward transform to equation (2.26) yields an easily solved ordinary differential equation based on a newly defined quantity $\boldsymbol{\phi}$.

$$\frac{d^2\widehat{\boldsymbol{T}}}{dy^2} - \boldsymbol{\phi}^{\boldsymbol{2}}\widehat{\boldsymbol{T}} = 0 \tag{2.29}$$

$$\boldsymbol{\phi}(\chi)_j = \sqrt{\psi\chi^2 + \frac{i2\omega_j\Delta x^2}{\alpha_y}} \qquad j = 1, 2, \ldots M \tag{2.30}$$

Here, j is the frequency index (M total frequency points). Δx is the width of the heated region. Also, the anisotropy ratio ψ and non-dimensional transform variable χ are defined as:

$$\psi = \frac{k_x}{k_y} \tag{2.31}$$

$$\chi = \Delta x \lambda \tag{2.32}$$

The temperature solution becomes:

$$\widehat{\boldsymbol{T}} = c_1 \sinh\left(\boldsymbol{\phi}\frac{y}{\Delta x}\right) + c_2 \cosh\left(\boldsymbol{\phi}\frac{y}{\Delta x}\right) \tag{2.33}$$

It is now useful to define the transform impedance $\boldsymbol{z}$.

$$\widehat{\boldsymbol{T}} = \widehat{\boldsymbol{Q}}\boldsymbol{z} \tag{2.34}$$

Fourier's law of conduction can be applied to equation (2.34) to solve for integration coefficients.

$$\widehat{\boldsymbol{Q}} = -k_y \Delta x L \frac{\partial \widehat{\boldsymbol{T}}}{\partial y} \tag{2.35}$$

Substituting equation (2.33) and (2.35) into equation (2.34) yields:

$$\boldsymbol{z}(\chi)_{\boldsymbol{j}} = \frac{1}{L k_{y1} \boldsymbol{\phi}(\chi)_j} \quad j = 1, 2, \ldots M \tag{2.36}$$

It is also necessary to define the boundary condition at the surface of the material. This is done by determining the transformed heat flux at the surface (i.e. integrating over the heated region.) The forward transform reduces to a cosine transform due to the symmetry of the heat flux about x=0.

$$\hat{Q}(\lambda) = \Delta x L \int_{-\Delta x/2}^{\Delta x/2} \boldsymbol{q} \cos(\lambda x) dx \tag{2.37}$$

Equation (2.37) can now be inserted into equation (2.34) to yield a boundary condition for the surface temperature ($\boldsymbol{Q} = \Delta \boldsymbol{x} L \boldsymbol{q}$).

$$\widehat{\boldsymbol{T}}_{\boldsymbol{j}} = 2\Delta x \boldsymbol{Q} \frac{\sin\left(\frac{\chi}{2}\right)}{\chi} \boldsymbol{z}(\boldsymbol{\chi})_{\boldsymbol{j}} \; j = 1, 2, \ldots M \tag{2.38}$$

A reverse transform can now be applied to equation (2.38), again symmetry reduces the reverse transform to a cosine transform.

$$\begin{aligned}\boldsymbol{T}(x)_j &= \frac{1}{2\pi}\int_{-\infty}^{\infty}\widehat{\boldsymbol{T}}_j\cos(\lambda x)d\lambda \\ &= \frac{\boldsymbol{Q}}{\pi}\int_{-\infty}^{\infty}\frac{\sin\left(\frac{\chi}{2}\right)\cos\left(\chi\frac{x}{\Delta x}\right)}{\chi}\boldsymbol{z}(\chi)_j d\chi \\ j &= 1,2,\dots M\end{aligned} \tag{2.39}$$

$$\boldsymbol{T}(x)_j = \boldsymbol{Z}(x)_j\boldsymbol{Q} \tag{2.40}$$

$$\boldsymbol{Z}(x)_j = \frac{1}{\pi}\int_{-\infty}^{\infty}\frac{\sin\left(\frac{\chi}{2}\right)\cos\left(\chi\frac{x}{\Delta x}\right)}{\chi}\boldsymbol{z}(\chi)_j d\chi \quad j = 1,2,\dots M \tag{2.41}$$

The surface transform impedance $\boldsymbol{z}(\chi)$ in equation (2.41) is a function of material properties, frequency and the integration variable χ. This rather complicated expression has eluded solution by analytical means. In fact, no known solution exists for even the simplest case. It is therefore requisite than any inverse method, which employs this solution, be equipped with an efficient means of evaluating the integral in equation (2.41). It is certainly possible to numerically integrate equation (2.41) by standard means; however, this process is made difficult by dramatic changes in $\boldsymbol{z}$ that occur over a range of frequencies. This difficulty can be largely circumvented through the use of a simple

variable substitution. Equation (2.42) defines a new dimensionless substitution variable that effectively expands the integration region directly about $\chi = 0$.

$$\chi = \xi(\eta) = \frac{\eta^5}{1+\eta^4} \tag{2.42}$$

$$\frac{d\xi(\eta)}{d\eta} = \frac{\eta^4(5+\eta^4)}{(1+\eta^4)^2} \tag{2.43}$$

Since the impedance function is symmetric about η, it is only necessary to integrate one haft of the total domain. Following the variable substitution, equation (2.41) can be rewritten as equation (2.44)

$$\boldsymbol{Z}(x)_j = \frac{1}{\pi}\int_{-\infty}^{\infty} \frac{d\xi(\eta)}{d\eta} \frac{\sin\left(\frac{\xi(\eta)}{2}\right)\cos\left(\xi(\eta)\frac{x}{\Delta x}\right)}{\xi(\eta)} \boldsymbol{z}\left(\xi(\eta)\right)_j d\chi \tag{2.44}$$

$$j = 1, 2, \ldots M$$

Although the limits of integration on equation (2.44) are infinite, it can be observed that the integration argument is essentially zero for values of η larger than 4π. The integration interval can, therefore, be truncated to ($-4\pi < \eta < 4\pi$).

In order to simplify the sample preparation process, wire elements have been used in place of patterned elements. In order to insure that the wires are in intimate contact with

the surface, the surface is first flattened and polished (if needed). After placement of the wire, a thin (<1μm) topcoat of contact agent is applied. Although this arrangement is experimentally simple, accurate treatment of the boundary conditions requires further development. This will be accomplished through modification of the incremental division method developed by Olsen [44].

The contact agent film can be divided into finite volume elements oriented at 45^{o} and a first order approximation of Fourier's law can be used to calculate the horizontal heat flow between elements (Figure 7).

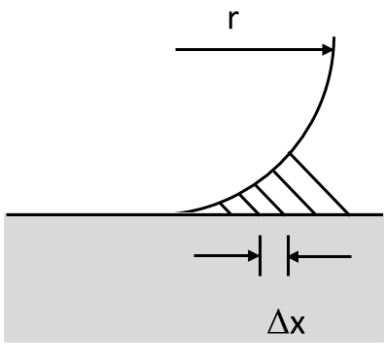

Figure 7 The finite volume division of the spin-on-glass coating. Elements are oriented at 45^{o}.

$$\{\boldsymbol{Q}_H\}_j = [S_H]_j\{\boldsymbol{T}\}_j \quad j = 1, 2, \ldots M \tag{2.45}$$

Here, $[S_H]$ is a tri-diagonal matrix of conduction coefficients $\left[kLH\sqrt{2}/_{\Delta x}\right]$ (the factor of $\sqrt{2}$ is included because the elements are oriented at 45°), $\{\mathbf{T}\}$ is the corresponding nodal temperature for each element, and *j* is the frequency index. The total heat transfer through the base of each element can be determined using the matrix form of equation (2.40).

$$\{\boldsymbol{T}_S\}_j = [\boldsymbol{Z}]_j\{\boldsymbol{Q}_S\}_j \quad j = 1, 2, \dots M \tag{2.46}$$

Here $\{\mathbf{T}_s\}$ is the temperature at the surface of the material. Fourier's law can also be used to relate the surface temperature to the nodal temperature.

$$\{\boldsymbol{Q}_S\}_j = [S_V]\{\boldsymbol{T}_S - \boldsymbol{T}\}_j \quad j = 1, 2, \dots M \tag{2.47}$$

Here $[S_V]$ is a matrix of vertical conduction resistances $\left[2kL\Delta x/_{\sqrt{2}H}\right]$. Combining equations (2.46) and (2.47) yields:

$$\{\boldsymbol{Q}_S\}_j = \left[[S_V][\boldsymbol{Z}]_j - [I]\right]^{-1}[S_V]\{\boldsymbol{T}\}_j \quad j = 1, 2, \dots M \tag{2.48}$$

where $[I]$ is the identity matrix. The total energy balance for the system of elements can be written in matrix form as:

$$\{\boldsymbol{Q}_H\}_j + \{\boldsymbol{Q}_S\}_j - \{\boldsymbol{Q}_W\}_j = [S_M]_j\{\boldsymbol{T}\}_j \quad j = 1,2, \dots M \tag{2.49}$$

where $[\mathbf{S}_\mathrm{M}]$ is a diagonal matrix of mass coefficients $\left[i2\omega_j \rho C \Delta x \Big/ \sqrt{2}LH \right]$, and $\{\mathbf{Q}_\mathrm{W}\}$ is the total heat transfer from each finite volume element into the wire. The energy balance equation can thus be rewritten:

$$[\boldsymbol{S}_T]_j\{\boldsymbol{T}\}_j = \{\boldsymbol{Q}_W\}_j \quad j = 1, 2, \dots M \tag{2.50}$$

$$[\boldsymbol{S}_T]_j = [\boldsymbol{S}_H] + \left[[S_V][\boldsymbol{Z}]_j - [I]\right]^{-1}[S_V] - [S_M]_j \quad j = 1, 2, \dots M \tag{2.51}$$

Fourier's law can again be employed to relate the temperature at the wire surface $\{\mathbf{T}_\mathrm{G}\}$ to the elemental temperature $\{\mathbf{T}\}$.

$$\{\boldsymbol{Q}_W\}_j = [S_V]\{\boldsymbol{T} - \boldsymbol{T}_W\}_j \quad j = 1, 2, \dots M \tag{2.52}$$

Using equation (2.48) in equation (2.46) yields:

$$\{\boldsymbol{Q}_W\}_j = \left[[I] - [S_T]_j[S_V]^{-1}\right]^{-1}[S_T]_j\{\boldsymbol{T}_W\}_j \quad j = 1, 2, \dots M \tag{2.53}$$

Equation (2.53) places the total rate of heat transfer into each incremental area in terms of the wire surface temperature. Assuming that the wire is isothermal, an arbitrary temperature can be assigned to $\{\mathbf{T}_w\}$ and $\{\mathbf{Q}_W\}$ can be calculated.

$$\boldsymbol{Z}_{W\,j} = \frac{\sum_m^{M_{incr}} \boldsymbol{T}_{W,m,j}}{M_{incr} \sum_m^{M_{incr}} \boldsymbol{Q}_{W,m,j}} \quad j = 1, 2, \ldots M \tag{2.54}$$

The wire impedance can be corrected for the influence of the wire mass using equation (2.55)

$$\widetilde{\boldsymbol{Z}}_j = \frac{1}{\frac{1}{\boldsymbol{Z}_{W\,j}} - i2\omega\rho C\pi r^2 L} \quad j = 1, 2, \ldots M \tag{2.55}$$

The properties of the material are determined by adjusting the model parameters to minimize the error between the measured impedance values and the analytical impedance values. This is typically done using a nonlinear optimization function which employs a simplex algorithm

$$E = \sum_j^M \left|\widetilde{\boldsymbol{Z}}_j - \widehat{\boldsymbol{Z}}_{\boldsymbol{j}}\right|^2 \tag{2.56}$$

It should be note that, by parameter fitting, approach, thermal conductivity can be determine in through-thickness and in-plane directions, which are k_y and k_x, respectively in (2.31). It should be also noted that, according to equation, it is possible to measure the thermal conductivity of the bulk material by embedding the platinum wire inside the sample. In this case, the boundary condition is much simpler and there is no need to used finite difference model in the previous section. Beginning with the heat conduction equations in cylindrical coordinates and employing a solution procedure similar to the one presented in reference [44], it is a straightforward exercise to derive the thermal impedance at the surface of the embedded wire:

$$\boldsymbol{\phi_j} = \sqrt{\frac{i4\pi r^2 f_j}{\alpha}} \tag{2.57}$$

$$\boldsymbol{Z_j} = \frac{1}{2\pi kL}\frac{\mathrm{K}_0(\boldsymbol{\phi_j})}{\boldsymbol{\phi_j}\mathrm{K}_1(\boldsymbol{\phi_j})} \tag{2.58}$$

where, K_0 and K_1 are modified Bessel functions. However, this method has a limitation: it requires the platinum wire be in the bulk material before test. Only neat epoxy or nanofiller epoxy composites can be measured using this method. Therefore, in this study, the wire-embedding method is only used for validation purpose.

2.3 Measuring Thermal Conductivities of Individual Fibers

2.3.1 Measuring Longitudinal Thermal Conductivities of Individual Fibers

2.3.1.1 Experimental principle

3ω method can be also used to measure thermal conductivity of material in shape of fiber filament. It is required that the sample must either electrical conductive or semi-conductive. The AC driven voltage or current is directly fed onto the specimen and the specimen itself will response as both heater and sensor. The fiber filament is usually suspended between two copper strips serving as both electrodes and heat sinks.

Compared to metal strip or metal wire on a hard surface, the suspended filament will experience higher convection compared with conduction. This is because the only conduction occurs at the two ends where the suspended fiber filament is connected to the heat sink. For eliminating the heat loss through gas convection, a high vacuum, typically in mini-torr scale, is needed. In order to depress the radial heat loss, radiation shielding is used.

2.3.1.2 Theory for determining thermal conductivity from 3ω response

The heat generation and diffusion of an AC electrical current of the form $I_o \sin \omega t$ passing through the suspended fiber filament can be described by the following partial differential equations and the initial boundary conditions (Figure 8):

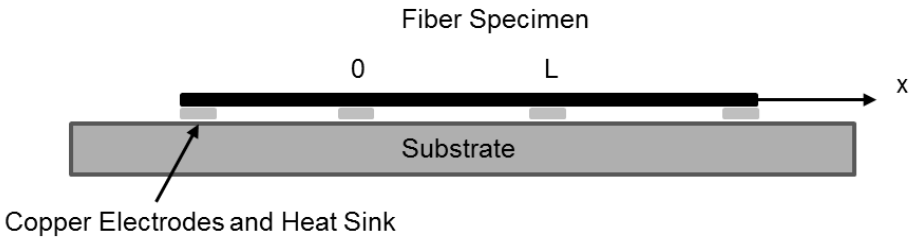

Figure 8 Illustration of the configuration for measuring the specific heat and thermal conductivity of a fiber filament specimen along fiber direction.

$$\rho C_p \frac{\partial T(x,t)}{\partial t} - k\frac{\partial^2 T(x,t)}{\partial x^2} = \frac{I_0^2 \sin^2 \omega t}{LS}[R + R'(T(x,t) - T_0)] \tag{2.59}$$

$$\begin{cases} T(0,t) = T_0 \\ T(L,t) = T_0 \\ T(x,-\infty) = T_0 \end{cases} \tag{2.60}$$

where $R' = (dR/dT)_{T_0}$. S is the cross section of the specimen. We have assumed that the electric current was turned on at $t = -\infty$.

Let $\Delta(x,t)$ denote the temperature variation from T_0, i.e., $\Delta(x,t)=T(x, t)-T_0$, equation (2.59) and (2.60) then become

$$\frac{\partial \Delta(x,t)}{\partial t} - \alpha\frac{\partial^2 \Delta(x,t)}{\partial x^2} - c\sin^2 \omega t \Delta(x,t) = b\sin^2 \omega t \tag{2.61}$$

$$\begin{cases} \Delta(0,t) = 0 \\ \Delta(L,t) = 0 \\ \Delta(x,-\infty) = 0 \end{cases} \tag{2.62}$$

where $\mathrm{b} = \mathrm{I}_0^2\mathrm{R}/\rho\mathrm{C}_\mathrm{p}\mathrm{LS}$, $\mathrm{c} = \mathrm{I}_0^2\mathrm{R}'/\rho\mathrm{C}_\mathrm{p}\mathrm{LS}$.

Using the impulse theorem, Δ(x,t) can be represented as the integral of the responses of the specimen to the instant "force" $b\sin^2\omega t$ at each time interval:

$$\Delta(x,t) = \int_{-\infty}^{t} z(x,t;\tau)d\tau \tag{2.63}$$

where $z(x,t;\tau)$ satisfies

$$\frac{\partial z}{\partial t} - \alpha\frac{\partial^2 z}{\partial x^2} - c\sin^2\omega t z = 0 \tag{2.64}$$

$$\begin{cases} z(0,t) = 0 \\ z(L,t) = 0 \\ z(x,\tau+0) = b\sin^2\omega\tau \end{cases} \tag{2.65}$$

$z(x,t;\tau)$ can be expanded in the Fourier series:

$$z(x,t;\tau) = \sum_{n=1}^{\infty} U_n \sin\frac{n\pi x}{L} \tag{2.66}$$

Substituting equation (2.66) into equation (2.64), we have

$$\sum_{n=1}^{\infty}\left[\frac{dU_n}{dt} + \left(\frac{n^2}{\gamma} - c\sin^2\omega t\right)U_n\right]\sin\frac{n\pi x}{L} = 0 \tag{2.67}$$

where $\gamma \equiv L^2/\pi^2\alpha$ is the characteristic thermal time constant of the specimen for the axial thermal process.

The term $c\sin^2\omega t$ can be neglected if $n^2/\gamma \gg c$, or equivalently

$$\frac{I_0^2 R' L}{n^2\pi^2 kS} \ll 1 \tag{2.68}$$

Condition (2.68) means that the heating power inhomogeneity caused by resistance fluctuation along the specimen should be much less than the total heat power. This condition is usually held. For example, in a typical measurement one could have I_0=10 mA, R'=0.1Ω/K, L=1 mm, S=10^{-2} mm2, and k=100 W/mK, the left-hand side of equation (2.68) is then about 10^{-3} even for the n=1 case.

After dropped off the $c\sin^2\omega t$ term, the solution of the ordinary different equation (2.67) is

$$U_n(t;\tau) = C_n(\tau)e^{-(n^2/\gamma)(t-\tau)} \tag{2.69}$$

where $C_n(\tau)$ can be determined using the initial condition in equation (2.65), together with the relation $\sum_{n=1}^{\infty}\{2[1-(-1)^n]/n\pi\}\sin n\pi x/L = 1$ for 0<x<L:

$$C_n(\tau) = \frac{2b[1-(-1)^n]}{n\pi}\sin^2\omega\tau \tag{2.70}$$

Using equation (2.69) and (2.70), equation (2.67) becomes

$$z(x,t;\tau) = \sum_{n=1}^{\infty}\sin\frac{n\pi x}{L}\frac{2b[1-(-1)^n]}{n\pi}\sin^2\omega\tau e^{-(n^2/\gamma)(t-\tau)} \tag{2.71}$$

Substituting equation (2.71) into (2.63) and remembering that $\Delta(x,t)=T(x,t)-T_0$, we obtain the temperature distribution along the specimen:

$$T(x,t) - T_0 = \Delta_0\sum_{n=1}^{\infty}\frac{[1-(-1)^n]}{2n^3}\times\sin\frac{n\pi x}{L}\left[1-\frac{\sin(2\omega t+\phi_n)}{\sqrt{1+\cot^2\phi_n}}\right] \tag{2.72}$$

where $\cot\varphi_n=2\omega\gamma/n^2$, and $\Delta_0 = 2\gamma b/\pi = 2\gamma b/\pi = 2I_0^2R/(\pi kS/L)$ is the maximum dc temperature accumulation at the center of the specimen. Δ_0 is only *k* dependent. The

information of C_p is included in the fluctuation amplitude of the temperature around the dc accumulation.

The temperature fluctuation will result in a resistance fluctuation, which can be calculated as

$$\delta R = \frac{R'}{L}\int_0^L [T(x,t) - T_0]dx \tag{2.73}$$

Using equation (2.72) and the relation $\int_0^L (\sin n\pi x/L)\, dx = [1-(-1)^n]L/n\pi$, the resistance fluctuation can be expressed as

$$\delta R = R'\Delta_0 \sum_{n=1}^{\infty} \frac{[1-(-1)^n]^2}{2\pi n^4}\left[1 - \frac{\sin(2\omega t + \phi_n)}{\sqrt{1+\cot^2\phi_n}}\right] \tag{2.74}$$

As a product of the total resistance $R + \delta R$ and the current $I_0 \sin\omega t$, the voltage across the specimen contains a 3ω component $V_{3\omega}(t)$. Obviously, the n=2 term in $V_{3\omega}(t)$ automatically vanishes. If only taking the n=1 term, which introduces a relative error of the order $\sim 3^{-4}$ at low frequencies, we have

$$V_{3\omega}(t) \approx -\frac{2I_0^3 RR'}{\pi^4 kS\sqrt{1+(2\omega\gamma)^2}}\sin(3\omega t - \phi) \tag{2.75}$$

where we have redefined the phase constant $\phi = \frac{\pi}{2} - \phi_1$ so that

$$\tan\phi \approx 2\omega\gamma \tag{2.76}$$

If using the root-mean-square values of voltage and current as what the lock-in amplifier gives, equation (2.75) becomes (hereafter we always let $V_{3\omega}$ denotes the rms value of $V_{3\omega}(t)$, and I denotes the rms value of $I_0\sin\omega t$):

$$V_{3\omega\_rms}(t) \approx -\frac{4I^3LRR'}{\pi^4 kS\sqrt{1+(2\omega\gamma)^2}} \tag{2.77}$$

By fitting the experimental data to this formula, we can get the thermal conductivity k and thermal time constant γ of the specimen. The specific heat can then be calculated as

$$C_p = \frac{\pi^2\gamma k}{\rho L^2} \tag{2.78}$$

The following alternative form makes it more clear how the 3ω voltage depends on the dimensions of the specimen:

$$V_{3\omega}(t) \approx -\frac{4I^3L\rho_e\rho_e{}'}{\pi^4 k\sqrt{1+(2\omega\gamma)^2}}\left(\frac{L}{S}\right)^3 \tag{2.79}$$

where ρ_e is the electrical resistivity of the specimen, $\rho_e' \equiv (\mathrm{d}\rho_e/\mathrm{d}T)$.

2.3.2 Measuring Transverse Thermal Conductivities of Individual Fibers

As mentioned in chapter 1, carbon fibers are, in fact, highly anisotropic structural materials due to the orientation of graphite-like micro-fibrils along the fiber direction. Therefore, the thermal conductivity of a carbon fiber is significantly higher in the longitudinal direction compared to the transverse direction.

In order to set up a complete study of the effect of CNFs on thermal conductivity of hierarchical carbon fiber and provide experimental input to the hierarchical CFRCs, an experimental technique and the corresponding analytical model for direct measurement of the transverse thermal conductivity of carbon fiber using the 3ω method is developed. The experimental principle and the theory to determine the thermal conductivity of this new technique are given in the following two sections.

2.3.2.1 Experimental principle

Similar to the technique for measuring longitudinal thermal conductivity of an individual fiber with 3ω method, the individual fiber specimen in this technique is also used as heating and sensing element. Instead of suspending the fiber in a vacuum environment, to measure transverse thermal conductivity, medium is needed to allow the heat flux flow through transverse direction of the carbon fiber. To achieve this controlled environment of transverse heat flow, the fiber is submerged in deionized water. The AC voltage of frequency ω is then applied to the specimen to heating up both the specimen and the surrounding medium to generate the 3ω response. The connections for the fiber also need to be adjusted to minimize the heat flowing from the two ends of the fiber.

Instead of copper strip, small piece of circuit board is used to create adiabatic boundary condition. Deionized water is selected as medium because: 1. it is the convenient to place the fiber inside deionized water; 2. deionized water is a liquid with high thermal conductivity and low electrical conductivity. The known thermal properties of deionized water can be used to calculate the thermal conductivity of the fiber specimen through heat conduction theory.

2.3.2.2 Theory for determining thermal conductivity from 3ω response

Schematic diagram of the heat conduction of the fiber submerged in a liquid medium is shown in Figure 9. Due to high aspect ratio (> 100) and significantly smaller dimensions of the fiber compared to the liquid reservoir the fiber is modeled as an infinite long cylinder inside an infinite medium (Figure 10). Assuming that the thermal conductivity is uniform over the cross section of the fiber and a perfect boundary condition is maintained at the interface between the fiber and the liquid medium, the governing equations of the heat conduction of an infinite long cylinder inside the infinite medium with periodic volumetric heat generation due to the applied alternating voltage in polar coordinate system, neglecting convection and radiation heat loss, can be written as,

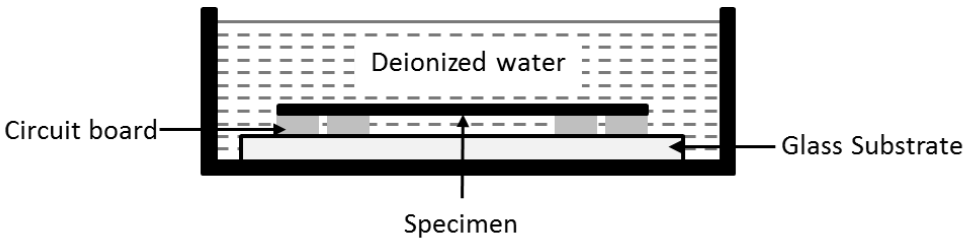

Figure 9 Schematic of the suspended fiber specimen submerging in deionized water.

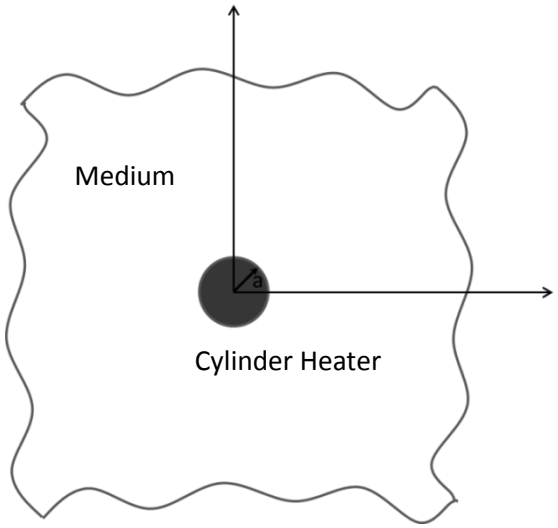

Figure 10 Schematic of a heat conduction of infinite long cylinder heater inside an infinite medium.

$$\rho_1 C_1 \frac{\partial \tilde{T}_1}{\partial t} = k_1 \left(\frac{\partial^2 \tilde{T}_1}{\partial r^2} + \frac{1}{r} \frac{\partial \tilde{T}_1}{\partial r} \right) + \tilde{g} \tag{2.80}$$

$$\rho_2 C_2 \frac{\partial \tilde{T}_2}{\partial t} = k_2 \left(\frac{\partial^2 \tilde{T}_2}{\partial r^2} + \frac{1}{r} \frac{\partial \tilde{T}_2}{\partial r} \right) \tag{2.81}$$

$$\tilde{T}_1\big|_{r=a} = \tilde{T}_2\big|_{r=a} \tag{2.82}$$

$$\tilde{T}_2\big|_{r=\infty} = 0 \tag{2.83}$$

$$k_1 \left.\frac{\partial \tilde{T}_1}{\partial r}\right|_{r=a} = k_2 \left.\frac{\partial \tilde{T}_2}{\partial r}\right|_{r=a} \tag{2.84}$$

where $\tilde{T}$ is the oscillating temperature and $\tilde{g}$ is the heat generation rate per unit volume;ρ, C, and k are density, specific heat and thermal conductivity, respectively. The subscript 1 is for the fiber and subscript 2 is for the medium. R, a and L are the electric resistance, radius and length of the fiber specimen, respectively. V is the amplitude of the AC voltage, ω is the angular frequency of the alternating voltage, and t is the time. Driven by ω periodic signal, temperature will also be also fluctuated in period of 2ω and can be written as

$$\tilde{T}_i = \Delta T_i \exp(i2\omega t) + T_0 \tag{2.85}$$

where T_0 is the ambient temperature, and

$$\tilde{g} = g \exp(i2\omega t) = \frac{V^2}{\pi R a^2 L} \exp(i2\omega t) \tag{2.86}$$

Substitute (2.85) and (2.86) into (2.80)-(2.84), we have:

$$0 = \left(\frac{\partial^2 \Delta T_1}{\partial r^2} + \frac{1}{r}\frac{\partial \Delta T_1}{\partial r}\right) + \frac{g}{k_1} - \frac{i2\omega}{\alpha_1}\Delta T_1 \tag{2.87}$$

$$0 = \left(\frac{\partial^2 \Delta T_2}{\partial r^2} + \frac{1}{r}\frac{\partial \Delta T_2}{\partial r}\right) - \frac{i2\omega}{\alpha_2}\Delta T_2 \tag{2.88}$$

$$\Delta T_1|_{r=a} = \Delta T_2|_{r=a} \tag{2.89}$$

$$\Delta T|_{r=\infty} = 0 \tag{2.90}$$

$$k_1 \frac{\partial \Delta T_1}{\partial r}\Big|_{r=a} = k_2 \frac{\partial \Delta T_2}{\partial r}\Big|_{r=a} \tag{2.91}$$

Solution of (2.88) is [51]:

$$\Delta T_2 = A\mathrm{K}_0(\beta_2 r) \tag{2.92}$$

where K_0 is the second kind modified Bessel function. For (2.87), let

$$u = \Delta T_1 - \frac{\alpha_1 g}{i2\omega k_1} \tag{2.93}$$

then the solution for (2.88) can be obtained as:

$$u = B\mathrm{I}_0(\beta_1 r) \tag{2.94}$$

$$\Delta T_1 = B\mathrm{I}_0(\beta_1 r) + \frac{\alpha_1 g}{i2\omega k_1} \tag{2.95}$$

where I_0 is the first kind modified Bessel function. $\beta_j = \left(\frac{2\omega i}{\alpha_j}\right)^{1/2}$ A and B are constants that can be obtained using boundary conditions (2.90) and (2.91)

$$A = \frac{\alpha_1 g}{i2\omega k_1} \frac{\gamma I_1(\beta_1 a)}{\gamma K_0(\beta_2 a) I_1(\beta_1 a) - K_1(\beta_2 a) I_0(\beta_1 a)} \tag{2.96}$$

$$B = \frac{\alpha_1 g}{i2\omega k_1} \frac{K_1(\beta_2 a)}{\gamma K_0(\beta_2 a) I_1(\beta_1 a) - K_1(\beta_2 a) I_0(\beta_1 a)} \tag{2.97}$$

where $\gamma = -\left(\frac{k_1}{k_2}\right)\left(\frac{\alpha_1}{\alpha_2}\right)^{1/2}$. $\alpha_j = k_j/\rho_j C_j$, $j = 1,2$ are the heat diffusivities of the specimen and the medium, respectively and i is the imaginary unit. The amplitude of periodic change in the resistance of the sample is

$$\Delta R(r) = R'\Delta T_1(r) \tag{2.98}$$

The average change of the resistance of the sample over the cross section is

$$\Delta R = \frac{2R' \int_0^a \Delta T_1(r) r dr}{a^2} \tag{2.99}$$

The amplitude of the 3ω signal is

$$V_{3\omega\_rms} = I_{rms}\Delta R = \frac{V_{rms}}{R}\left(\frac{2R' \int_0^a \Delta T_1(r) r dr}{a^2}\right) \tag{2.100}$$

or

$$V_{3\omega\_rms} = \frac{2V_{rms}R'}{R}\left(\frac{BI_1(\beta_1 a)}{\beta_1 a} + \frac{\alpha_1 g}{4i\omega k_1}\right) \tag{2.101}$$

where the subscript “rms” denotes root mean square of the AC signal.

2.3.2.3 Uncertainty analysis

In this section, we analyze the uncertainty of the present developed technique for measuring transverse thermal conductivity of an individual fiber. Since the thermal conductivity is implicit in equation (2.101), the total uncertainty in the thermal conductivity measurement can be determined by calculating the root sum-of-squares of the uncertainties of all the contributing measured quantities, including diameter, length, voltage, electric resistance, and temperature coefficient of electric resistance, which can be expressed as [52, 53]:

$$\delta\lambda = \sqrt{[\delta\lambda]_d^2 + [\delta\lambda]_l^2 + [\delta\lambda]_V^2 + [\delta\lambda]_R^2 + [\delta\lambda]_{\alpha_{CR}}^2} \tag{2.102}$$

For the uncertainties in the dimensions, the maximum deviations from the average values are taken as uncertainties from independent measurements. The diameter of the carbon fiber is measured from the SEM images, and the relative uncertainty is estimated to be less than 1.5%. The length is measured under the microscope by comparing with rhonchi ruling of 0.1 mm/cycle as reference scale. The uncertainty of the thermal conductivity caused by length is estimated to be less than 2.07%.

Since the electric voltage and current were measured by an Agilent 8.5-digit digital multimeter and the standard resistance, the relative uncertainties in the electrical resistance and the ac voltage mainly came from signal noises. By taking the fluctuation of

the quantities during measurement as uncertainties, the uncertainties of resistance and voltage are estimated to be 0.15% and 0.13%, respectively. The uncertainty in the temperature coefficient of resistance α_{CR} is correlated to the uncertainties of electrical resistance and the temperature values. In the present study, it is estimated by comparing the mean value of the maximum and the minimum of electrical resistances over the temperature range between measured data and the best fit results from linear regression of $R{\sim}T$ curves. The total uncertainty in ρ'_e is about 3%. Using the aforementioned uncertainties of the contributing quantities, the uncertainty of the measured transverse thermal conductivity is estimated to be less than 5.06% using equation (2.102).

Chapter 3 Materials and Experimental Methods

3.1 Introduction

This chapter describes the experimental detail for measuring thermal conductivity of carbon fiber and carbon fiber epoxy composites using 3ω method including the materials selection, samples preparation, experimental setup and experimental protocol. Finally the selection of parameters for systematically studying the effect of CNFs on hierarchical fibers and composites is discussed.

Three catalogs of materials are used in this study. The first two catalogs are hierarchical carbon fiber and hierarchical CFRCs, which are the focus in this research. An additional catalog is the hybrid carbon fiber composites, which means that CNFs were blended into the matrix to make the CFRCs. This catalog is for studying the efficiency of CNF on improving the thermal conductivity with different CNFs reinforced CFRCs system and to confirm the value on measuring the thermal conductivity of hierarchical CFRCs.

For the sample preparation and protocol, the wire-based 3ω method was chosen to measure the thermal conductivity for bulk materials in this study due to the low expense for the sample preparation as discussed in chapter 2. This raises some practical challenge and issues in preparing the sample and in accurately measuring the thermal conductivities of CFRCs. A unique designed apparatus and a modified sample preparation protocol are thus developed to solve these issues. Detail will be discussed in section 3.3.1.

The same 3ω setup was used to measure thermal conductivities in longitudinal and transverse directions of an individual fiber. The configuration of sample assembly is slightly different for these two measurements. The details are given in 3.3.2 and 3.3.3 respectively.

Finally, a general introduction of the components in the 3ω setup will be given in section 3.4.1. Parameter settings for different measurements are presented in 3.4.2.

3.2 Materials

3.2.1 Raw Materials

At the early stage of this study, two types of standard materials were used to validate the sample preparation, the measurement technique and the experimental setup for bulk material. These standard materials respectively were Pyrex 7740 glass (Glass Dynamics LLC.), and EPON 862 epoxy with EPICURE curing agent W (Monentive, Performance Materials Inc.). For the measurement of longitudinal thermal conductivities of individual carbon fibers, platinum wire and tungsten (California Fine Wire Company, 99.95%) wire and two types of commercial carbon fiber, AS4 and IM10 (Hexcel corp.) were used for validation. For the technique to measure transverse thermal conductivities of an individual carbon fibers, platinum wire, tungsten wire and wires coated with polymer Spin-on-glass (IC1-200, futurrex inc.) were used for validation. Consequently, the improved wire-based 3ω method was used to measure CFRCs, hybrid CFRCs and hierarchical CFRCs with hierarchical carbon fabric. For all the epoxy composites system, Epon862/EPIKURE W was used as the matrix.

For all the bulk material measurement, platinum wire with 10 μm diameter was used as the heater and senor. Spin-on-glass was used as both the adhesive material to attach the wire on the surface of the specimen and the electrical insulation material.

For carbon fabric reinforced epoxy composites, the carbon fabric used in the study was T650/15 Pan-based plain weaved laminated carbon fabric from Indianapolis, Indiana USA. The fibers of this kind of fabric have relatively low thermal conductivity and electrical conductivity but have high Young's modulus. The CNFs used to fabricate hybrid CFRCs for comparison with hierarchical CFRCs are commercial vapor grown CNFs which are Pyrograf III PR24 with AGLD grade. The lengths of the CNFs range from 30 μm to 100 μm while the diameters of them range from 60 nm to 150 nm. The functionalization of the CNFs was achieved by oxidation of the surface of the CNFs with the help of nitric acid. The oxidation generated rough surface on the nanofibers introducing strong mechanical locking between CNFs and the epoxy matrix. In this study, 0.01%, 0.05% and 0.1% CNFs were used selected as the mass percent to both neat CNFs and oxidized CNFs to fabricate the hybrid CFRCs.

3.2.2 Hierarchical Carbon Fiber and Hierarchical Carbon Fabric

Hierarchical carbon fabrics were fabricated by growing CNFs on the surface of the carbon fabrics. The process used to produce growth of CNFs on carbon fiber fabric in this study followed the chemical vapor deposition process presented by Downs and Baker. Various amounts of nickel nitrate and copper nitrate salts were mixed in isopropanol at a 9:1 Ni:Cu ratio and deposited on the surface of the carbon fiber fabric with the help of a Paasche H0609 siphon-fed hobby airbrush. The carbon fiber fabric was then inserted into

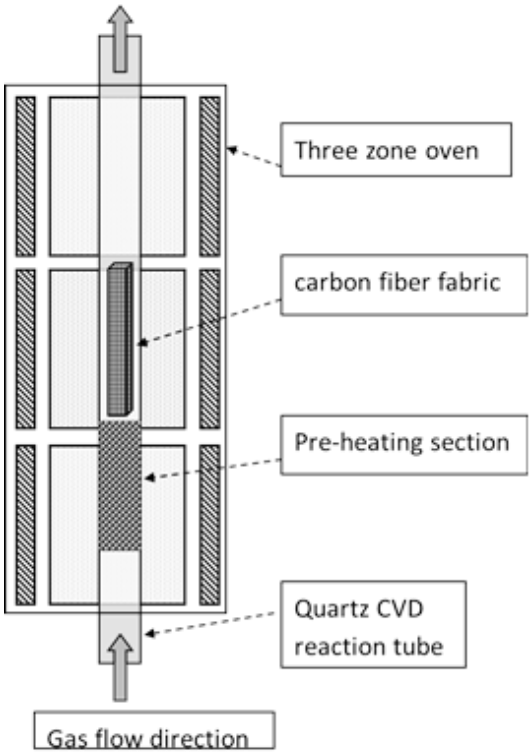

Figure 11 Schematic for chemical vapor deposition (CVD) process for CNFs growth on carbon fabric.

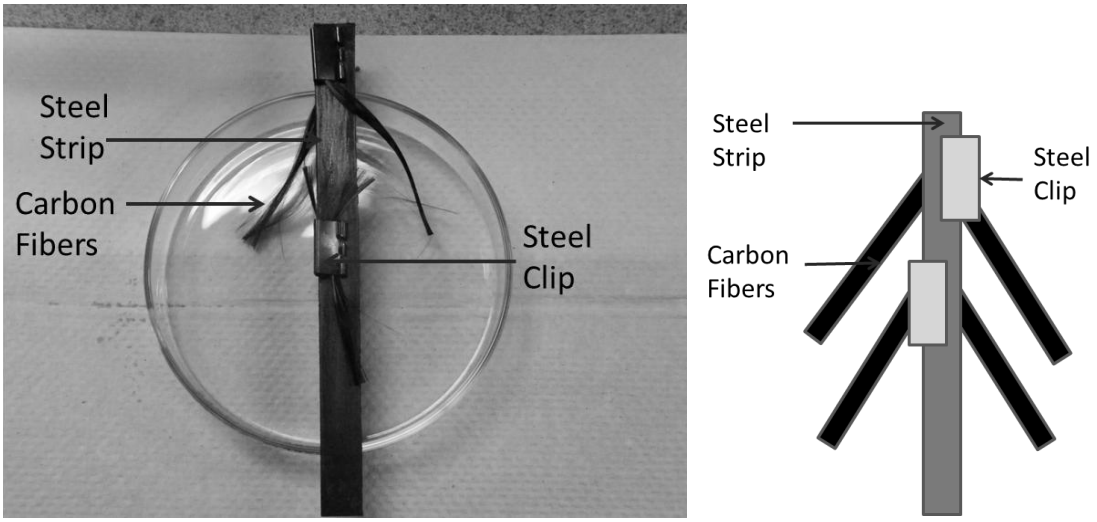

Figure 12 Configuration for holding the carbon fiber tow inside the reactor for growing CNFs. Left: Picture of the real samples assembly for reaction; Right: Schematic of the samples assembly for reaction

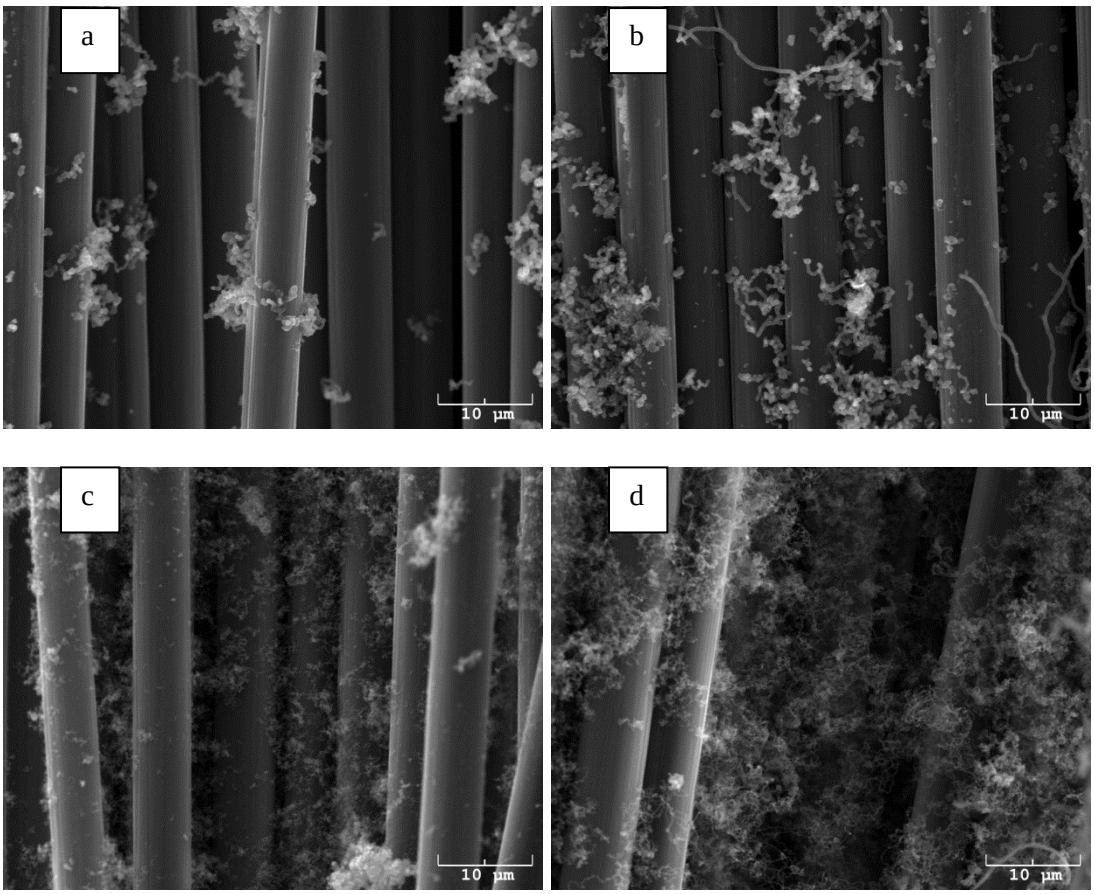

Figure 13 SEM images of CNF grown on the carbon fibers with a) 0.2, b) 0.3, c) 0.5 and d) 1.2 wt% catalysts.

a quartz reaction tube in a three zone vertical furnace (Figure 11). The catalyst was calcified in air at 300 ^{o}C for 1 hour to convert from metal nitrates to oxides, and then reduced in pure hydrogen at 500 ^{o}C for 30 minutes to de-oxidize the catalyst nanoparticles. Ethylene was flowed through the reaction tube to serve as a carbon source for the CNF growth, which took place at 750 ^{o}C for 30 minutes. The reaction tube was then purged and the samples were cooled to room temperature in a pure nitrogen environment.

For the individual fiber study, the carbon fiber tows were drown out from the carbon fabric after catalyst solution was sprayed on the surface and it was dried for 10 minutes. The fiber tows were then held on a steel strip with steel clips and vertically inserted into the reaction tube (Figure 12). Figure 13 illustrated the SEM images of typical pattern of CNF grown on the surface of carbon fiber.

3.2.3 Carbon Epoxy Composites

Vacuum assisted resin transfer molding (VARTM) was used to fabricate CFRCs. In this process incorporating a reference dam, the fibers within the preform were aligned to the reference dam to create a straight edge after the laminate is cured. The VARTM process used a single hard tooling flat plate and a vacuum bag as the opposite mold line. Vacuum pressure was used to impregnate the preform as the matrix is drawn into and through the layup through the following path which is depicted in Figure 14. The matrix was heated up to approximately 121℃ during the infusing. After infusion, the sample assembly was heated up to 177 ℃ and maintained at this temperature for 90 minutes, and then allowed to be naturally cooled overnight. The integrity of the vacuum bag was verified by checking that the leak rate was less than 25 mm of mercury in five minutes.

To fabricate hybrid CFRCs, the epoxy was first modified by blending CNFs, and then brought into the procedure of VARTM. Since CNFs tend to agglomerate in the as-received condition, we applied mechanical shearing and ultransonication to disperse the fillers into the epoxy to fabricate the composites precursor. CNFs were first dispersed in isopropyl alcohol (IPA) under bath ultrasonic treatment for 1 hour. The suspension was then mixed with acetone and Epon862 epoxy resin using a mechanical mixer for 5 min at

400 rpm. The mixture was further sonicated for 20 min, followed by drying in the vacuum oven for 24 hours at 50 ℃ and 48 hours at 60 ℃, respectively, and then finally heated to 105 ℃ to flash the mixture until all the IPA and acetone were removed. The mixture was sonicated for another hour. EPIKURE W curing agent was then added into the mixture, followed by mechanical mixing for 10 min at 250 rpm. The resultant mixture was bath sonicated for 5 min, and then degassed under vacuum for 4 hours. This mixture was then used in the VARTM to fabricate the hybrid CFRCs.

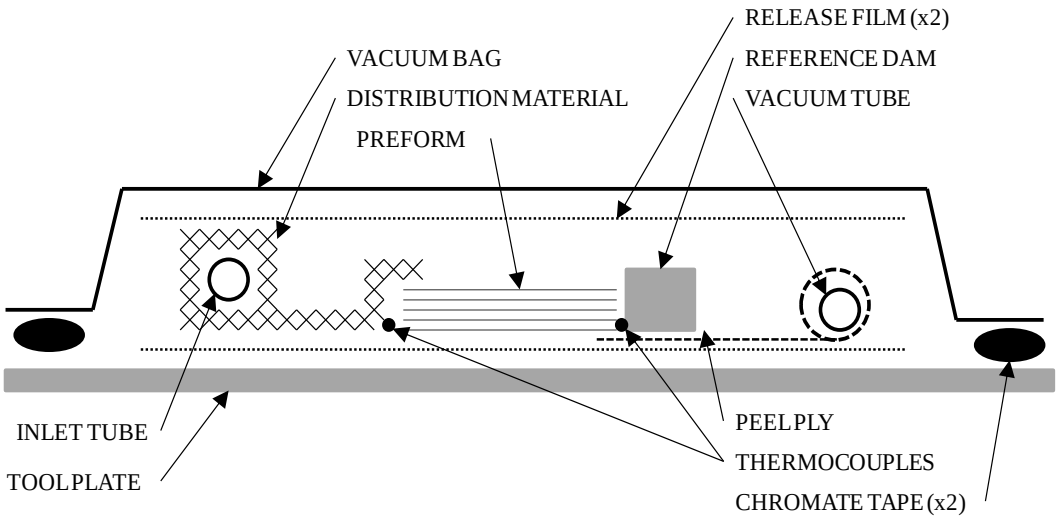

Figure 14 Schematic of the cross section of VARTM layup. The resin will flow from the inlet tube on the left, through the preform to the vacuum tube on the right.

The Second type of the CNFs modified CFRC is hierarchical CFRC. CNFs was grown onto the surface of the neat carbon fabrics and these carbon fabrics were then used to manufacture the fiber reinforced epoxy composites with the VARTM procedure following the same protocol for fabricate hybrid carbon epoxy composites. For

hierarchical composites with CNFs growth, study has been focused on the weight percent of growth. By applying different mass amount of catalyst (0.2%, 0.3%, 0.5%, 1.2%, and 3%), we have achieved 5.145%, 8.19%, 17.4%, 38% and 252% growth. The thermal conductivity study was also rendered on the individual fibers measurement for both longitudinal and transverse directions with different controlled amount of catalysts. In this study, 0.2%, 0.3%, 0.5%, and 1.2% of catalysts were used to grow CNFs on T650 carbon fiber tows. Fibers were randomly drawn from these tows and thermal conductivities of them were characterized in a statistical way.

3.3 Test Sample Preparation

3.3.1 Test Sample Preparation for Bulk Materials with Surface-Mounting

The sample was first flattened with diamond cutter and then polished with a polishing machine with a series of sand paper of different grits from coarse to fine: 80 grits, 150 grits, 200 grits, 500 grits, 800 grits, 1000 grits, and finally 2000 grits. The sample was then cut into small specimens with length about half an inch. The width and the thickness of the specimen are various depend on the type of the materials. Usually the width is between 5 mm to 10 mm, the thickness is between 2 mm to 10 mm. Two small pieces of circuit boards with size of 2 mm by 5 mm by 1 mm were secured on the edge of the sample with super glue and maintained in plane with the surface of the specimen by placing them upside down as shown in Figure 15. For thick specimen, on the bottom of the circuit boards, several droplets of quick cure acrylic epoxy (Allied High Tech Products Inc.) were applied and dried or 15 minutes to ensure the connection between the circuit boards and the specimen were strong enough. These two small pieces of circuit

boards served as two electrodes to connect the platinum wire to the 3ω analysis circuit. The platinum wire was then stretched and soldered over the two electrodes in contact with the surface of the specimen serving as the heater and sensor.

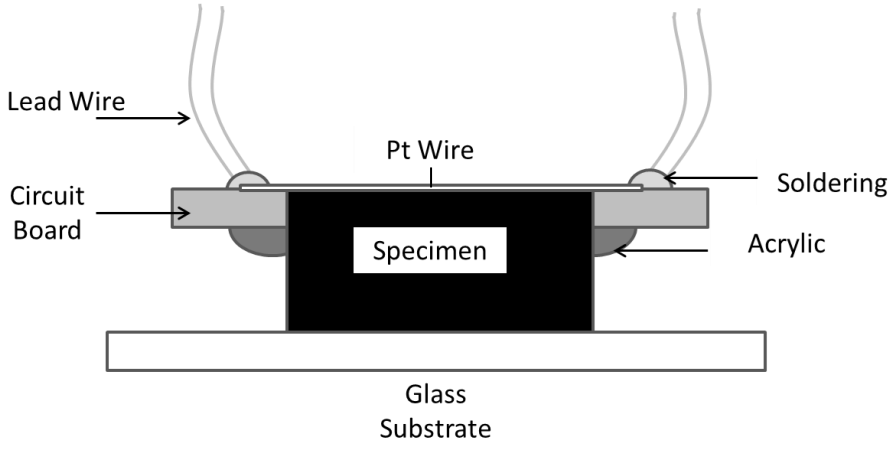

(a)

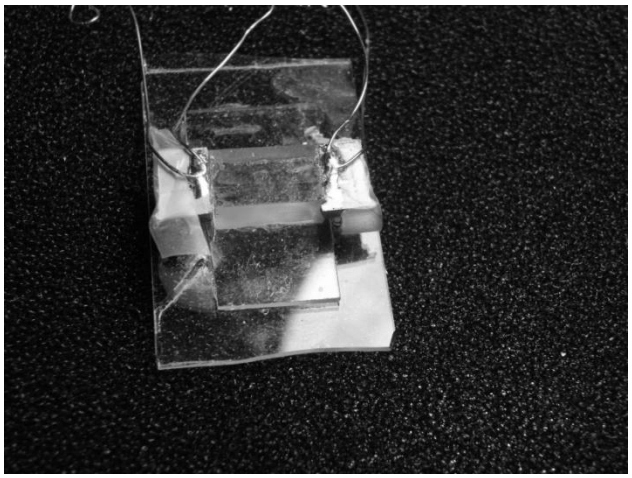

(b)

Figure 15 Sample assembly for measuring thermal conductivity of bulk material with wire-based 3ω method: (a) schematic and (b) a picture of sample assembly of lime glass.

As can be seen in 2.2.2, using the wire-based 3ω and the corresponding scheme to calculate the thermal conductivity is much cost-effect than using a lithographic strip. However, there are also some challenging and issues here.

One of the most important drawbacks of this method is the highly skill-required sample preparation procedure. In this protocol, a metal wire (e.g. platinum) with diameter around 10μm is needed to be perfectly mounted on the surface of the specimen. A typical way is to transport the wire with tape and stretch the wire manually over the surface of the specimen. Under the tension, the wire might be in touch with the specimen.

There are two possible failures of the sample even before measurement: 1. the failure of the wire under over-applied tension; 2. the wire fails to be fully in touch with the surface the specimen due to the bending of the wire if not enough tension is applied. In the first situation, no result can be obtained due to the open circuit. The second situation is more difficult to inspect, because the adhesive material introduced in the next step may flow in the spacing between the wire and the surface of the specimen and bring in significant measurement error.

As a result, a precise control apparatus must be designed to apply proper tension to the wire to both maintain the force within the failure range of the wire and supply enough stress to make sure the wire is in contact with the surface of the specimen. Meanwhile, it should be flexible for different dimension of the specimen because if the wire and the surface of the specimen are not in the same plane, additional stress on the wire will occur at the edge of the specimen.

In order to ensure full contact between the small-dimension wire and the surface of the specimen and to handle such a delicate configuration manually without breaking the wire, a unique designed mounting-stage was built (Figure 16). This apparatus is composed of two translation stages: a z direction stage to align the sample to a reference plane, and a y direction stage to stretch the wire on sample after wire is placed on the surface of the sample. The z direction stage is a home-made lifting stage with coarse thread and spring, which can be controlled by turning the screw on the bottom. This z direction stage provided the flexibility for measuring specimen with thickness from 1 mm to 20 mm. The y direction stage is a linearly translation stage driven by 0.25mm pitch with maximum 6.4 mm travel distance from Thorlabs Inc. After the surface of the sample and the reference plane are aligned (In fact, the surface of the sample was intentionally maintained slightly higher than the reference plane in most of the cases to ensure the stretching of the wire.), a platinum wire with length of about 25 mm was transported with the help of marking tape (marking tape was chosen because it is easy to remove it from smooth surface.) on to the sample. The wire is then secured on the y stage and the sample with scotch tapes. The whole apparatus was then put under the microscope and the y stage was manually controlled to move and stretch the platinum wire up to the point that there is no gap between the wire and the surface of the sample observed. Super glue is then applied to both ends of the wire on the electrodes. Two lead wires with length about 50 mm were soldered on the two electrodes for connection into the 3ω measurement system. After the super glue was solidified, the sample was removed from the stages system and prepared for the next step.

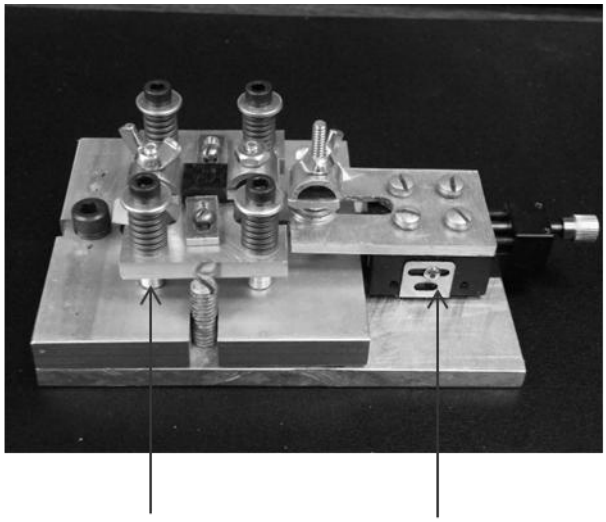

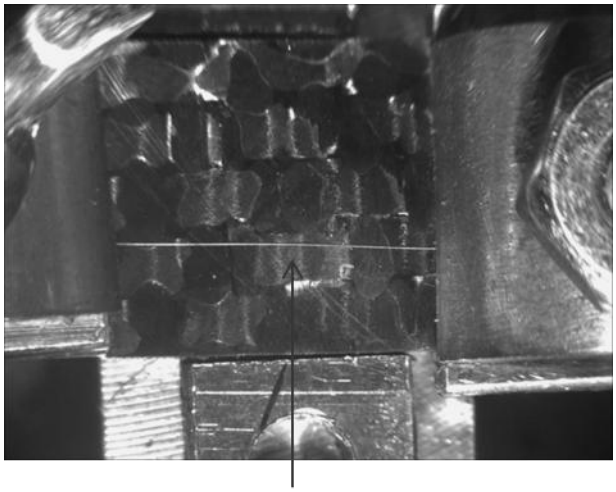

Figure 16 A mounting-stage for 3ω sample assembly: (a) the over view and (b) closer look at the specimen section.

In order to establish a robust thermal contact between the wire and the surface of the sample, adhesive named spin-on-glass (SOG) was used to fill gap between the non-contacted area of the bottom surface of the wire and the surface of the sample (Figure 6). After the wire was mounted and secured with super glue on both ends, its surface with the wire was coated with the SOG with a spinning coating machine at 1500 RPM for 30 seconds. The sample was then allowed to be baked at 50 ℃ for 5 minutes to evaporate the solvent of the coating. The integrity of the thermal path between the wire and the sample was formed using this thin top-coat layer of adhesive. Sample was then connected to the 3ω circuit with a resistive bridge system and ready for measurement.

For non-electrical conductive material, the aforementioned technique is proper. However, carbon fabric is semi-conductive material. After the carbon fabric epoxy composite is polished, some parts of the fabric are exposed on the surface. Directly contact between the platinum wire and the carbon fabric can lead to electric leakage and generate wrong measurement results. In order to overcome this issue, a thin coating of SOG (thickness smaller than 1μm) was first applied on the surface of the carbon fabric composites before the platinum wire was mounted. To compensate the effect induced by the additional SOG layer, a lower frequency range was used during the measurement to generate higher penetration depth. Figure 17 shows the measured thermal conductivities of SOG coated Pyrex 7740 using different maximum frequencies where the minimum frequency was set to be 1Hz and number of data points was set to be 20 with logarithmic spacing. It is found that, when the maximum frequency is below 4 Hz, the thermal conductivity converges to the value of pure Pyrex 7740. This is due to the fact at low frequency the depth of penetration is large enough to cover large volume of the Pyrex

comparing to the small volume of the coating, and thus the effect of the coating is negligible. This can be also validated with comparing two standard material samples with and without insulation coating. Figure 18 shows the comparison between two Pyrex 7740 samples with different sample preparation: one is with insulation layer and the other is without insulation layer. It can be seen that, the maximum of error is about 0.02 W/m-K (3.6% of the thermal conductivity of Pyrex 7740), induced by the additional insulation layer if lower frequency range (below 4 Hz) is used.

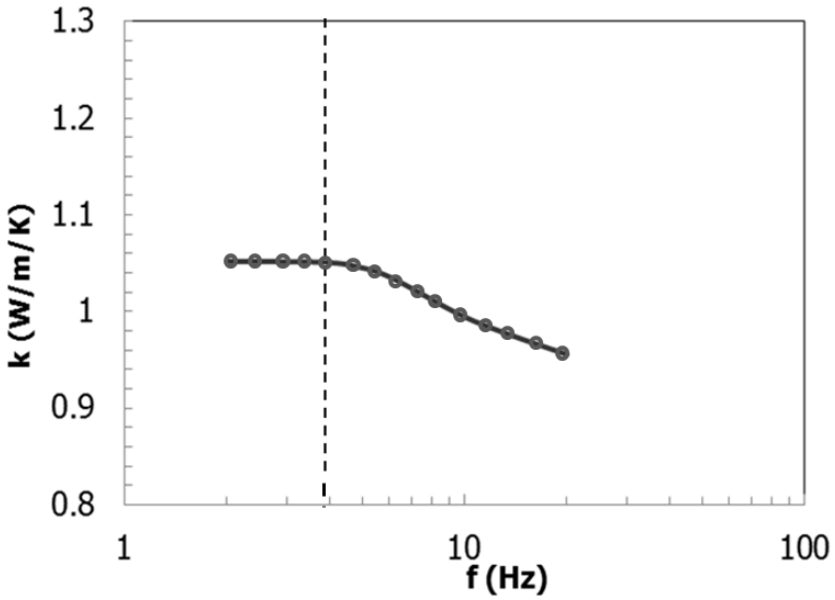

Figure 17 Measured thermal conductivity of SOG-coated Pyrex with 3ω method using different frequency ranges.

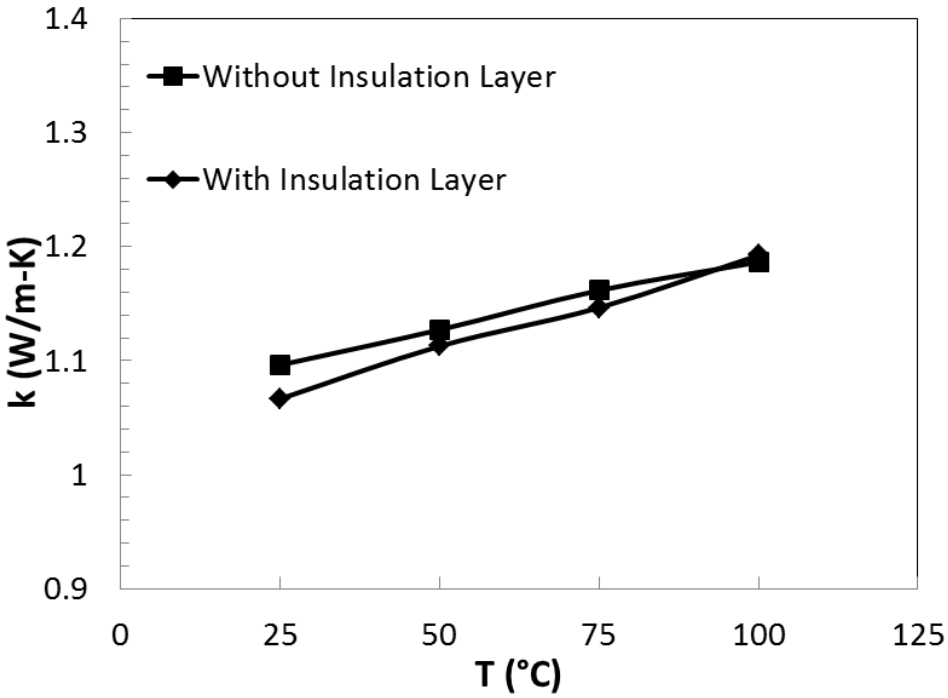

Figure 18 Comparison of measured thermal conductivity of Pyrex 7740 with insulating layer and without insulation layer in frequency range below 4 Hz using 3ω method.

3.3.2 Test Sample Preparation for Individual Carbon Fiber-Longitudinal Direction

As demonstrated in Chapter 2, 3ω method can be also used to measure thermal conductivities of individual fiber filament samples. In this case, the sample itself will serve as both the heater and the sensor.

The configuration for the sample preparation for measuring thermal conductivity of an individual fiber filament is shown in Figure 8. Four copper strips were immobilized on a piece of alumina ceramic with silver epoxy (MG Chemicals Inc.). The distance between the four copper strips were adjusted according to the requirement of the length the

specimen. These four strips functioned as both electrodes and heat sinks, thus copper was selected due to its high electrical and thermal conductivity. The substrate requires high thermal conductivity and high dielectric performance. Thus alumina ceramic was selected as the substrate material and silver epoxy was used as adhesive to conduct heat from the copper strips to the substrate.

The fiber specimen was carefully stretched over the four copper strips with the help of scotch tape for transportation. During the stretching, the fiber was ensured to be straight with the aid of the optical microscope. It should be noted that, although small bending of the fiber specimen will not affect the 3ω response, the waviness geometry of the fiber can introduce error in measuring the length of the fiber. In order to avoid disturbing of the fiber specimen, the fiber was connected to the electrodes with cold soldering using silver paste. After that, due to the difficulty to solder lead wire on the thick copper strips, the sample assembly was connected to the 3ω circuit using alligator clips and the copper strips at the later stage of the study were replaced with two copper crimp terminals with hole in the center (Figure 19).

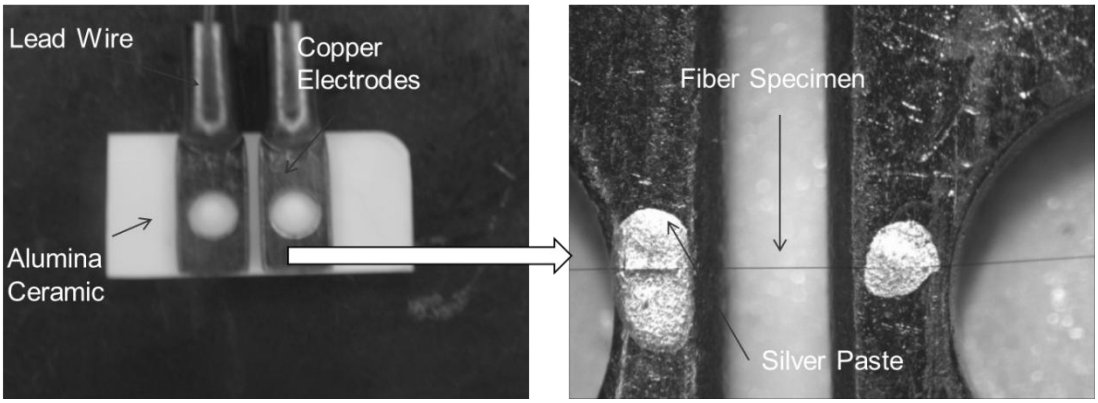

Figure 19 Sample assembly for measuring longitudinal thermal conductivity of an individual fiber using 3ω method.

3.3.3 Test Sample Preparation for Individual Carbon Fiber-Transverse Direction

In order to measure the transverse thermal conductivity of a fiber specimen, medium was introduced to fully encapsulate the whole specimen. There were two requirements for the medium: 1. the medium must be dielectric material 2. The volume of the medium should be much larger than the fiber specimen. For convenience, in this study, material that was liquid phase at room temperature was chosen as medium. There was also consideration of the boiling point of the liquid during the study of thermal conductivities of the fiber specimen under different temperature, where, the temperature of the medium need to be monitored. So at this study, deionized water was finally chosen as the medium because water has a relatively high thermal conductivity (0.6 W/m-K at 20 ℃ [54]) among the liquids and an extremely high electrical resistivity (1.8×105 Ω·m at 20 ℃ [55]).

Figure 20 shows the configuration of the sample assembly for measuring the transverse thermal conductivity of an individual fiber. Two pieces of circuit board of dimension of 2 mm by 5 mm by 1 mm were stick onto a piece of glass substrate with a gap according to the material of the specimen. The fiber specimen is then bridged between the two circuit boards on the glass substrate. Since there is no challenging issue of contact like that for surface mounting in measuring bulk material, there was no need to ensure the wire is straight and under tension, but the length of the wire must be accurately measured. (The detail of measuring the length of the specimen will be discussed in section 3.4.1.) Two lead wires with length of 50 mm are then soldered onto the two circuit boards for connection to the 3ω measurement system. The whole system consisting with glass substrate, circuit boards, platinum wire and the lead wires was considered as a sample assembly.

The sample assembly was then completely submerged inside the medium inside a reservoir and the lead wires were then connected to the 3ω circuit. The electrical resistant of the fiber was measured before and after the sample assembly was put into the water medium to ensure there was no electrical leakage due to any contamination (Figure 9).

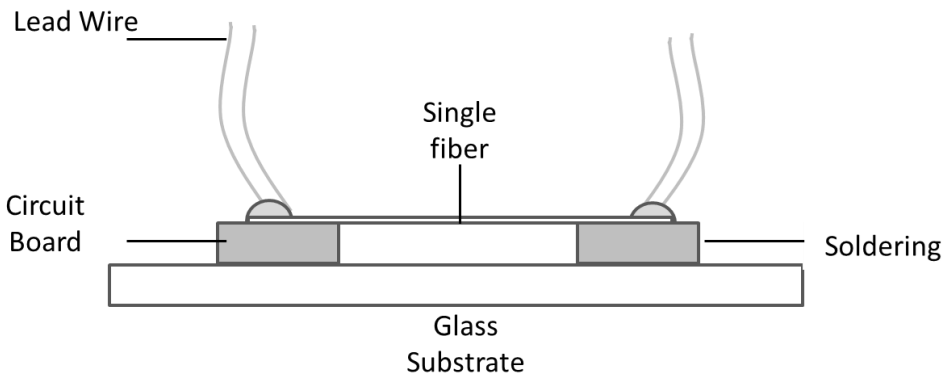

Figure 20 Schematic of sample assembly for transverse thermal conductivity measurement for an individual fiber filament.

3.4 Measurement

3.4.1 Experimental Setup

For all kinds of measurement object, including bulk material, fiber filament in longitudinal direction, and fiber filament in transverse direction, the same 3ω circuit setup was used. This system was built up with similar schematic as that was proposed by Cahill et.al [29], which consists of a function generator, a Whitestone cancelling circuit, a digital multimeter, and a virtual lock-in amplifier system (Figure 21 and Figure 22).

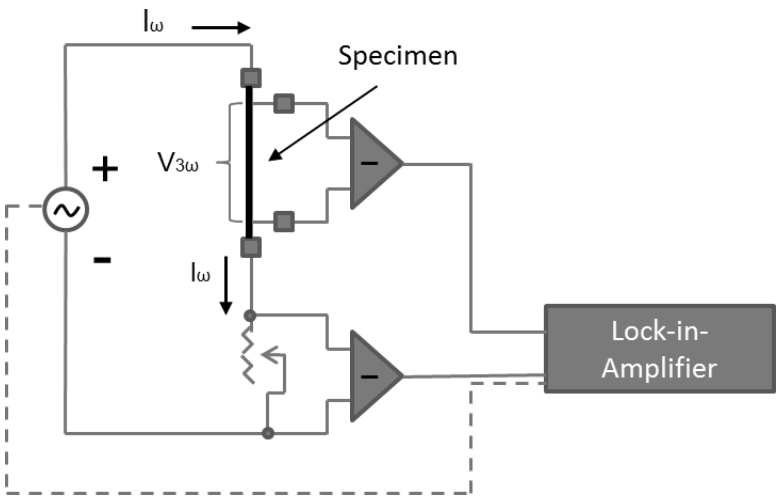

Figure 21 Block diagram of the 3ω measurement circuit.

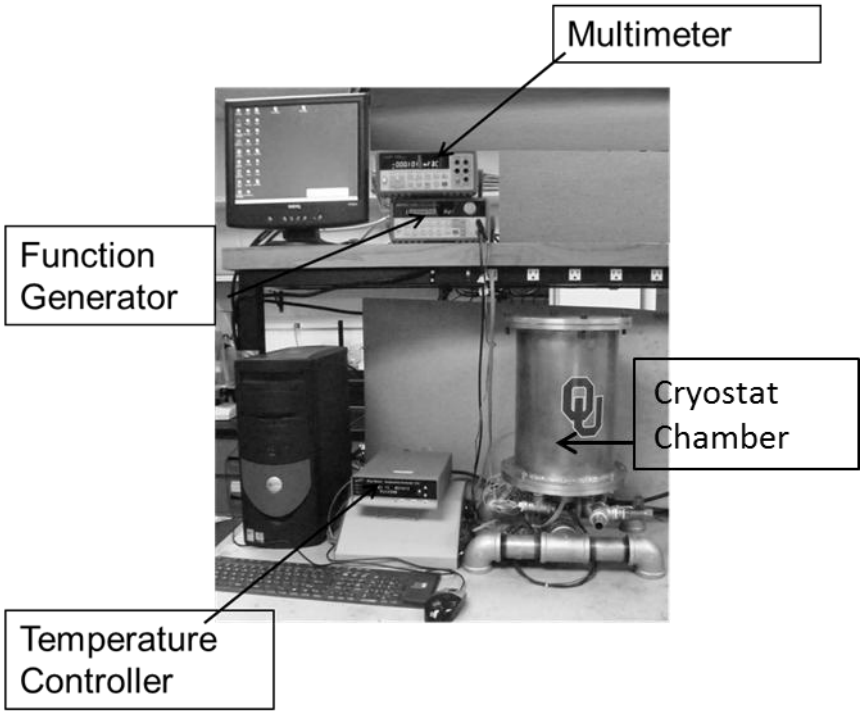

Figure 22 Picture of 3ω measurement system for measuring bulk materials.

During the measurement, the function generator supplied the driven signal in the frequency of ω to the platinum wire or to the carbon fiber filament through the analog data cables. The function generator is an arbitrary waveform generator of model HP 3312A purchased from Hewlett-Packard Company. The function generator is able to generate sine, triangle, ramp and square wave form outputs up to 15 MHz with amplitude of 50 m Vpp dc output. Before the signal reached the sample section, it goes through a Wheatstone cancelling circuit with two bridges to balance out the background signal and the noise (Figure 21). A potentiometer series are utilized for this by adjusting its electrical resistant as close to the electrical resistant of the sample section as possible. This potentiometer series contain two potentiometers: a coarse linear potentiometer with range from 0 to 5000 Ω that was controlled manually during the measurement and a potentiometer with fine step ranging from 0 to 500 Ω with step resolution of about 0.5 Ω that was controlled with the help of a step programmed motor during the measurement. When a sample assembly with low electrical resistance is tested, the coarse potentiometer is manually adjusted to zero Ω and only the fine potentiometer is used to balance the Wheatstone Bridge controlled with a LabVIEW program which will be discussed in detail later. When a sample assembly with electrical resistance higher than 500 Ω is tested, the coarse potentiometer is manually adjusted to roughly match the resistance of the specimen and then the fine potentiometer is used to balance the Wheatstone Bridge.

The multimeter in the system is a digital multimeter with limit of 1000 volts and resolution of 6-1/2 digits that can transport analog result through GPIB cable (Agilent 34401A, Agilent Technologies, Inc). The voltage and the current across the sample

assembly are measured with this multimeter. Electrical resistance of the sample assembly is also calculated with the voltage and the current.

The last important component in the 3ω circuit is a virtual lock-in amplifier. In this study, a LabVIEW programmed data acquisition system is used to both acquire and digitally filter voltage signals while remotely control the power supply. The system consists of two data acquisition cards (M-PCI6254, National Instrument) and the data acquisition cables (GPIB-USB-B, National Instrument). The 3ω response of the sample assembly is locked-in through wave form analysis modules along with the LabVIEW7.0. The program is also used to supervise the temperature controller for the cryostat chamber used for temperature-thermal conductivity study. The cryostat chamber is made of aluminum with sealing for vacuum level up to 29 inHg and two ventilation holes that for connection to vacuum pump and for electric wires for electrical components inside. Inside the chamber, heat cable is tired around a pole that support the specimen stage, where there are 4 poles to connect the lead wire of the sample assembly (Figure 23). The heat cable was monitored by a temperature controller of model EW-89000 from Digi-Sense with a thermocouple located right under the specimen stage. The temperature setting of the temperature controller is controlled by a PC through a USB converter cable (U232-P9, Magic Control Technology Corp.) with aforementioned LabVIEW program according to the user's setting at the beginning of the test.

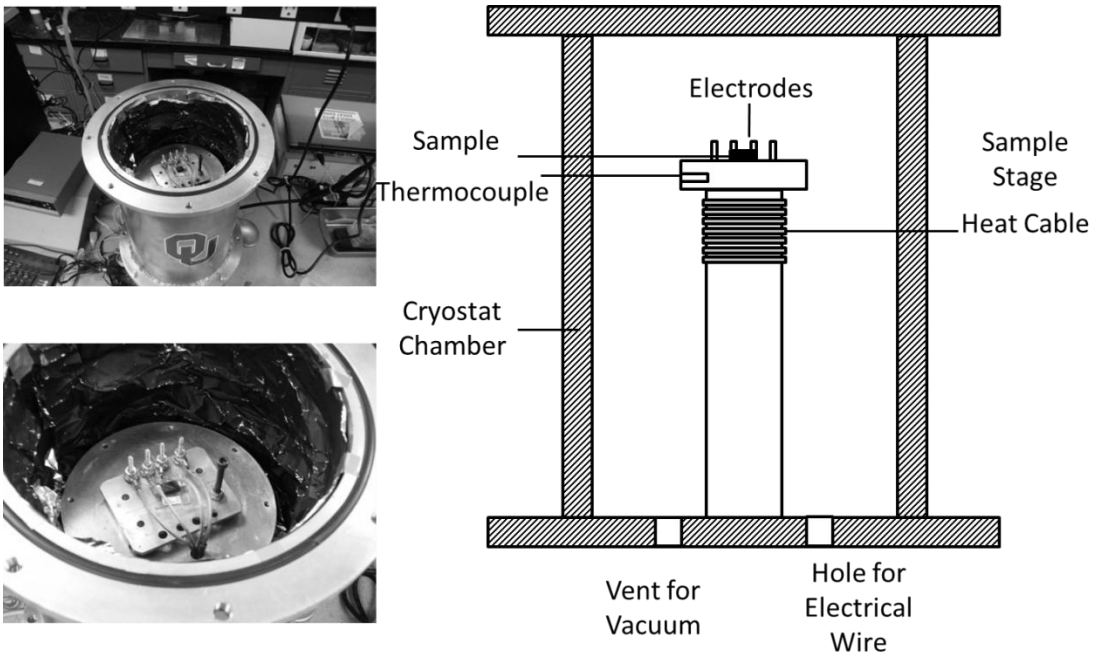

Figure 23 The computer-monitored cryostat chamber. Top left: outer view. Bottom left inner view. Right: Schematic of the computer-monitored cryostat chamber.

For the measurement of the longitudinal thermal conductivity of the fiber filament, a smaller cryostat chamber is manufactured. This Cryostat can be vacuumed inside up to 500 mini-torr with the help of a high-vacuum pump (HVP6, Uniweld Product, Inc). The level of vacuum was investigated with a high sensitive vacuum gauge (20011 Stinger, InstruTech, Inc), which can measure vacuum level up to 1.0×10^{-4} Torr (Figure 24 (a)). A radiation heat shield made of silicate rubber and aluminum foil is also used to cover the sample assembly during the measurement. For the measurement of the transverse thermal conductivity of the fiber filament, a water reservoir made of silicate rubber was put on the specimen stage (Figure 24 (b)).

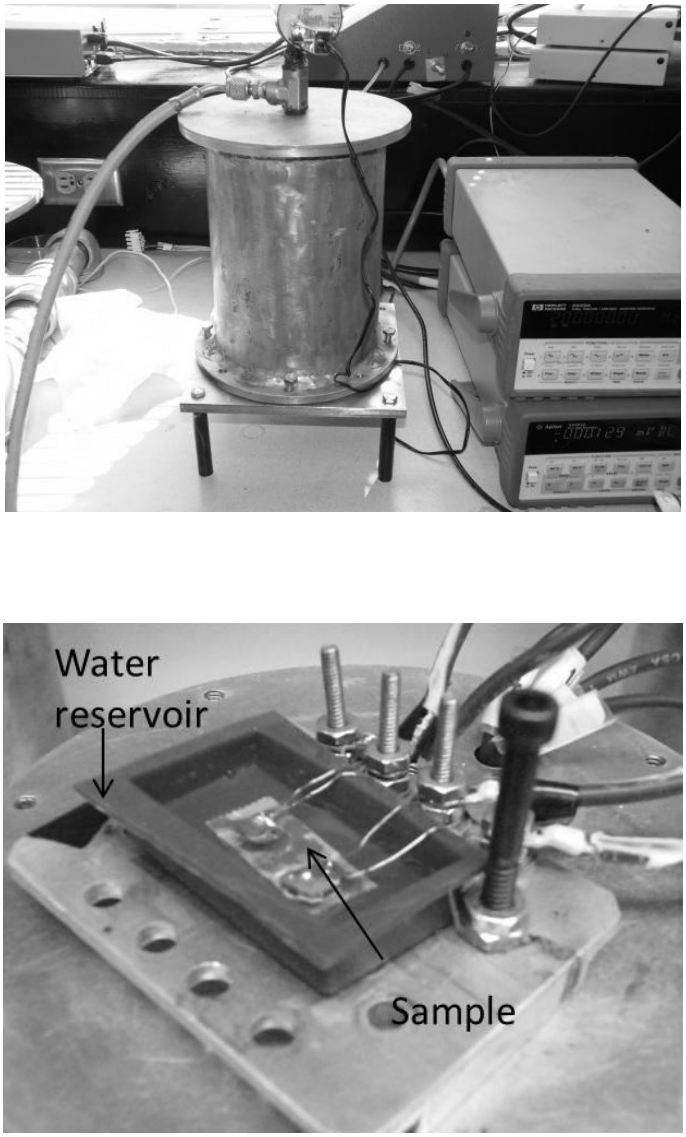

Figure 24 (a) The vacuum chamber cryostat chamber for measuring longitudinal thermal conductivity of an individual fiber. (b) A silicate rubber water reservoir for measuring transverse thermal conductivity of an individual fiber.

3.4.2 Parameters Setting and Measurement Procedure

For the carbon fiber composites, each sample was tested at 20 logarithmically spaced frequency points covering the range 1-4 Hz. For the validation sample such as Pyrex7740

and epoxy, and for individual fiber filaments since there is no need to pre-coat the specimen with SOG, thus a broader frequency range was used (10-200 Hz), and the number of frequency points is chosen as 50. At least 500,000 instantaneous data points were collected to determine the magnitude and phase of the signal at each frequency.

For composites, the driven voltage was set to be 3V. The composites sample temperature in the cryostat chamber was allowed to stabilize to within 0.1 ℃ of the set value before sampling begin by putting it into a cryostat chamber. For each temperature point, it took about half an hour for the temperature to stabilize, and then it took about another 2 minutes to measure the 3ω response. For most of the composites samples, four temperature points were tested: 25 ℃, 50 ℃, 75 ℃, and 100 ℃. Although the temperature coefficient of resistance is known for platinum, to eliminate the errors introduce through variation of the platinum wire; such coefficient was measured through the test by calculating the slope of the temperature-resistance curve of the platinum wire.

For an individual fiber filament, especially for measuring the thermal conductivity in longitudinal direction, since the fiber was suspended in a vacuum environment as the heater, to avoid overheating the fiber, the driven voltage was set to be 1V. The unknown temperature coefficients of resistance were measured separately by a four point resistance measurement method inside a temperature-monitored oven (Stabletemp oven, Cole-Parmer). The resistance of each specimen was measured at several temperature points at a step of 2 ℃ from 20 ℃ to 30 ℃ and then linear regression was used to calculate the temperature coefficient of resistance. At each temperature, the specimen was maintained for 30 minutes to stabilize. A DC voltage ranging from 1.1V to 2.3V was applied to the specimen with the help of a potentiometer. The voltage and the current over the fiber was

then measured by two separate digital multimeters (Agilent 34401A, Agilent Technologies). All the specimens were found to be ohmic over the entire temperature range. Electrical resistances of the specimens were then obtained by calculating the slope of the voltage-current curves. The temperature coefficient ρ'_e was calculated from the following equation:

$$R(T) = R(T_0)(1 + \rho'_e T) \tag{3.1}$$

where R is resistance and T_0 is the reference temperature that is chosen to be 20 ℃.

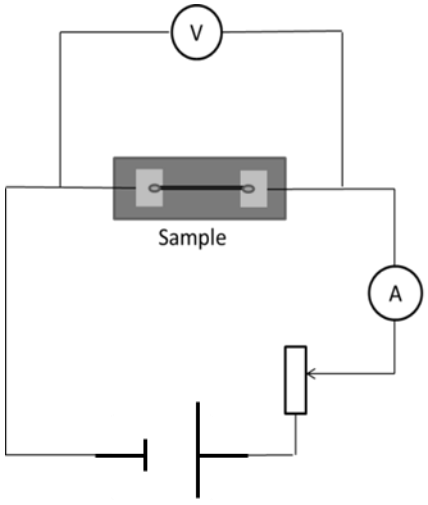

Figure 25 Schematic of the measurement of temperature coefficient of resistance using a four-probe method.

To measure the transverse thermal conductivities of individual fiber filaments, the specimen was carefully put into a water reservoir without breaking the fiber specimen and bringing in bubbles. The electrical resistance of the sample assembly was measured before and after putting into the reservoir to ensure that there was no electric leakage. In temperature study, a thermocouple was also submerged into the reservoir and kept as close to the fiber specimen as possible. Similar to measuring longitudinal thermal conductivity for an individual fiber, temperature coefficient also need to be measured to calculate the transverse thermal conductivity of the fiber. Since temperature coefficient does not depend on material geometry, for the same type of material, the same value was used for both transverse thermal conductivity measurement and longitudinal thermal conductivity measurement.

The length of the platinum wire used for measuring the thermal conductivity of composites and the length of the individual fibers were determined using a stereo microscope (3601, Accu-Scope Inc.). A picture was taken for each sample under the microscope and the length was calculated with the pixels of the specimen in the image and the pixel/length ratio obtained from an image of reference with known dimension under the same magnitude as that used for the specimen. In this study, Rhonchi's ruling (Edmund Optic Inc.) of 0.1 mm /cycle was used as reference scale and a free software Imagj was used for the digital image processing to determine the length of the specimen from its image.

After the 3ω response of the specimen, the temperature coefficient of the heater/ specimen, and the length of the heater/specimen were measured, a MatLab coded programmed was then used to determine the thermal properties of the specimen through

searching for optimal thermal properties that minimizes the difference between experimental result and the theoretical solution according to the theories presented in chapter 2. In the program, the algorithm to achieve the optimization is a gradient-based method called trust-region-reflective algorithm, which has been built in MatLab function "fmincon". Detail of the algorithm is out of the scope of this dissertation and can be found in [56] and [57].

Chapter 4 Results and Discussion

4.1 Introduction

In this chapter, results of measuring thermal conductivities of carbon fibers, CFRCs with CNFs will be presented as the following sequence. The second section of this chapter gives the general validation of the 3ω method and the experimental setup. Two types of standard materials were used for validation: Pyrex 7740 and Epon862 epoxy. In the third section of this chapter, the results of carbon fiber epoxy composite with CNFs filled into the epoxy will be presented first, which will serves as a comparison for studying hierarchical CFRCs. Consequently, thermal conductivity of CFRCs with CNFs growth will be shown in the fourth section. Similar to Section two, before applying wire-based 3ω method to measure the thermal conductivities for carbon fibers, validation was done to ensure the technique is implementable and the experimental setup is robust. Two types of metal wires, platinum and tungsten were used for the validation purpose. For measurement of thermal conductivity in transverse direction of an individual fiber filament, there is a need to investigate whether the technique and the setup are sensitive to the isotropy of the material. Therefore, metal wires coated with SOG were also measured with the method discussed in 4.5.2.2. The sample will be treated with different types of surface treatment, including: heat treatment and CNFs growth. Also the temperature effect of the correlated carbon fiber has been studied. And the results will be given in section 4.5.3. Finally, discussion and conclusion will be given in section 4.6.

4.2 Validation for Bulk Material Measurement

To evaluate the accuracy of the wire-based 3ω method, Pyrex7740 glass was first utilized for validation. Figure 26 shows the measured thermal conductivity of the

standard material Pyrex 7740 with wire-based 3ω method. The error bars is ±2.5% uncertainty of the measured results. For this material, a large range of numbers of thermal conductivity is reported from different literatures [28, 58, 59]. The data measured with wire-based 3ω fall in the middle of these numbers, and is about 2% different from Cahill's traditional 3ω method. From the experiments on Pyrex 7740 we have verified the validity of the sample preparation process as well as the accuracy of the wire-based 3ω set up.

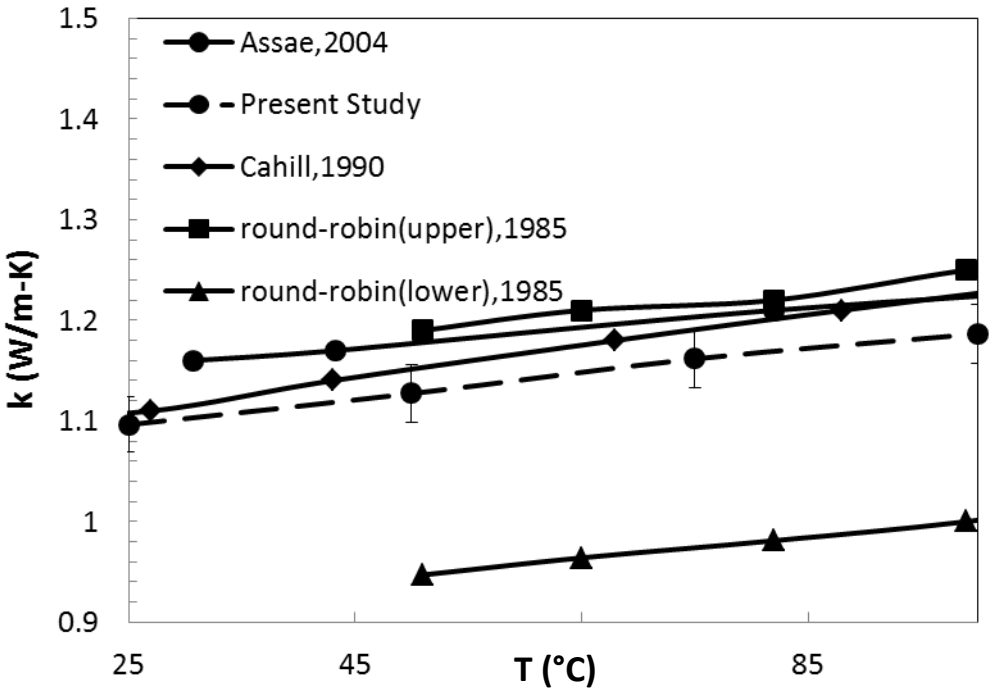

Figure 26 Thermal conductivity of Pyrex7740 from room temperature to 100 ^{o}C.

As discussed in the chapter 2, there are two ways to measure the thermal conductivities of bulk materials using wire-based 3ω method. The first way is to mount

the wire on the surface of the bulk material, and the second way is to embed the wire inside the material before it cures or is formed if it is possible. Epoxy is one of the examples. Although for measuring CFRCs only surface-mounting method is used, for measuring transverse thermal conductivity of an individual carbon fiber, the fiber is submerged into the deionized water, which is in a similar configuration of a platinum heater embedded inside the testing sample. To confirm that this configuration does generate a radial heat flow from the heater to the medium, validation was perform for the wire-embedded method as well. The thermal conductivity of epoxy Epon862 was investigated and compared between using wire-on-surface and wire-embedment methods. Figure 27 shows the thermal conductivities of Epon862 measured from these two methods. It can be seen that, there is only less than 0.5% difference between the results from these two methods. We also compared our measured results with the literature data, which shows a good agreement: there is less than 5% difference for Epon862 (Figure 27). This confirms that by embedding the heater inside medium and using the present configuration, a radial heat flow is generated as expected.

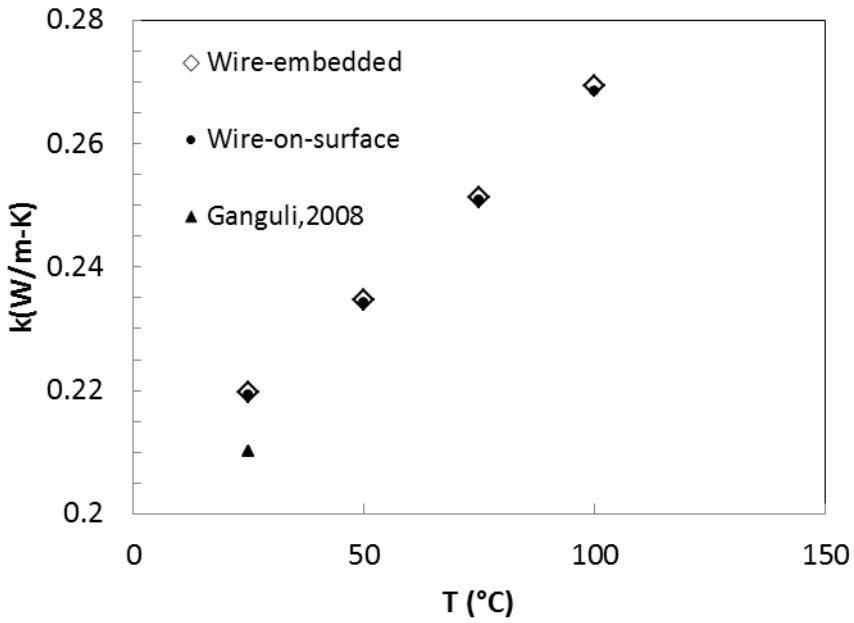

Figure 27 Thermal conductivity of Epon 862 epoxy measured with wired-based 3ω method.

The last set of validation for bulk material measurement is to confirm that SOG coating technique is able to achieve the goal of measuring thermal conductivity of carbon fiber composites. For this, the thermal conductivities of neat laminated CFRCs measured in this study are compared with existed thermal conductivity data of similar composites. The composites in this work are fabricated with T650/Epon 862 system with volume faction about 60% comparing to the reference composites fabricated with F263/Mia100 system with volume faction about 61% [4]. Figure 28 shows the comparison of the data of present study and that reported in the literature in both in-plane and through-thickness direction. The error bars are the standard deviation of 5 tests. Our results agree favorably with the literature value at room temperature.

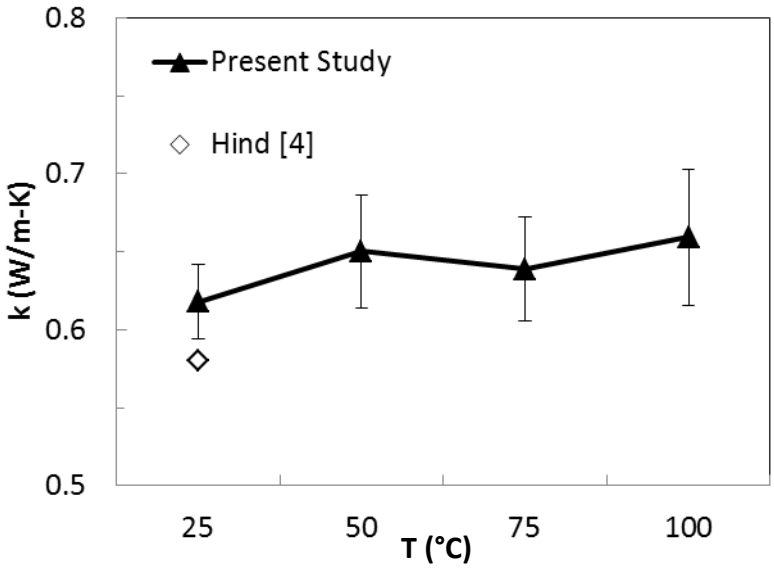

(a)

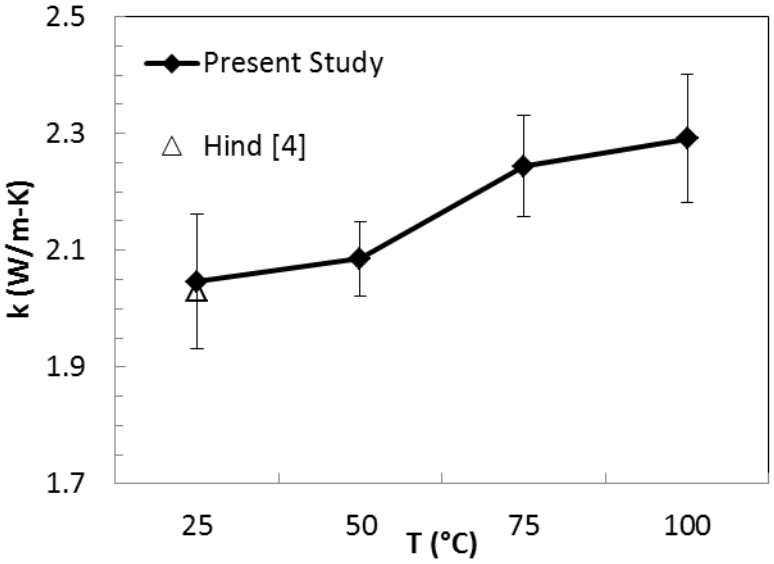

(b)

Figure 28 Comparison of thermal conductivity of laminated carbon fiber epoxy composites between present study and literature data: (a) through-thickness direction and (b) in-plane direction.

In summary, the present experimental setup and wire-based 3ω method are reliable and robust to measure the thermal conductivity of CFRCs and thus ready to be applied to measure the thermal conductivities of hierarchical CFRCs.

4.3 Thermal Conductivities of Hybrid Carbon Fiber Reinforced Composites

In this section, thermal conductivities of hybrid CFRCs are presented. The purpose of investigating this type of carbon composites is that: through comparison between hybrid CFRCs and hierarchical CFRCs, whether hierarchical CFRCs is a better option to utilize CNFs to enhance the through-thickness thermal conductivity can be determined. During the process of fabrication of hybrid CFRCs, sonication was used to help the dispersion of the CNFs into the epoxy. The effect of sonication was also investigated here by measuring the thermal conductivity of neat CFRCs with sonicated epoxy. Lastly, the effect of a typical surface treatment for CNFs, oxidation, was also investigated. For different types of composites, at least five samples were measured in both through-thickness and in-plane direction at four temperature points, 25 ℃, 50 ℃, 75 ℃ and 100 ℃.

4.3.1 In-Plane Thermal Conductivities

The results of in-plane thermal conductivities of hybrid CFRCs measured with 3ω method are shown in Figure 29. Despite the slightly larger deviation comparing to through-thickness thermal conductivity, analysis of variation (ANOVA) of the data shows that the F-value is 1.33, much lower than the F_{crit} of 2.31. Therefore the in-plane thermal conductivities of all eight types of CFRCs are almost identical to each other in term of average values over five samples, which indicates that, the filled CNFs do not have effect on the thermal conductivity in in-plane direction. This obviously is due to the

dominating heat path formed by the carbon fabric in the composites. The typical value of CNF-epoxy composites is between 0.2-0.4 W/m-K [60]. Comparing to the in-plane thermal conductivity of carbon fabric (14 W/m-K), this number is relatively small; therefore the CNFs do not have significant effect in the in-plane direction for CFRC. A closer look at all the in-plane thermal conductivities at room temperature of all eight types of hybrid CFRCs have been tested is given in Figure 29.

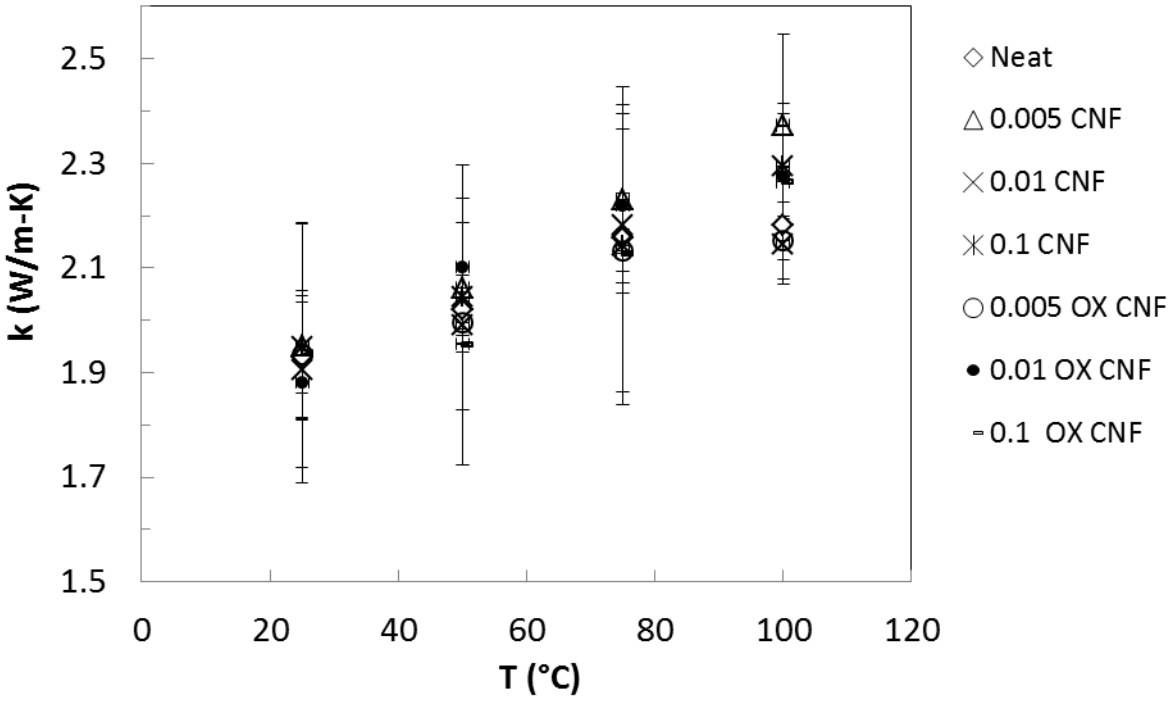

Figure 29 In-plane thermal conductivities of hybrid CFRCs with different CNF loading. The error bars are the standard deviation of five specimens.

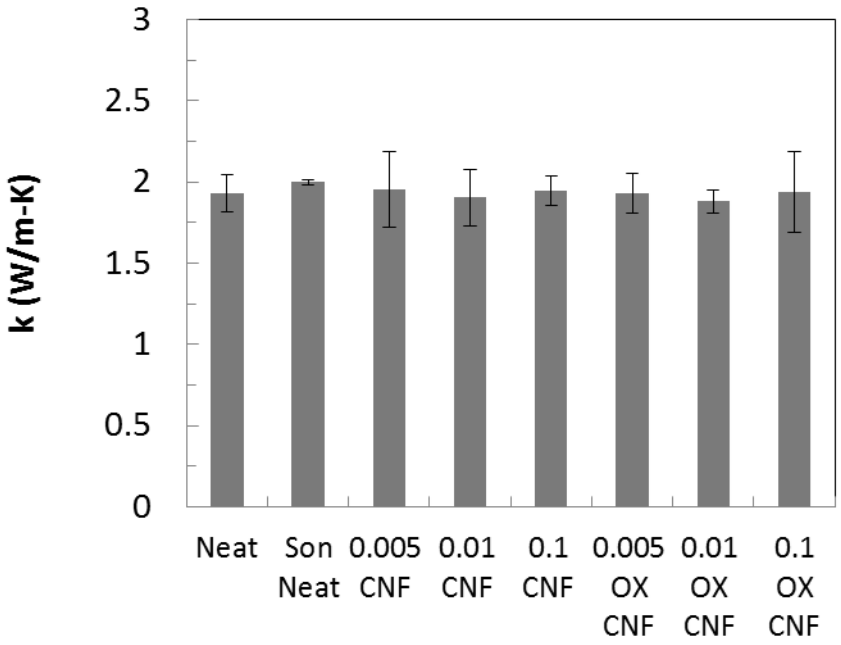

Figure 30 In-plane thermal conductivities of hybrid CFRCs with different CNF loading at room temperature. The error bars are the standard deviation of five specimens.

4.3.2 Through-Thickness Thermal Conductivities

Figure 31 shows the through-thickness thermal conductivities of neat CFRCs and CFRCs fabricated with epoxy sonicated for 2 hours. At room temperature the through thickness thermal conductivity of CFRC with sonicated epoxy in average is about 3% lower than the neat CFRCs. But this small discrepancy is even smaller than the standard deviation of the values of both types of CFRCs. Thus generally speaking, sonication for the epoxy does not affect the through-thickness thermal conductivity of CFRC.

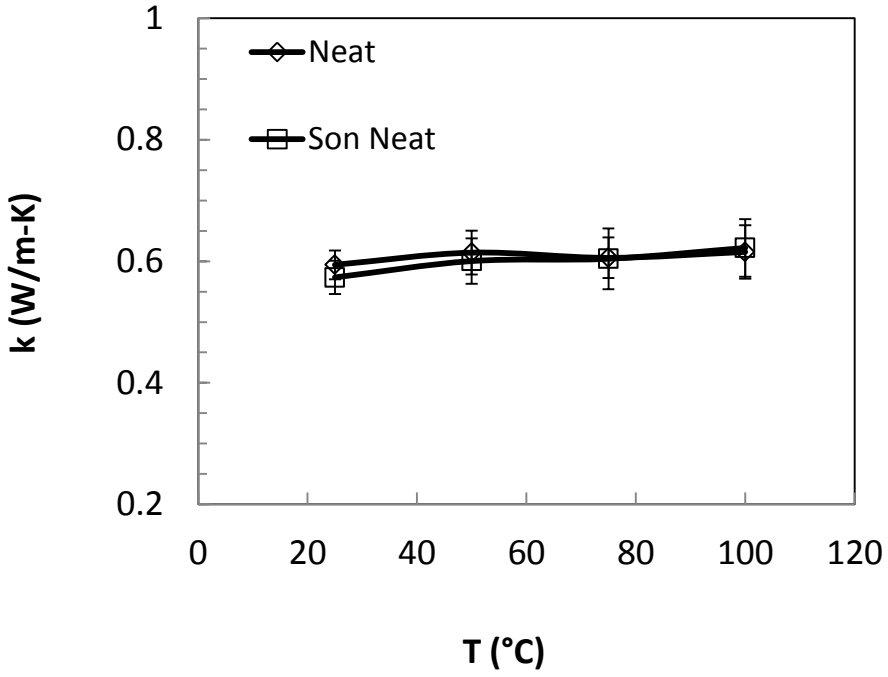

Figure 31 Through-thickness thermal conductivity of neat laminated carbon fabric epoxy composite and neat laminate carbon fabric epoxy composite with sonicated epoxy. The error bars are the standard deviation of five specimens.

Figure 32 shows the through-thickness thermal conductivities of hybrid CFRCs. ANOVA of the data show that F value is 5.75, which is higher than F_{crit} of 2.87. It proves that the incorporated CNFs do improve the through-thickness thermal conductivity of neat CFRCs as expected. With 0.005% CNFs mixed into the epoxy, there is no significant enhancement, but with 0.01% CNFs, the through thickness thermal conductivity is enhanced by about 9.5% at room temperature. However, such enhancement reaches asymptote very fast: with 0.1 CNFs incorporated, there is only 11% enhancement for transverse thermal conductivity. This is probably due to the fact that

after the CNFs forming a connection network in some resin-rich area, accumulating CNFs will not enhance the thermal path anymore. In fact, it has been observed that incorporating more CNFs will diminish the mechanical bonding between the carbon fabric and the epoxy, and hence significant defects such as void, can be induced to the composites. Meanwhile, as discussed in section 1.2, large amount of CNF fillers also can bring in many processing issues such as agglomeration of CNFs during the matrix preparation step and filtration of the CNFs during the VARTM process. Therefore, in this study, we limit the total mass of CNFs to 0.1% of the epoxy.

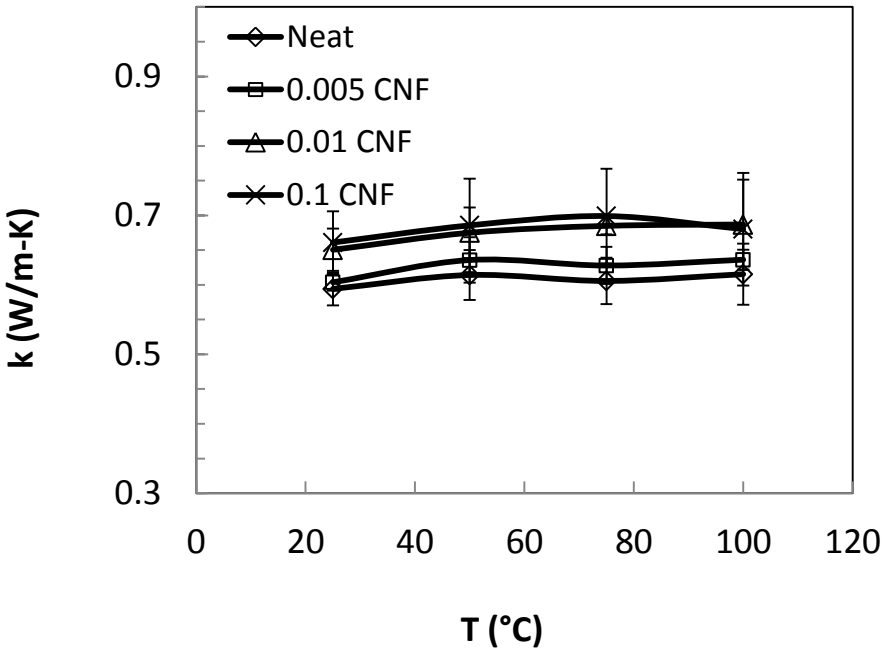

Figure 32 Through-thickness thermal conductivity of laminated carbon fabric epoxy composite filled with CNFs. The error bars are the standard deviation of five specimens.

For CNF as a filler, oxidation is a typical way to enhance the wettability [61] and improve the mechanical interlocking between the CNFs and the matrix [62]. Here, the effect of oxidation of the CNFs on the transverse thermal conductivity of hybrid CFRCs is also investigated. The transverse thermal conductivities of CFRCs reinforced with oxidized CNFs are shown in Figure 33. ANOVA of the data shows that F value is 8.81 higher than the F_{crit} of 3.24, which means that oxidized CNFs do affect the thermal conductivity of the CFRCs. However, unlike pristine CNF, the 0.005% and 0.01% oxidized CNFs in average give 6.6% and 4.7% enhancement of through-thickness thermal conductivity, respectively. The lower enhancement of thermal conductivity stems from the stronger interfacial resistance between the CNFs and the epoxy matrix. The rough surface caused by the oxidization process may strengthen the mechanical interlocking between the CNFs and the cured epoxy, but oxidizing group also creating thermal barrier that makes the phonon boundary scattering more intensive across the CNF-epoxy interface [63]. Thus, drop down of thermal conductivity is observed. When 0.1% oxidized CNFs was added to the epoxy matrix, the final fabricated composites shows a 6.6% drop down of the through-thickness thermal conductivity in room temperature, which indicates that overloading of CNFs not only cause decreasing the mechanical properties, but can also lead to a diminishing of the thermal conductivity of CFRC [64]. The threshold of the amount of CNFs is before 0.1%.

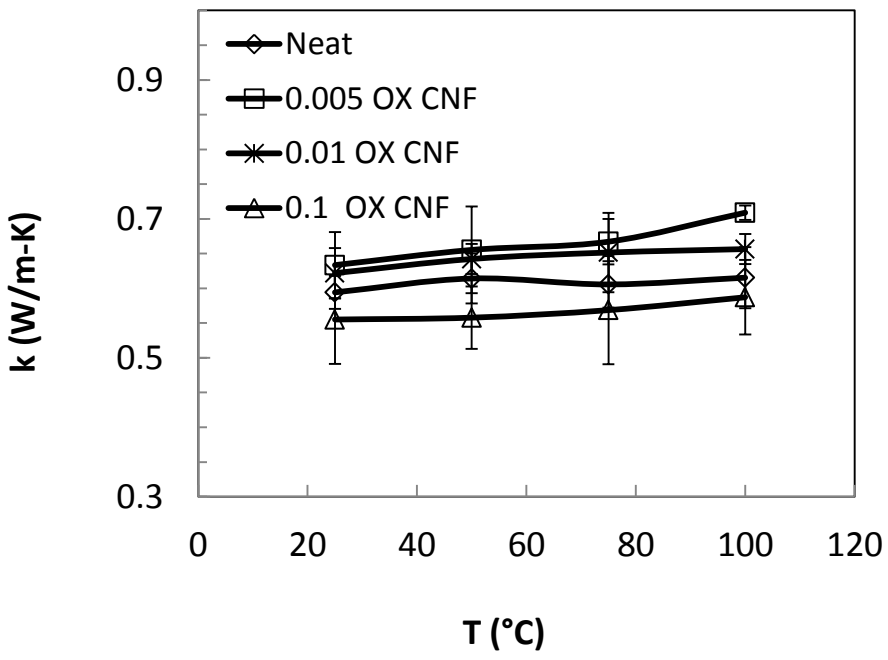

Figure 33 Through-thickness thermal conductivity of laminated carbon fabric epoxy composite filled with oxidized CNFs. The error bars are the standard deviation of five specimens.

A closer look at the through-thickness thermal conductivities at room temperature of all eight types of hybrid CFRCs have been tested is given in Figure 34. Generally speaking, by incorporated CNFs into the epoxy to fabricated hybrid CFRCs, in average only about 2% enhancement of thermal conductivity through-thickness can be achieved due to the limit amount of CNFs that can be used to fabricate the hybrid CFRCs. The enhancement also reaches a plateau very fast and even becomes decrease as the amount of CNFs increases. This is more significant when the CNF was oxidized; the rough surface of the CNF can cause higher thermal interfacial resistance. So it can be concluded

that, filling epoxy with CNF to fabricate hybrid CFRCs is not an effective way to improve the thermal conductivity of CFRC, especially in through-thickness direction.

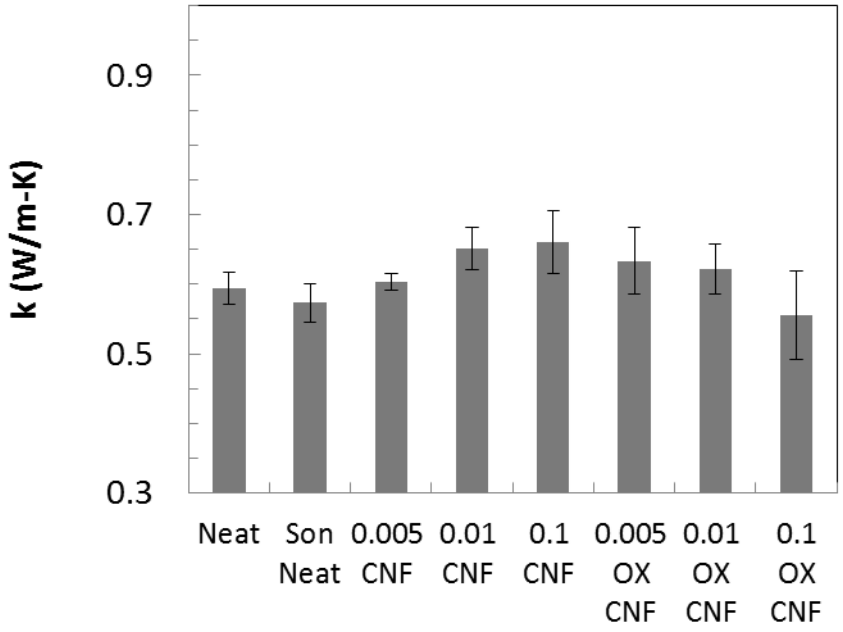

Figure 34 Through-thickness thermal conductivities of hybrid CFRCs with different CNF loading at room temperature. The error bars are the standard deviation of five specimens.

4.4 Thermal Conductivities of Hierarchical Carbon Epoxy Composites

Figure 35 (a) shows the in-plane thermal conductivity of the hierarchical CFRCs with CNFs growth on the surface of carbon fibers. With growth lower than 38 wt%, the change of the thermal conductivities of the composites is less than 5%. But when growth increases to 250 wt% there is about 10% enhancement, and the enhancement increases as temperature increases. The reason for this could be due to the bending of the CNF forest

by the vacuum pressure, thus aligning them in-plane direction. Enhancement of thermal conductivities in the through-thickness direction is much more significant. The largest enhancement is reached with 252 wt% growth where about 33% improvement is shown in Figure 35 (b). With higher growth of CNFs, more CNFs were bridging between the reinforcement and the matrix and thus overcoming the effect of phonon scattering. A closer look at the in-plane and through-thickness thermal conductivities hierarchical CFRCs at room temperature is given in Figure 36.

It can be also seen that, as the temperature increased, the enhancement of thermal conductivity also increases. This can be clearly seen from hierarchical CFRCs with 252% CNFs growth. At 100 ℃, the enhancement for in-plane and through-thickness thermal conductivity is about 38% and 86%, respectively. This can be due to the reduction of thermal interfacial resistance between the CNFs and the matrix as temperature increases [65].

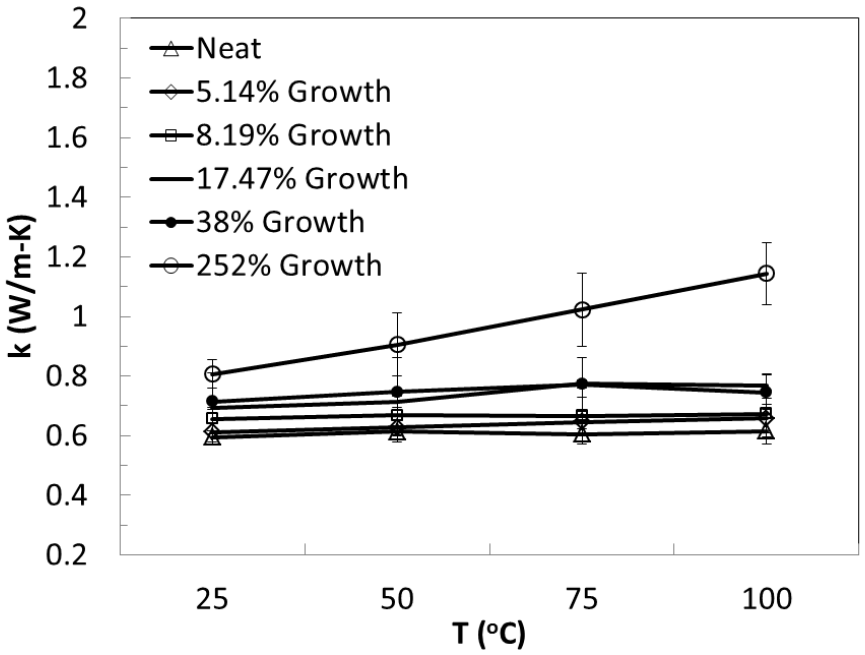

(a)

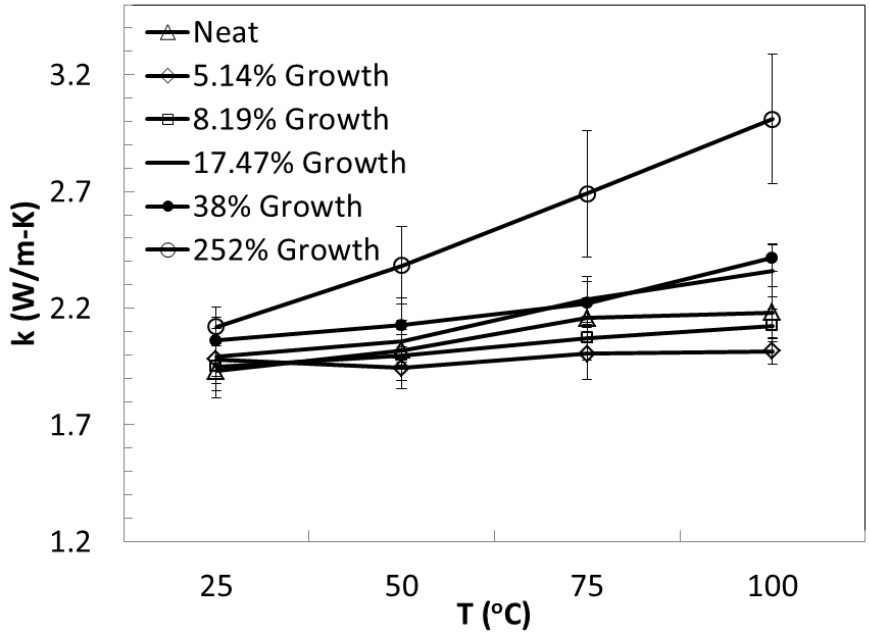

(b)

Figure 35 (a) In-plane thermal conductivity of CNF grown CFRCs at various temperatures. (b) Through-thickness thermal conductivity of CNF grown CFRCs at various temperatures. The error bars are the standard deviations of five specimens.

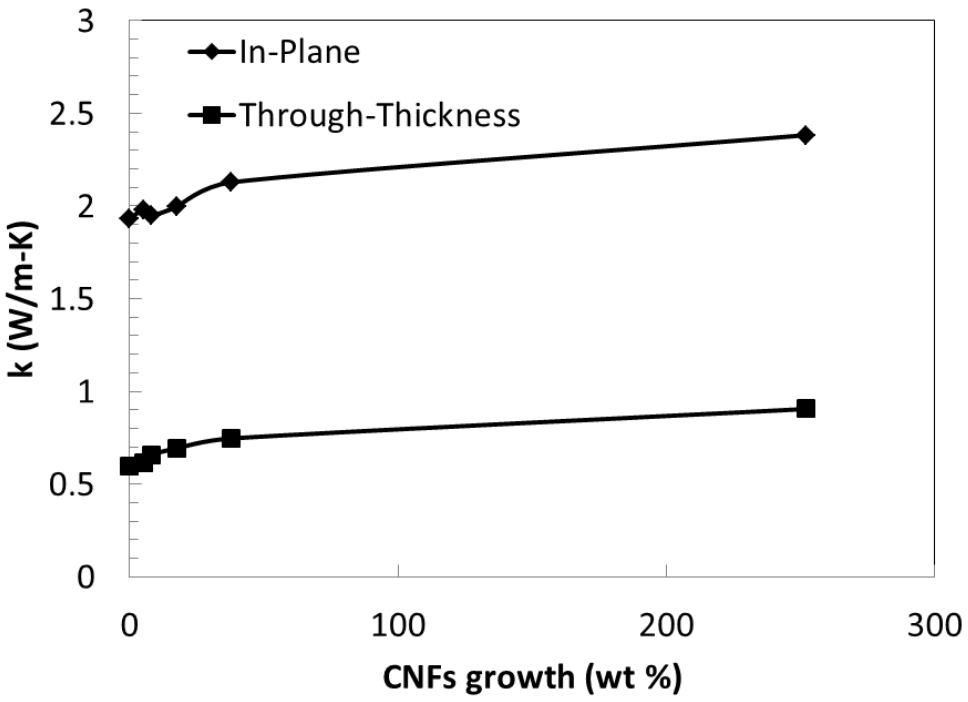

Figure 36 Thermal conductivities of hierarchical CFRCs with different amount of CNFs growth at room temperature.

It is mentioned that the volume fractions of fiber in the composites with CNF growth are in the range from 42-48 wt% whereas the volume fraction of fiber in the neat composite is about 60 wt%. According to the finite element analysis reported in the literature [66] the through-thickness thermal conductivity depends on the volume fraction of fiber in the composite. Since CRFCs with CNFs growth has smaller fiber content the through-thickness thermal conductivity values are corrected for the same fiber content as neat CFRCs (e.g. 60 wt%) using the empirical relationship of the data shown in Figure 37. Figure 38 shows the corrected through-thickness thermal conductivity of CFRCs with CNF growth normalized with the neat CFRCs containing the same carbon content at

room temperature. It can be seen that the through-thickness thermal conductivity of CFRCs with 252 wt% CNF growth is about 9 times higher than the neat CFRCs. Even with modest CNFs growth in the amount of 5 wt% the increase in through-thickness thermal conductivity is about 60%, which is significantly higher than CNF filled CFRCs. Therefore, modification carbon fabric with CNFs growth is more effective to enhance through-thickness thermal conductivity of CFRCs. Considering that CNFs is generally lighter than carbon fiber, introducing CNFs into CFRCs opens new ways to fabricate light weight structure with improved through-thickness thermal conductivity.

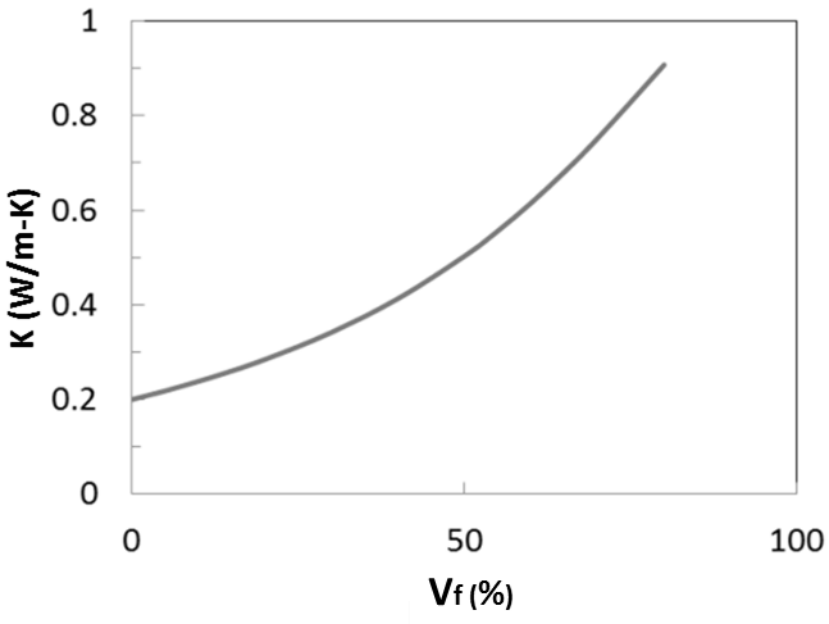

Figure 37 Predicted through-thickness thermal conductivity of CFRCs as a function of volume fraction of carbon fiber [66].

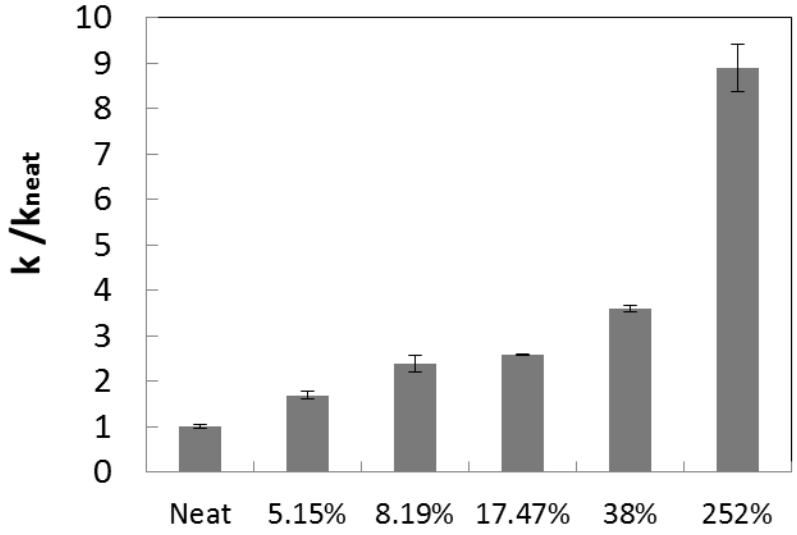

Figure 38 Normalized through-thickness thermal conductivities of CFRCs with CNFs growth containing 60% fiber content at room temperature. The vertical axis represents thermal conductivity normalized by the thermal conductivity of neat composites. The percentages indicate the growth in weight percent. The error bars are the standard deviations of five specimens.

4.5 Thermal Conductivities of Individual Carbon Fibers

4.5.1 Validation for Measuring the Longitudinal Thermal Conductivities for Individual Carbon fibers

4.5.1.1 Validation with metal wires

To evaluate the accuracy of the 3ω method and the experiment setup for measuring individual carbon fiber filament in longitudinal direction, a platinum wire of 10 μm

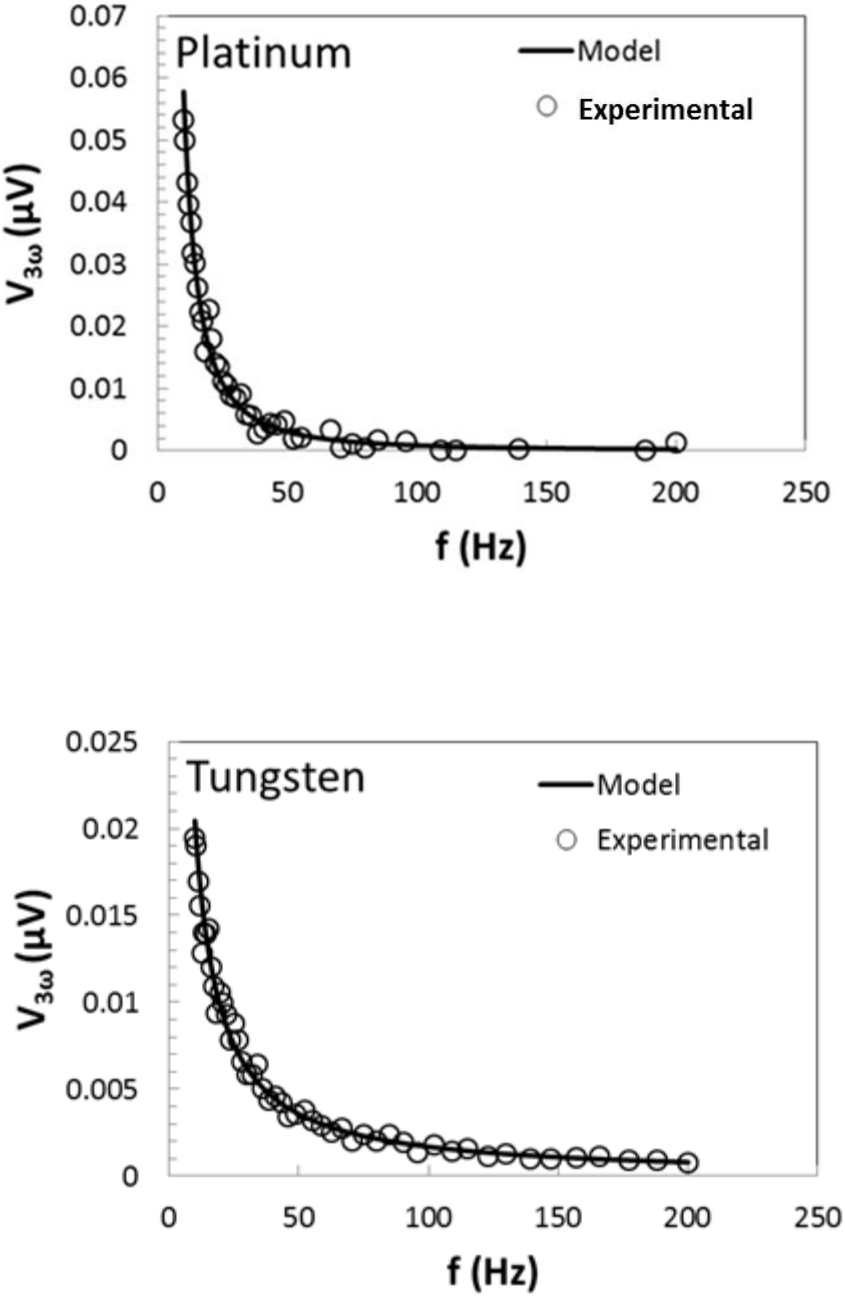

Figure 39 Typical data for measuring longitudinal thermal conductivity of an individual fiber: amplitude of real part of experimental and theoretical 3ω voltage as function of frequency of metal wires.

diameter with length about 8mm and a tungsten wire of 25 μm diameter with length about 3 mm were first utilized for validation. Figure 39 illustrates a typical plot of 3ω signal of the platinum wire and tungsten wire as a function of applied frequency. The results of validation measurement are shown in **Error! Not a valid bookmark self-reference.**, where the standard deviation of five measurements for each sample is also listed. The temperature coefficients, the thermal conductivities and the heat capacities of platinum and tungsten measured in present study agree well with the reported data in literature.

Table 1 Temperature coefficients, thermal conductivities and heat capacities of the standard materials

Material	ρ_e' (1/^{o}C)		k (W/m -K)		ρC (MJ/m^3 -K)	
	Measured	Reference [67]	Measured	Reference [68]	Measured	Reference [68]
Platinum	0.0039 ±0.0003	0.0039	69.1 ±4.2	71.6	2.61 ±0.12	2.79
Tungsten	0.0043 ±0.0002	0.0045	165.8 ±8.8	173.0	2.69 ±0.06	2.50

4.5.1.2 Validation with commercial carbon fibers

Two commercial carbon fibers with known longitudinal thermal conductivities were used for validation. The dimension of the carbon fiber specimens are listed in Table 2 Figure 40 illustrates a typical plot of 3ω signal of the carbon fiber AS4 and IM10 as a function of applied frequency. Table 3 summarizes the temperature coefficients of resistance and the thermal conductivities of different types of carbon fibers. The average and standard deviation are shown based on testing of at least five measurements for each sample. Similar to metal wire, the measured longitudinal thermal conductivities of carbon fibers also agree favorably with the material information reported from the vender

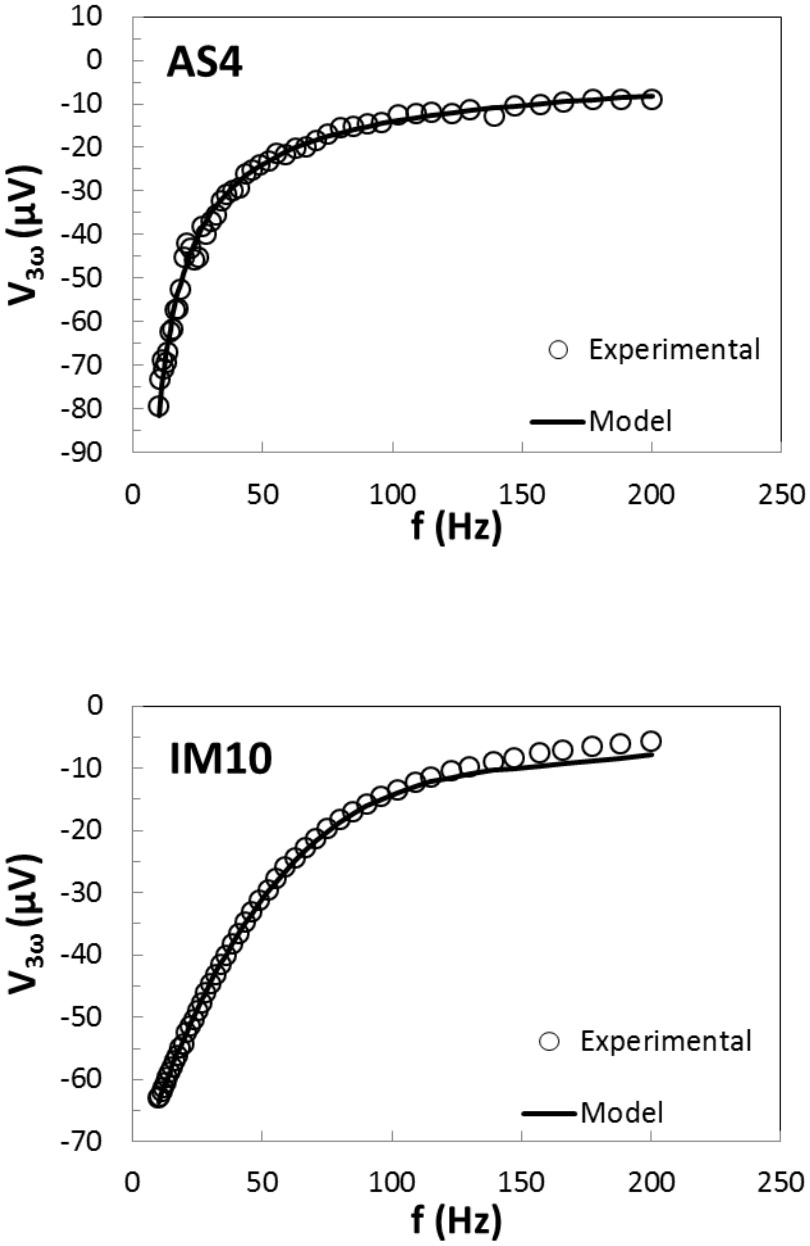

Figure 40 Amplitude of real part of experimental and theoretical 3ω voltage as function of frequency of carbon fibers.

Table 2 Dimensions of the validation materials for measuring longitudinal thermal conductivities

Test Material	Diameter (μm)	Length (mm)
AS4	7.1±0.4	1.50±0.08
IM10	4.4±0.2	1.43±0.07

Table 3 Temperature coefficients of resistance, thermal conductivities and heat capacities of different types of commercial carbon fibers

Carbon Fiber Type	Measured ρ_e' (10^{-4}/℃)	Measured k (W/m-K)	Reference k (W/m-K)	Measured ρC (MJ/m^3-K)	Reference ρC (MJ/m^3-K)
AS4	-4.60±0.3	6.5±0.2	6.8[69]	1.99±0.01	2.02[69]
IM10	-4.20±0.4	6.9±0.4	6.14[70]	1.49±0.06	1.57[70]

4.5.2 Validation for Measuring the Transverse Thermal Conductivities for Individual Carbon Fibers

4.5.2.1 Validation of the measurement technique

In order to assess the validity of the 3ω measurement technique for measuring transverse thermal conductivity of individual fiber filament, two types of standard materials (platinum and tungsten wires) were tested (Table 4). Figure 41 shows typical curve fittings of the analytical expression of 3ω (Equation (2.101)) and experimental data for platinum and tungsten wire specimens. The measured transverse thermal conductivity and heat capacity are shown in Table 5 along with the reference values from the literature. As seen from Table 5 the transverse thermal conductivities of the wires are very close to the reference values. The difference between the measured and reference values are

within 2.3% and 4.6% for platinum wire and tungsten wire, respectively. It is to be mentioned that the reference values represent the thermal conductivity of bulk platinum and tungsten metals. Since bulk metals generally consist of homogeneous structure it is expected that the metal wires show isotropic behavior as implied in the present results. It should be noted that the heat capacity the test material can also be simultaneously determined during the curve fitting process. The measured heat capacity of the metals also agrees favorably with the published data, showing the accuracy and validity of the measurement technique. The standard deviations for five measurements for each specimen are also listed in Table 5.

Table 4 Dimensions of the reference material for validation of transverse thermal conductivity

Test Material	Diameter (μm)	Length (mm)
Platinum wire	10.1 ±0.1	8.51 ±0.17
Tungsten wire	24.9 ±0.4	13.32 ±0.22

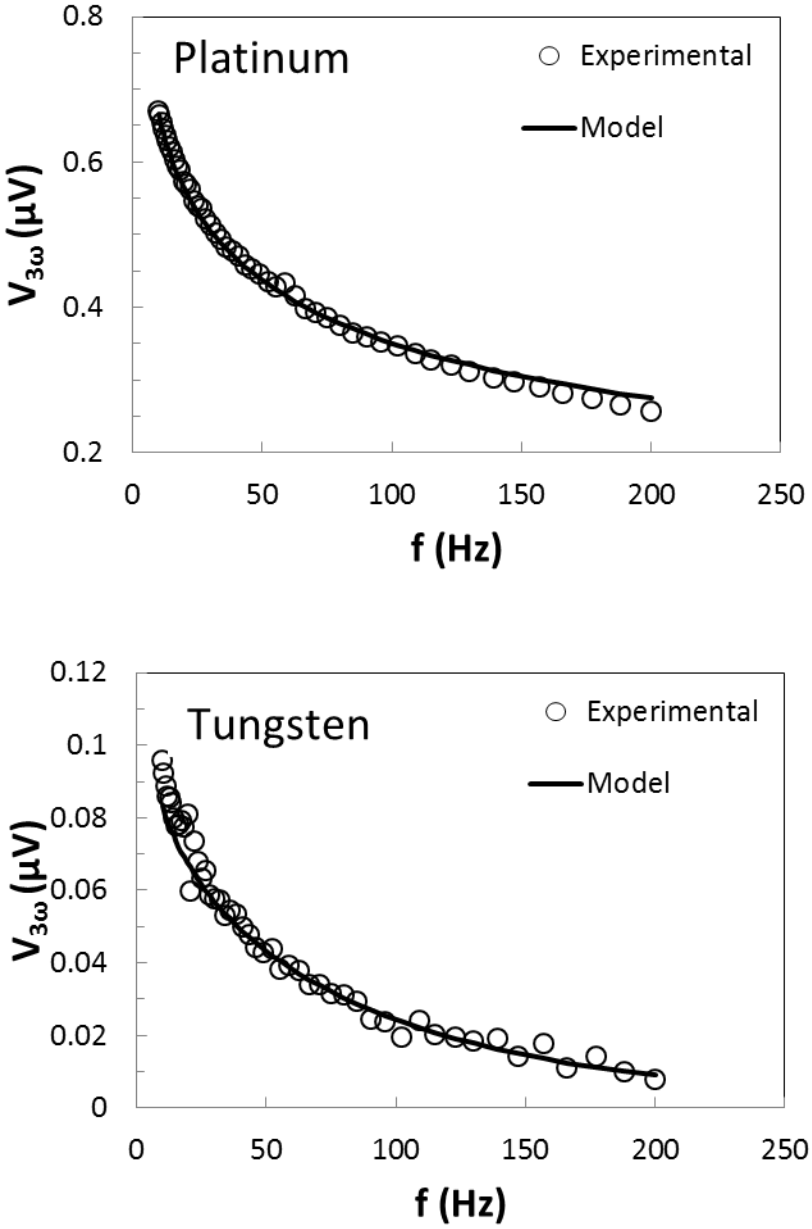

Figure 41 Amplitude of real part of experimental and theoretical 3ω voltage as function of frequency of metal wires.

Table 5 Comparison of the thermal conductivities and heat capacities of the metal wires between the measurement and the reference data

Test Material	k (W/m-K)		ρC (MJ/m^3-K)	
	Measured value	Reference value [68]	Measured value	Reference value [67]
Platinum wire	69.93 ±1.99	71.6	2.88 ±0.06	2.79
Tungsten wire	165.01 ±6.42	173.0	2.76 ±0.11	2.50

4.5.2.2 Validation for sensitivity to anisotropy

To evaluate the sensitivity of the measurement technique to anisotropy, a platinum wire and a tungsten wire were coated with SOG to fabricate wires with anisotropy. The dimensions of the two wires are listed in Table 6. The diameters of the specimens were measured with the help of SEM (Zeiss NEON FEG-SEM, SEMTechSolutions, Company) images, which are shown in Figure 42 and Figure 43.

Table 6 Dimensions of the validation material for sensitivity of anisotropy test

Test Material	Diameter (μm)	Length (mm)	Thickness of SOG coating (μm)
SOG-coated platinum wire	10.9 ±0.2	4.70 ±0.09	0.4 ±0.09
SOG-coated tungsten wire	26.1 ±0.1	28.27 ±0.43	0.6 ±0.04

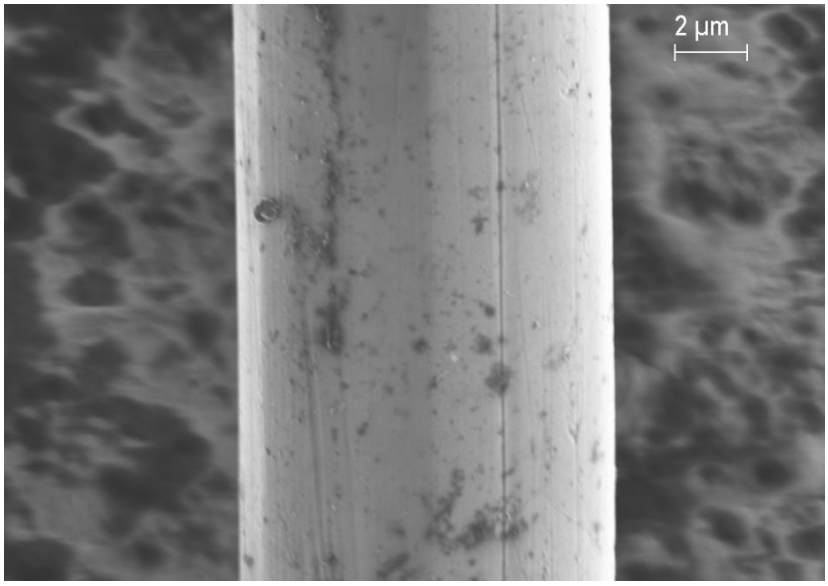

(a)

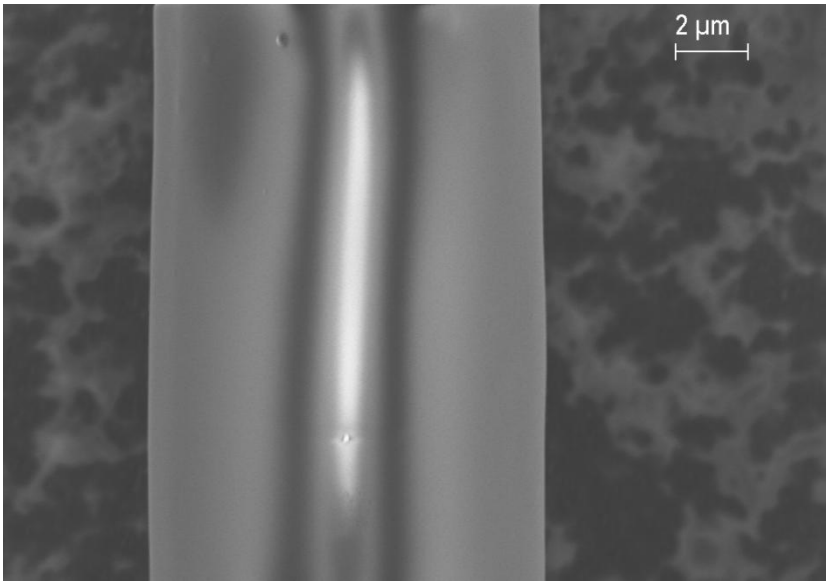

(b)

Figure 42 SEM images of (a) as-received and (b) SOG coated platinum wires.

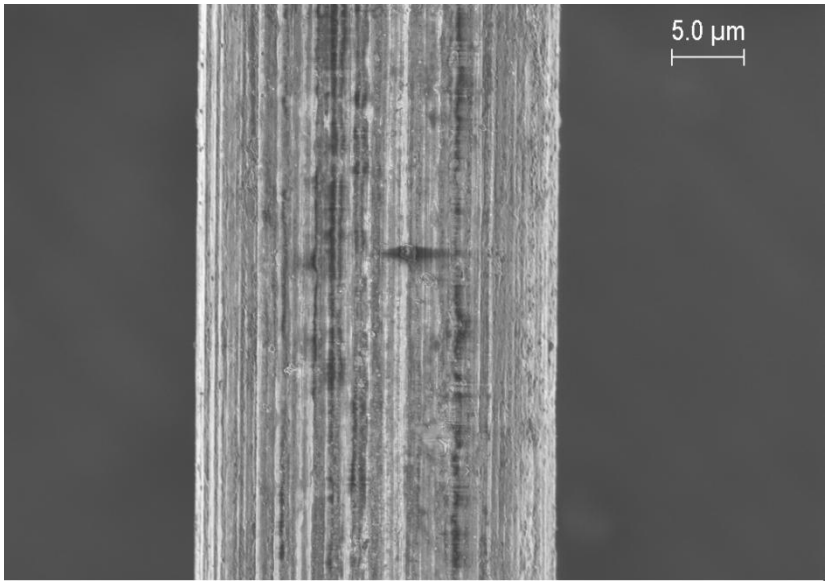

(a)

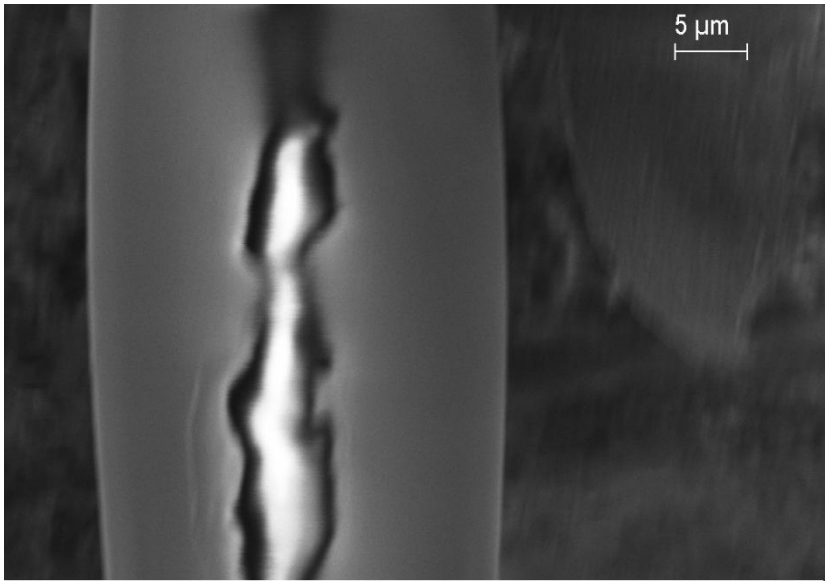

(b)

Figure 43 SEM images of (a) as-received and (b) SOG coated tungsten wires.

Figure 44 shows typical curve fittings of the analytical expression of 3ω and experimental data for platinum and tungsten wire specimens. The thermal conductivity values of the SOG coated metal wires in both directions are listed in Table 7 Since the thermal conductivity of SOG polymer is about 0.25 W/m-K, which is much lower than that of platinum (71.6 W/m-K) and tungsten (173 W/m-K), as expected, the measured thermal conductivity of the SOG coated wires exhibits remarkable anisotropy; the transverse thermal conductivity of the coated fiber are only about 2.7% and 3.3% of the longitudinal thermal conductivity for platinum and tungsten wire, respectively. Along the longitudinal direction, the core material provides the dominant heat transfer, thus the longitudinal thermal conductivities of the metal wires are not affected by the presence of thin SOG coating. However, along the transverse direction, the heat transfer process depends on the type of coating, coating thickness, and interphase. In this case the low thermal conductivity of the SOG leads to dramatically reduction of transverse thermal conductivity of the coated wires.

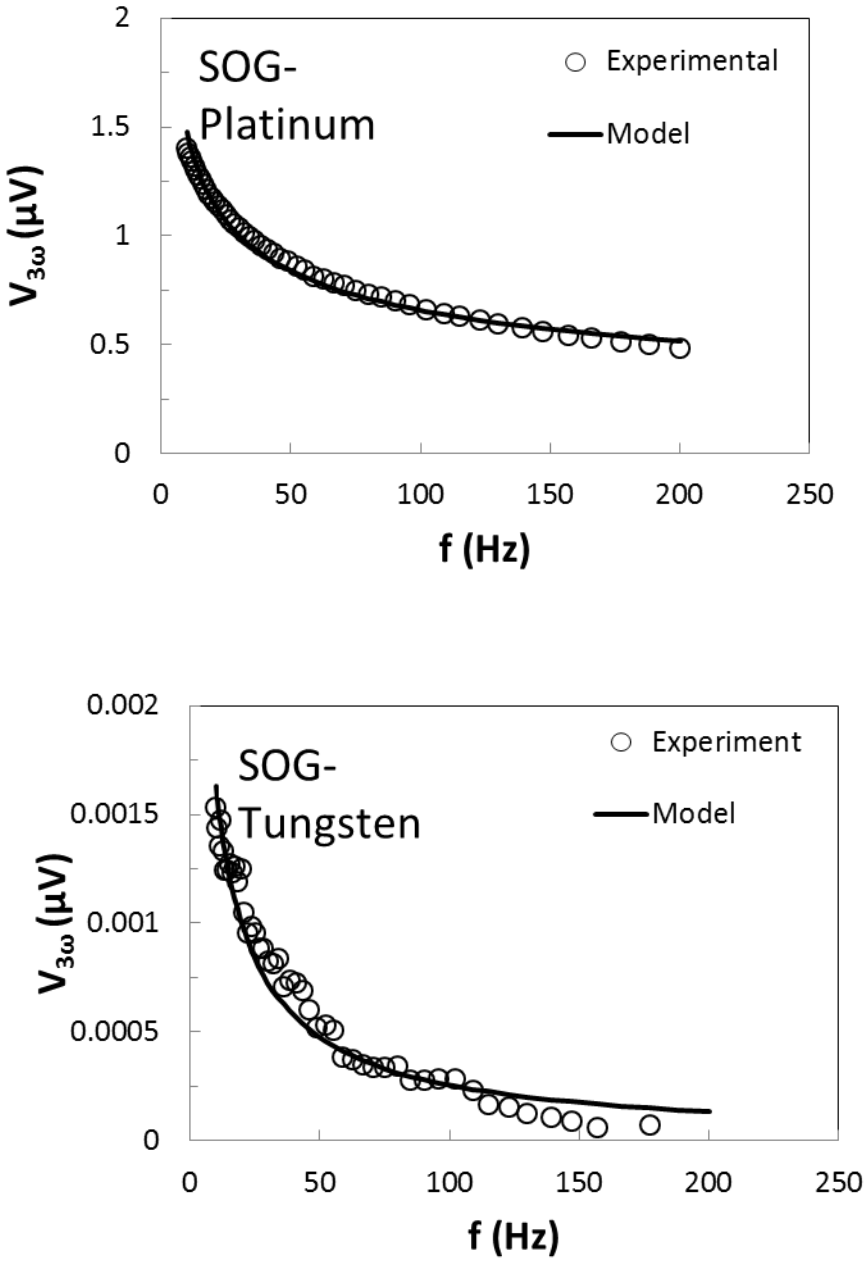

Figure 44 Amplitude of real part of experimental and theoretical 3ω voltage as function of frequency of SOG coated wires.

Table 7 Thermal conductivity of the SOG coated metal wires

Material	Longitudinal Thermal Conductivity (W/m-K)		Transverse Thermal Conductivity (W/m-K)	
	Measured value	Reference value [68]	Measured value	Effective Medium Theory (Equation (4.1))
Platinum wire	74.99 ±2.50	71.6	3.04 ±0.10	5.69
Tungsten wire	165.07 ±8.08	173.0	5.48 ±0.25	11.00

In order to corroborate this finding, a complex fiber model similar to the model proposed by Xue and Xu [71] was developed. The complex fiber is a two-phase fiber system and the effective thermal conductivity of the complex fiber in the transverse direction can be estimated according to the equation:

$$k_t = k_f \frac{k_c + k_f + \alpha(k_c - k_f)}{k_c + k_f - \alpha(k_c - k_f)} \tag{4.1}$$

$$\alpha = \left(\frac{R_f}{R_f + t_c}\right)^2 \tag{4.2}$$

where k_c and k_f are the thermal conductivity of the coating layer and fiber, respectively. R_f is the radius of the fiber and t_c is the thickness of the coating. The detail

derivation will be given in next chapter. In our case, k_f is 71 W/m-K for platinum wire, 173 W/m-K for tungsten wire, and k_c is 0.25 W/m-K for SOG coating. The values of R_f and t_c of the SOG coated wires are given in Table 6. The estimated thermal conductivities of the SOG coated wires are shown in Table 7. The measured transverse thermal conductivity of the SOG-coated platinum wire and tungsten wires both are only about 50% of the estimated value. This could be due to the fact that the SOG coating is not uniform along the wire length. Another more crucial reason that can lead to such a discrepancy is the imperfect interface between the coating layer and the wire. In fact, assuming the thickness of the thermal interface between the imperfect coating and the wire is half of the thickness of the coating, using equation (4.1) and the equation of thermal resistance of a hollow cylinder:

$$R_c = \frac{\ln(b/a)}{2\pi kL} \tag{4.3}$$

The Kapitza resistances of the interface here estimated as 1.74×10^{-6} m^2K/W for SOG-coated platinum and 3.00×10^{-6} m^2K/W for SOG-coated tungsten, which is about ten times of the Kapitza resistance of interface between carbon nanotube and polymer [72]. Obviously, the poor interface significantly decreases the transverse thermal conductivity of the SOG-coated metal wire. Despite the reasonable discrepancy between the estimated and measured values, it can be concluded that the individual fiber measurement technique is very sensitive to the anisotropic heat transfer behavior of the material.

4.5.3 Validation for Measuring Thermal Conductivities of Individual Fibers Under different Temperatures

In order to parallel to the study of thermal conductivity of carbon fiber composites in different temperatures, thermal conductivities of individual fibers were also measured in different temperatures in both longitudinal and transverse directions. Unlike measuring thermal conductivity of bulk material, the directional thermal conductivities need to be measured separately according to the directions. In the longitudinal direction, the specimen was heated up from the bottom through the substrate with a heat pat. The temperature was monitored by attaching a thermocouple to the copper strips as close as the specimen. In the transverse direction, the specimen was heated up indirectly through the deionized water, and the temperature was also monitored through controlling the temperature of the deionized water.

To validate the measurement technique and setup for temperature study, two types of metal wires were used: platinum wire and tungsten wire. The longitudinal and transverse thermal conductivities of these two types of wire under different temperatures measured with 3ω method are shown in Figure 45 and Figure 46 respectively. All the results are based on the measurement from five samples. The error bars in the figure is the standard deviation.

It can be seen that, for both platinum wire and tungsten wire, the thermal conductivity in longitudinal direction and transverse direction consistent with each other although different measurement methods were used for properties in direction

orientations. This agrees with the presumption that the metal wires are isotropic. For platinum, there is a large deviation among literature values in term of the thermal conductivity-temperature relation. However, the present results are between the upper bound and lower bound of these literature data and the different between these two bounds is actually very trivial (about 2% difference). For tungsten wire, the present results agree favorably with the reference data. For both types of wires, the trend of the thermal conductivity over the temperature matches that has been reported in literature: the thermal conductivity of platinum increases while the thermal conductivity of tungsten decreases when the temperature increases in temperature range between 20 ℃ and 60 ℃. And both the changes of thermal conductivity over temperature are very small: for platinum, there is about 4% increase; while for tungsten, there is about 2.5% decrease over the 40 ℃ span.

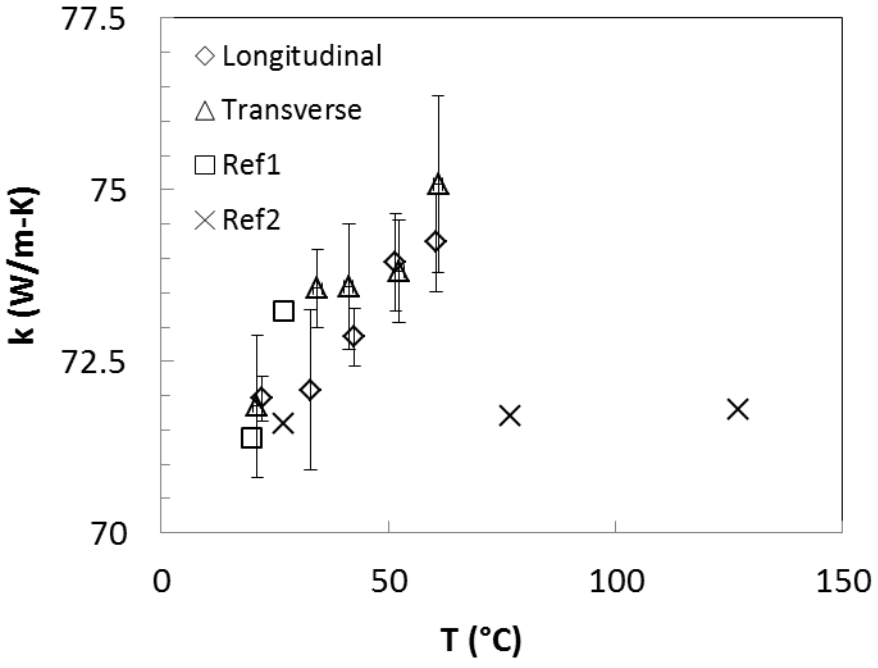

Figure 45 Thermal conductivity of platinum wire in both longitudinal direction and transverse direction. Data from two references are used for comparison, which are labeled as “Ref1” [73] and “Ref2” [74]. The error bars are the standard deviations of five specimens.

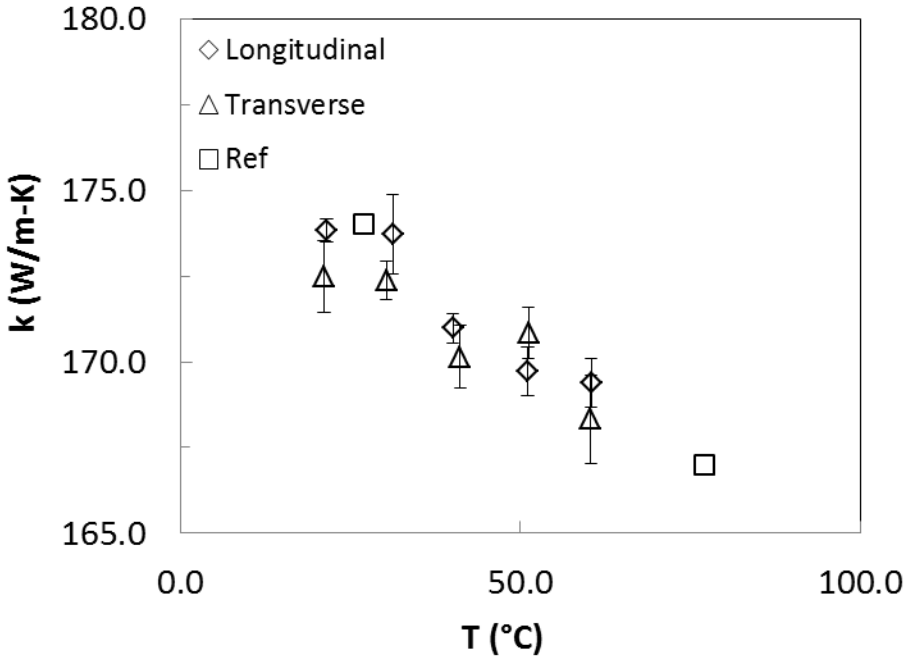

Figure 46 Thermal conductivity of tungsten wire in both longitudinal direction and transverse direction. Data from the reference used for comparison is labeled as “Ref” [75]. The error bars are the standard deviations of five specimens.

4.5.4 Thermal Conductivity of T650 Carbon Fiber

4.5.4.1 Anisotropy of Thermal Conductivity of T650 Carbon Fiber

In this study T650 carbon fabric was used for fabricating hybrid CFRCs and hierarchical CFRCs. Parallel to the composites level study, thermal conductivities of

individual T650 carbon fibers were measured in longitudinal and transverse direction. Figure 48 shows typical curve fitting of the 3ω responses between the experimental results and the theoretical values for longitudinal and transverse thermal conductivity measurement. Table 8 shows the measured thermal conductivities and heat capacity in longitudinal and transverse directions. For comparison, literature values of the thermal conductivities of carbon fibers are also listed in Table 8. It should be noted that the transverse thermal conductivity in the reference is for T300, which is estimated from a carbon fiber composites. Since this is the only transverse thermal conductivity data for such type of PAN-based carbon fiber to the author's knowledge, hence it is listed here for illustration. The standard deviations of 5 samples from different tows are also listed in Table 8.

It can be seen that the thermal conductivities of T650 carbon fiber exhibits significant anisotropy: the transverse thermal conductivity is only about 1/10 of the longitudinal thermal conductivity. This is due to the strong anisotropic structure of the T650 carbon fiber (Figure 47). In PAN-based fibers such as T650, the linear chain structure is transformed to a planar structure during oxidative stabilization and subsequent carbonization. Basal planes oriented along the fiber axis are formed during the carbonization stage. These graphite plane structures have a high axial preferred orientation and thick crystallite stack, which provide continue heat path along the fiber axis direction [76]. On the other hand, in the transverse or radial direction, the layer spacing between the discrete onion-like structures forms micro-barrier damping the heat wave transferring through the fiber [77]. Therefore, significant difference of thermal conductivity is seen between longitudinal direction and transverse direction.

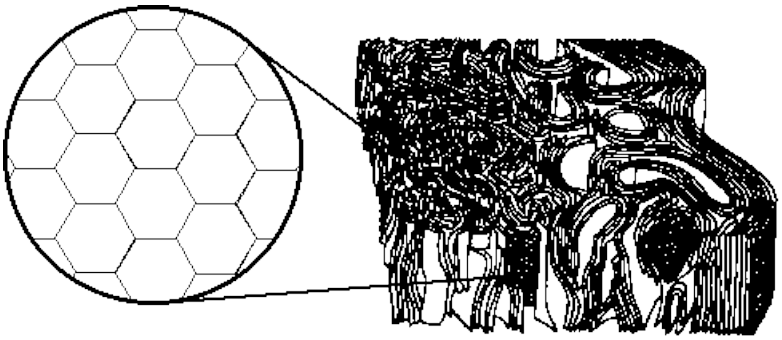

Figure 47 Microstructure of carbon fiber. (Image from http:// www. Chem. Wisc.edu)

Table 8 Measured thermal conductivity and heat capacity of different types of T650 carbon fibers

Direction	Transverse Thermal Conductivity (W/m-K)		Heat Capacity (MJ/m3-K)	
	Measured value	Reference value	Measured value	Reference value
Longitudinal	13.7±0.6	14	1.97±0.20	--
Transverse	1.5±0.2	0.8 [4]	1.92±0.15	--

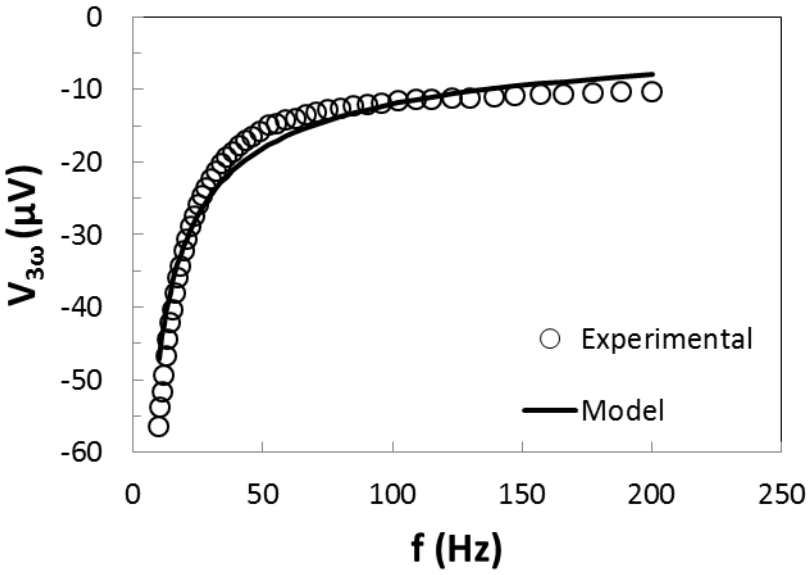

(a)

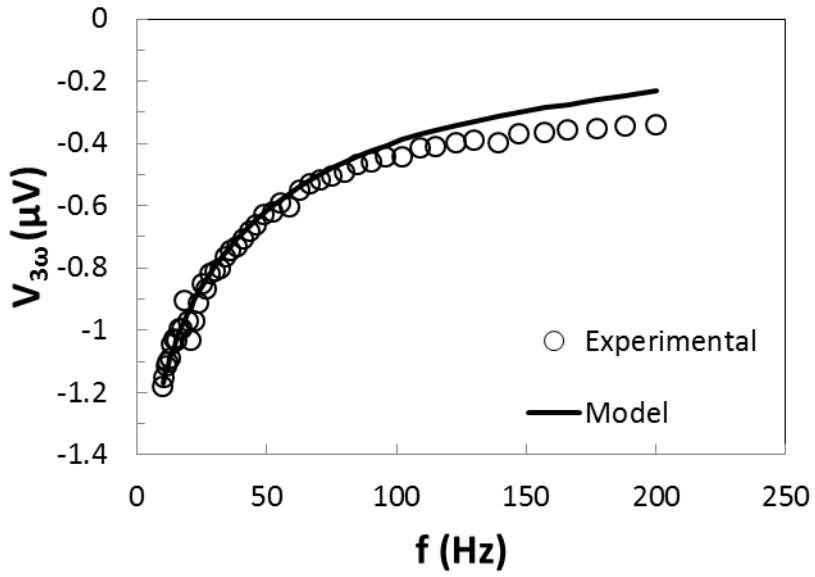

(b)

Figure 48 Amplitude of experimental and theoretical 3ω voltage as function of frequency of a carbon fiber in (a) longitudinal direction (b) transverse direction of the fiber.

4.5.4.2 Temperature Effect on Thermal Conductivity of T650 Carbon Fiber

Heat transferred in solid is mainly by two types of carriers: phonons (lattice vibration waves) and electrons. Generally speaking, for semiconductor like carbon fiber, phonon conduction dominates in heat transfer [78], which is sensitive to the stability of the material microstructure. Meanwhile, in carbon fiber, carbon atoms line up regularly and orderly, form mesh structure with layers piling up and entwining each other, which forms a fairly stable structure around room temperature (300 K-400 K in this study) [79]. Therefore the thermal conductivity is not expected to vary significantly in this temperature range due to the stability of phonon transfer. However, to confirm this presumption, thermal conductivities of T650 carbon fiber at temperature between 20 ℃-60 ℃ were measured with the present 3ω techniques. The measured longitudinal thermal conductivities and transverse thermal conductivities of five T650 Carbon fibers at 20 ℃, 30 ℃, 40 ℃, 50 ℃ and 60 ℃ are shown in Figure 49. As expected, the thermal conductivities of T650 carbon fiber in longitudinal and transverse directions both exhibit an almost zero increase over the temperature span. In the small temperature span around room temperature used in this study, there is no significant meaning to measure thermal conductivity at different temperature. Therefore in next section, thermal conductivity will be only presented in room temperature.

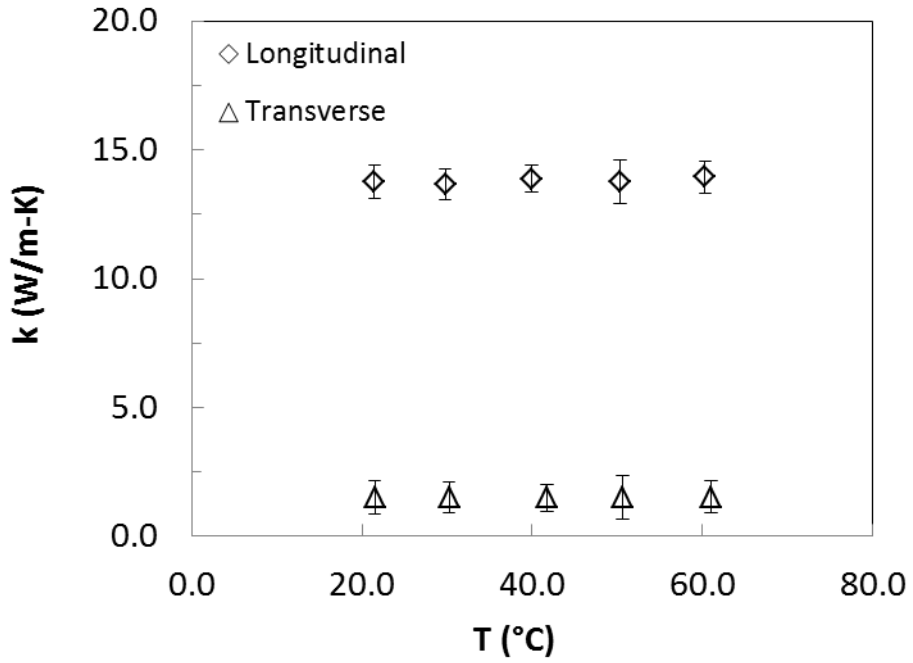

Figure 49 Thermal conductivities of T650 in longitudinal and transverse directions from room temperature up to 60 ℃. The error bars are the standard deviations of five specimens.

4.5.5 Heat Treated T650 Carbon Fiber

During the process of chemical vapor deposition for growing CNFs, the carbon fibers go through a series of high temperature environment. It has been reported that mechanical properties decay during such a high temperature process [80]. In order to investigate whether high temperature treatment also decreases the thermal conductivity of carbon fiber, the neat T650 carbon fibers were put inside the reactor and ran through the process the same as that for growing CNFs but without using catalysts. The thermal conductivities of heat treated carbon fiber are shown in Figure 50. In longitudinal direction, the thermal conductivity of heat treated carbon fiber is only about 4.6% lower than that of neat carbon fiber, but the deviation among samples are almost double. In

transverse direction, there is about 38% decrease of the thermal conductivity causing by the heat treatment process. By carefully investigate with SEM (Figure 51), no obviously structural damage on the surface is observed. However, as discussed in the last section, T650 carbon fiber has an onion-like graphite layer microstructure piling up along the radius direction and the outer layers are more regular stacked than the core layers. During the heating treating process, the spacing between the graphite layers will increase as the bonding between them is not as strong as that inside the graphite layers. After heat treatment, the spacing tends to close up but may not recover to the original location and size, which can become submicron scale damage inside the carbon fiber. Therefore, in radial direction, thermal conductivity significant degrades while in longitudinal direction, thermal conductivity only exhibits a trivial decrease.

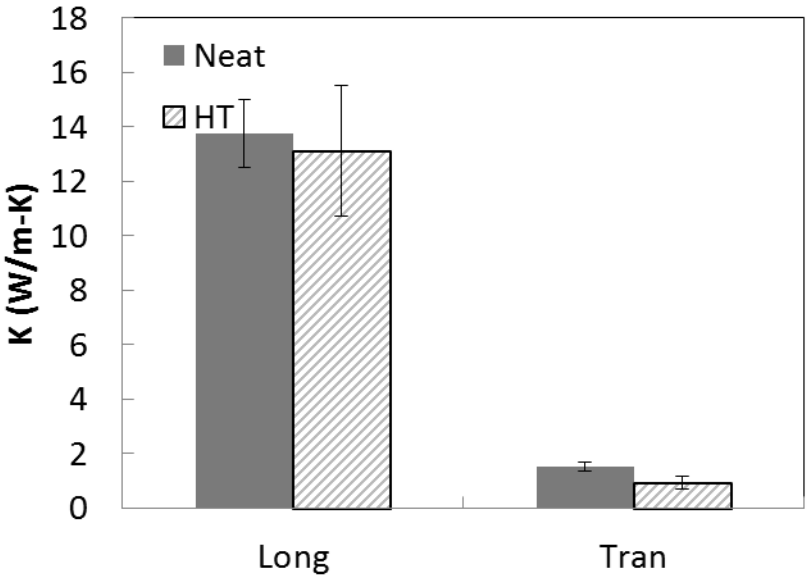

Figure 50 Effect of heat treatment on thermal conductivities of T650 carbon fiber. Five samples of neat carbon fiber and 10 samples of heat treated carbon fiber were measured. The error bars are the standard deviations of the specimens.

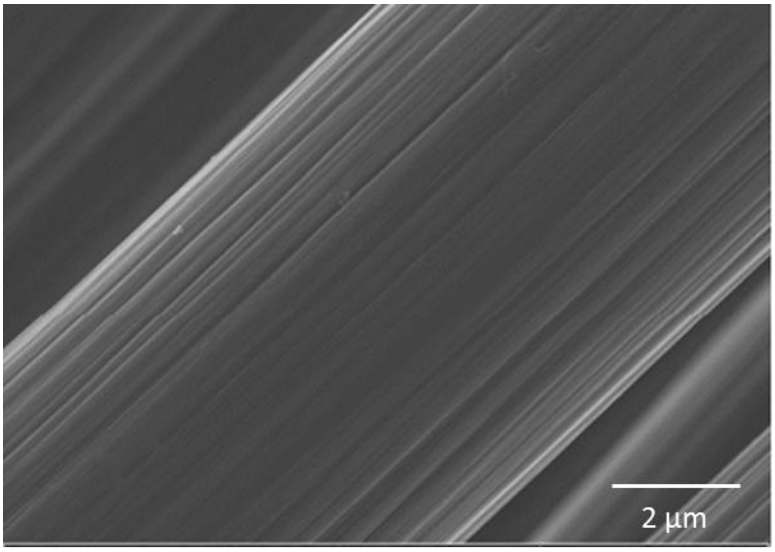

Figure 51 SEM image of heat treated T650 carbon fiber.

4.5.6 Thermal Conductivities of Hierarchical Carbon Fiber

In this Section, results of measured thermal conductivities of individual hierarchical T650 carbon fibers are presented. The hierarchical carbon fibers are fabricated by growing CNFs on the surface of carbon fiber tows using chemical vapor deposition method described in chapter 3. Four different amounts of catalysts were used to grow CNF, which are 0.2%, 0.3, 0.5 and 1.2 %. The relation between weight percent of growth and the catalysts applied on the tow is shown in Table 9. It should be noted that at this stage, the control of the growth of CNFs is only limited to the amount of catalysts used and the grown CNFs may not evenly distribute over the carbon fiber tows. Therefore, the results of thermal conductivities for the individual carbon fibers are presented in statistical way.

Table 9 Relation between weight percent of catalysts and weight percent of growth

Catalyst wt %	CNF Growth wt%
0.2	6.7
0.3	13.9
0.5	25.2
1.2	38.1

4.5.6.1 Longitudinal thermal conductivities

Longitudinal thermal conductivities of T650 carbon fiber with different weight percent of CNF growth are shown in Figure 52. The error bars shows the 95% confidential interval of 10 samples. Although the CNFs are intended to be grown to enhance the transverse thermal conductivity of the carbon fiber, it has been shown that in longitudinal direction there is also a minor enhancement and the enhancement generally increases as the growth increases. The highest enhancement of longitudinal thermal conductivity is seen for carbon fiber with 1.2% catalysts applied, which is about 24%. This enhancement could stem from the fact that the CNFs do not align perpendicular to the carbon fiber axis. Those CNFs that incline to or even align along the longitudinal direction serve as additional heat path along the fiber axis, which improve the global heat transfer the carbon fiber and thus enhance the longitudinal thermal conductivity of the carbon fiber.

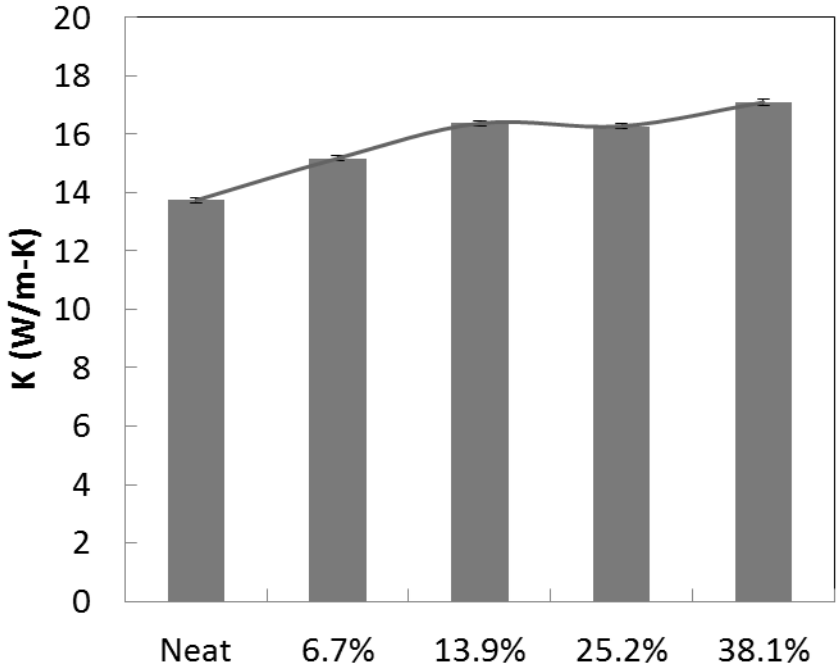

Figure 52 Longitudinal thermal conductivity of T650 carbon fiber with different weight percents of CNF growth. (10 specimens for each type of hierarchical carbon fiber)

4.5.6.2 Transverse thermal conductivities

Longitudinal thermal conductivities of T650 carbon fiber with different amounts of CNF growth are shown in Figure 53. The error bars shows the 95% confidential interval of 10 samples. As expected, growing CNFs on the surface of the carbon fiber significantly increases the thermal conductivity along the transverse direction of the carbon fiber. The enhancement of transverse thermal conductivities increases constantly with the weight percent of growth but it reach a plateau quickly. With 6.7% growth of CNFs, a 46% enhancement of transverse thermal conductivity is observed, while with 38.1% of CNFs, about five more folds growth, only 71% enhancement is seen. Considering there is a 24% enhancement of longitudinal thermal conductivity at this

amount of growth, it implies that when the CNFs grow longer, they prone to incline to the axial direction of the carbon fiber.

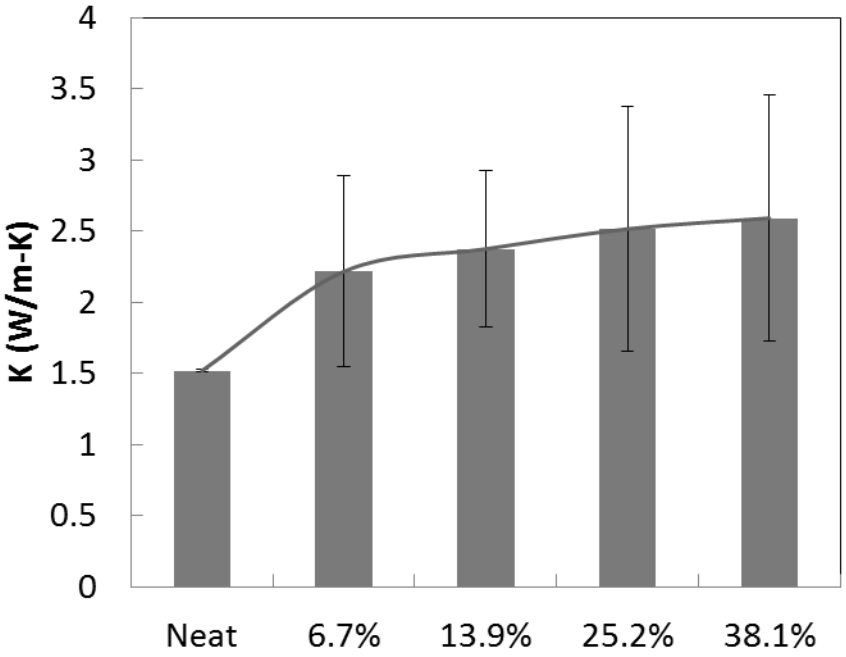

Figure 53 Transverse thermal conductivity of T650 carbon fiber with different weight percent of CNF growth. (10 specimens for each type of hierarchical carbon fiber)

4.6 Discussion and Conclusion

A technique based on wire-based 3ω method has been extended to measure the thermal conductivities for carbon composites materials and carbon fiber in both longitudinal and transverse directions. The technique and the experimental system were validated with standard materials before they were applied to the objects. For bulk material, validation has been done on pyrex and epoxy. For individual fibers, platinum wire and tungsten wire were used for validation. The measured results agree favorably

with the existed literature data. Based on that, measurement has been done on hybrid CFRCs and hierarchical CFRCs. In fiber scale, measurement has been done on carbon fibers with heat treatment and with CNF growth in both longitudinal and transverse directions.

Several conclusions can be drawn as follow:

(i) Surface treatment to the CNF has great effect on the thermal conductivities of the hybrid carbon fiber composites. Generally speaking, by oxidizing the CNF, degradation of the thermal performance was seen. This can be greatly related to the thermal resistance between the CNFs and the matrix. Oxidation, though generate good bonding between the matrix and the CNFs, it is very weak on transporting phonon. As is well known that, for semiconductive material, phonon is dominating approach for the heat transfer. Oxidation damps the phonon transfer thus also reduce the thermal conductivities of the hybrid carbon fiber composites system.

(ii) By comparing the two techniques: modifying the matrix with CNFs and modifying the carbon fabric with CNFs, it can clearly see that there is advantage of the latter technique over the former one. By incorporating CNFs into the epoxy matrix, only a mildly improvement of thermal conductivities has been seen for the hybrid CFRCs. On the other hand growing CNFs on the surface of the carbon fabric can bring in a high CNFs content limit. Meanwhile the location of the CNFs is relatively easily been controlled. The maximum enhancement of through-thickness thermal conductivity is about 33% when 252% CNFs are grown onto the carbon fiber. If all carbon contents are considered, with the same amount of carbon contents, through-thickness thermal conductivity of hierarchical CFRC can be nine times of neat CFRC. Therefore, it is a

better approach to improve the thermal conductivities of laminated carbon fabric-epoxy composites.

(iii) For individual carbon fibers, it has been found that CNFs improve the thermal conductivities in both longitudinal and transverse direction. Ideally, the purpose of growing nanofiber on the surface of the carbon fiber is to enhance the transverse thermal conductivity. However, due to the geometry of the CNFs, it is impossible to make the CNFs completely aligns vertically to the carbon fiber. Thus there is also an extent of enhancement of thermal conductivity in longitudinal direction but it is not as high as that in transverse direction. The present results clearly show that enhancement of transverse thermal conductivity is higher than the enhancement of longitudinal thermal conductivity, which matches the expectation.

(iv) As the weight percent of growth of CNFs increases, continue enhancement of thermal conductivities of carbon fiber in both longitudinal and transverse direction has been observed. In transverse direction this enhancement reaches a plateau very fast and shifts to enhancement in longitudinal direction. As the amount of CNFs growth increase, the CNFs start to form a mat-like network and then this network becomes denser and thicker. Ideally increasing the applied catalysts may continue to increase the amount of CNF growth and thus enhance the thermal conductivity of the carbon fiber. However, when the amount of catalysts increases, the catalysts tend to agglomerate into large size and grow CNFs in larger diameter and finally amorphous carbon. Meanwhile, when the CNF network forms, it may also reduce the flow rate close to the surface of the carbon fiber and thus reduce the reaction. The study of

controlling of CNF growth is out of the scope of this dissertation. More study may be done in the future work.

(v) By varying the temperature from room temperature to 100 ℃, a clearly trend of increase of thermal conductivity can be seen for the carbon fiber composite, the hybrid carbon fiber composites and the hierarchical carbon fiber composites. However, such trend is insignificant when investigating the thermal conductivities of carbon fibers. In fact, a minor decrease is observed when the temperature increases from room temperature to about 60 ℃. On the other hand, neat epoxy in the validation section shows a similar trend. Another important fact is that thermal interfacial resistance decrease as the temperature increase [65]. Based on these, it can be conclude that the increase of the thermal conductivity with temperature stem from the increase of the thermal conductivity of the epoxy and the decrease of the thermal interfacial resistance.

Although 3ω method has been widely used to measure fiber and thin film, it is the first time it has been used to systematically study the hierarchical CFRCs. Meanwhile, it is the first time the transverse thermal conductivities of individual carbon fibers come into scope. Therefore, these results generate significant meaning for instruction for designing hierarchical CFRCs. In the next chapter, a model based on the experimental work was derived.

Chapter 5 Prediction of Transverse Thermal Conductivities of Hierarchical Carbon Fiber Reinforced Composites

5.1 Introduction

Although hierarchical CFRCs has been existed for more than a decade, so far, modeling studies on thermal conductivity of hierarchical composites with CNF modified fiber is still limited on heat transportation in fiber scale. No analytical or simulation model was found for depicting the effective transverse thermal conductivity of the entire hierarchical structured composites. Meanwhile, recently, our research group is attempting to develop multi-scale carbon composites by growing different scales of CNFs onto conventional micron scale carbon fibers. The building of analytical are required to establish guideline for further development of hierarchical CFRCs and to give a deeper understanding of the mechanism behind the improvement of thermal conductivity.

In this chapter, a thermal resistance series representative volume element (RVE) model based on analogy between Fourier' s Law and Ohm's law is presented to predict the transverse thermal conductivity of the hierarchical CFRCs [81, 82]. The grown CNFs on the surface of carbon fiber with the wetting matrix were modeled as a homogenized layer using effective medium theory. The effects of thickness of the layers and the thermal conductivities of the homogenized layers were investigated by parameters study. Modeling issues for different types of growth morphology and the corresponded composites were also discussed.

5.2 Modeling of Thermal Conductivities of Hierarchical CFRCs

5.2.1 Model of Plain-Weave Laminated Composites

A composite lamina is a periodic material consists of repeating unit cells (Figure 54), therefore a RVE can be considered as a model to predict its properties. The model is characterized by the selection of a unit cell, which encloses the smallest periodic repeated volume in the plain weave lamina [83, 84] (Figure 56). For each unit cell, since its width (typically 5 mm) is much larger than its thickness (typically 50 μm, Figure 55), if there is temperature gradient between the top surface and the bottom surface of the lamina, the heat flow can be approximate as one-dimensional. The lamina properties can now be calculated with the tow properties using a thermal-electrical analogy, in which the unit cell is transformed into an electrical circuit where the resistance can be depicted as:

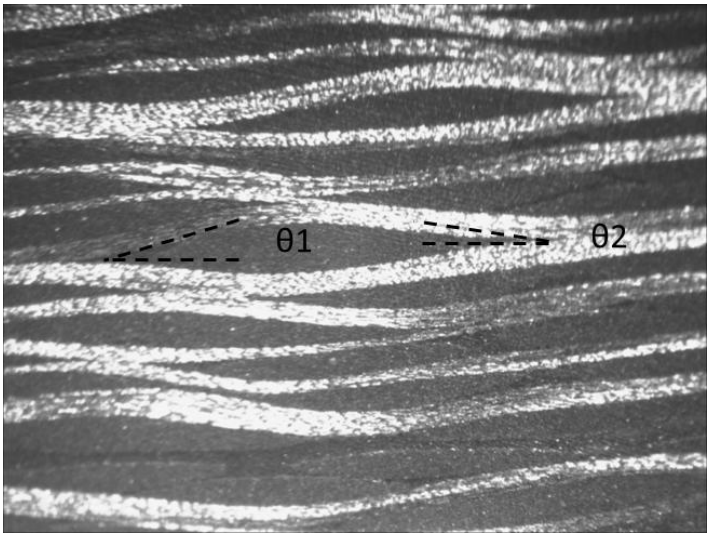

Figure 54 Typical cross section of plain-weave CFRC. The fiber orientation angles are labeled.

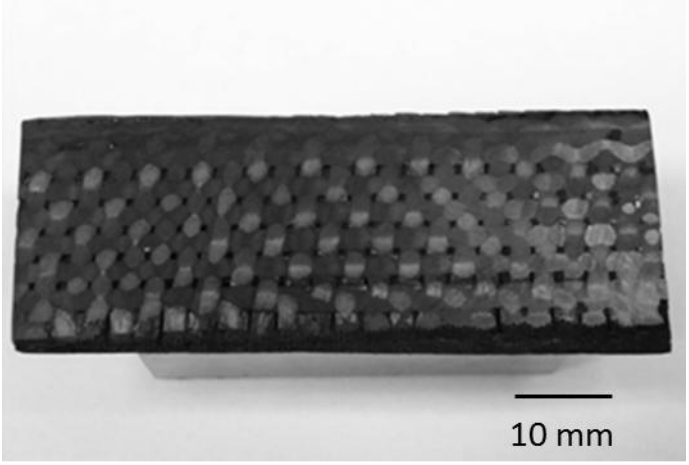

Figure 55 Top view of typical laminated CFRCs. The surfaced has been polish to expose the morphology of carbon fabric laminate structure.

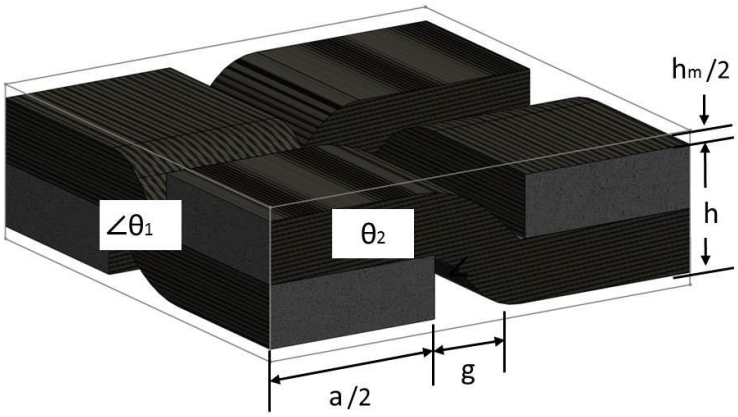

Figure 56 Schematic of the idealized unit cell of plain weave laminated composites.

$$R = \frac{L}{kA} \tag{5.1}$$

where R is thermal resistance, L and k are respectively, the length and effective thermal conductivity of conduction element in the direction of heat transfer, and A is the area of the conduction element cross section perpendicular to the direction of heat transfer.

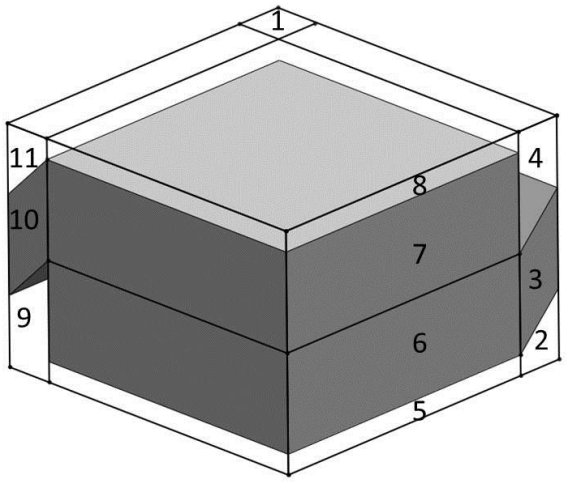

(a)

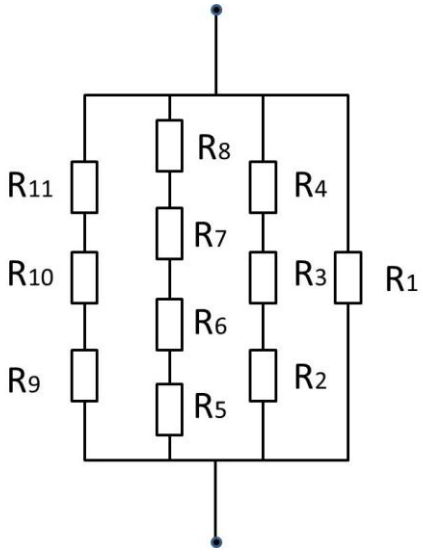

(b)

Figure 57 (a) The quarter idealized unit cell of plain-weave laminated composites. (b) Analogical electric circuit of the quarter idealized unit cell of plain-weave laminated composites.

For transverse thermal conductivity, due to the symmetry of boundary conditions, only quarter of the unit cell needs to be considered. The quarter unit is further divided into elements arranged in series, depending on the material components, denoted by 1-11(Figure 57(a)). The analogical electrical circuit is shown in Figure 57(b). The calculation for each element can be done with equation (5.2). The thermal conductivity of the inclined piecewise yarn $\boldsymbol{k_i}$ can be expressed as the transformation equation (5.3).

$$R_1 = \frac{4(h+2h_m)}{k_m g^2} \qquad R_2 = \frac{g\tan\theta_1 + 2h_m}{k_m a g}$$

$$R_3 = \frac{4h}{k_1 a g} \qquad R_4 = \frac{4h + 2h_m - g\tan\theta_1}{k_2 a g} \qquad (5.2)$$

$$R_5 = R_8 = \frac{2h_m}{k_m a^2} \qquad R_6 = R_7 = \frac{4h}{k_2 a^2}$$

$$R_9 = \frac{4h + 2h_m - g\tan\theta_2}{k_m a g} \qquad R_{11} = \frac{g\tan\theta_2 + 2h_m}{k_m a g} \qquad R_{10} = \frac{4h}{k_1 a g}$$

$$k_i = k_{ya}\cos^2\theta_1 + k_{yt}\sin^2\theta_1 \qquad (5.3)$$

where thermal conductivity of yarn in uniaxial direction k_{ya} can be found simply with rule of mixture:

$$k_{ya} = V_{fy}k_{fa} + (1 - V_{fy})k_m \tag{5.4}$$

and thermal conductivity of yarn in transverse direction k_{yt} can be found with a semi-empirical Clayton model [85]:

$$k_{yt} = k_m \left[\frac{\sqrt{(1 - V_{fy})^2 \left(\frac{k_{ft}}{k_m} - 1\right)^2 + \frac{4k_{ft}}{k_m}} - (1 - V_{fy})\left(\frac{k_{ft}}{k_m} - 1\right)}{2} \right]^2 \tag{5.5}$$

where k_{fa} and V_{fy} are respectively thermal conductivities of fiber in uniaxial direction and fiber volume fraction of the impregnated yarns. The total effective thermal resistance can be expressed in terms of its components as follows:

$$\frac{1}{R} = \frac{1}{R_1} + \frac{1}{R_2 + R_3 + R_4} + \frac{1}{R_5 + R_6 + R_7 + R_8} + \frac{1}{R_9 + R_{10} + R_{11}} \tag{5.6}$$

Assuming a balanced reinforcement (same tow density in the warp and fill directions), the fiber volume fraction of the lamina, can be calculated by [84]:

$$v_f = v_{fy} \frac{\left(1 - \frac{h_m}{h}\right)}{\left(1 + \frac{g}{a}\right)} \tag{5.7}$$

where h_m, h, g, and a are lamina geometric parameters can be seen in Figure 56.

5.2.2 Growth Morphology

Before growing CNFs onto the surface of the carbon fabric, catalyst solution was usually applied on the surface of laminates by spraying with paint spray gun. The catalyst solution wetted the carbon fabric unevenly: while most of the catalysts remained on the surface of the fabric, some of the catalysts flowed into the tows inside. After the reaction, the growth of the CNFs hence mainly covered the outer surface of the fabric (Figure 58(a)) and there was some growth inside the fabric as is confirmed by the SEM (Figure 58(b)).

In order to model the growth morphology of CNFs, two extreme cases are first studied. The first case is that CNFs only grow on the top and bottom surface of the fabric. The second case assumes that CNFs uniformly grow onto all the carbon fibers. In next two sections, two types of techniques are used to modify the RVE model to represent the CNFs growth in the aforementioned cases.

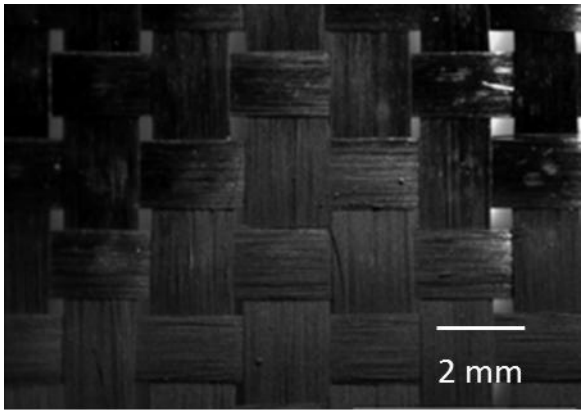

(a)

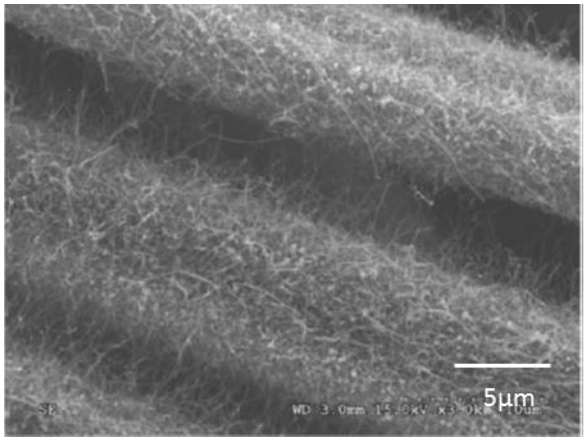

(b)

Figure 58 Typical hierarchical carbon fiber. [20] (a) CNF grown on the surface of carbon fabric (b) SEM image of hierarchical carbon fiber

5.2.3 Case I CNFs Grown on the Surface of Fabric (Surface Growth)

Assuming that the growth of CNFs gives a uniform thickness and is even over the whole surface of each lamina, the layer of growth can be modeled as a homogenized CNFs-matrix layer. Therefore we can modified the aforementioned quarter idealized unit

cell by adding extra layer 12-17 as shown in Figure 59(a). The analogical electric circuit is hence modified into Figure 59(b). The additional resistance from the CNFs can be described as:

$$R_{12} = R_{13} = \frac{4t}{k_g a^2} \tag{5.8}$$

$$R_{14} = R_{15} = R_{16} = R_{17} = \frac{4t}{k_g a g} \tag{5.9}$$

The total thermal resistance is:

$$\begin{aligned} \frac{1}{R} = \frac{1}{R_1} &+ \frac{1}{R_2 + R_3 + R_4 + R_{16} + R_{17}} \\ &+ \frac{1}{R_5 + R_6 + R_7 + R_8 + R_{12} + R_{13}} \\ &+ \frac{1}{R_9 + R_{10} + R_{11} + R_{14} + R_{15}} \end{aligned} \tag{5.10}$$

The through thickness thermal conductivity can be calculated as:

$$k_e = \frac{4h}{R(a+g)^2} \tag{5.11}$$

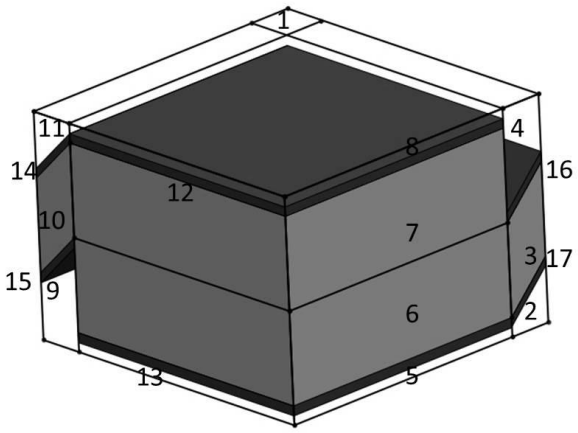

(a)

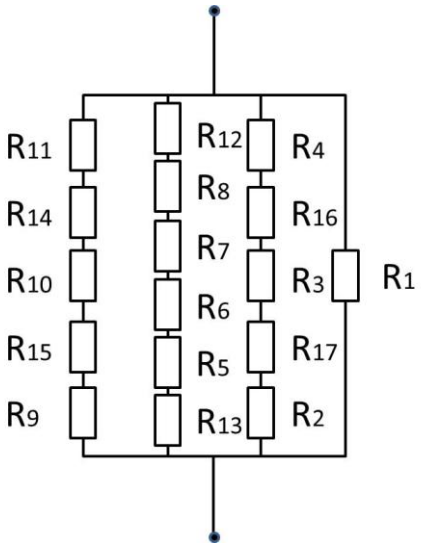

(b)

Figure 59 (a) The quarter idealized unit cell of plain weave laminated composites with CNFs growth. (b) Analogical electric circuit of the quarter idealized unit cell of plain weave laminated composites with CNFs growth.

5.2.4 Case II CNFs Grown Evenly on the Surface of Each Carbon Fiber (Full Growth)

Assuming that the micron scale carbon fibers have perfect cylindrical geometry and uniform alignment throughout the whole matrix (Figure 58), a 2-D quadratic unit can be used to represent the CFRC (Figure 60(a)). Also given that the growth of CNFs has uniform thickness over the carbon fiber and that the conductivity of the carbon fiber is in-plane isotropic, the growth of the CNFs with the matrix wetting the growth can be simplified as a homogenized layer between the carbon fiber and the rest of the matrix (Figure 60 (b)). Again, this layer together with the carbon fiber can be further homogenized as a complex fiber in the matrix (Figure 60 (c)). The transverse thermal conductivity of this simplified representative element could be easily obtained with the Springer model if we know the thermal conductivity of complex fiber [86]:

$$\frac{k_e}{k_m} = 1 - 2\sqrt{\frac{v_f}{\pi}} + \frac{1}{S}\left[\pi - \frac{4}{\sqrt{1-\frac{v_f S^2}{\pi}}}\tan^{-1}\left(\frac{1+\sqrt{\frac{v_f S^2}{\pi}}}{\sqrt{1-\frac{v_f S^2}{\pi}}}\right)\right] \tag{5.12}$$

where

$$S = 2\left[\frac{k_m}{k_c} - 1\right] \tag{5.13}$$

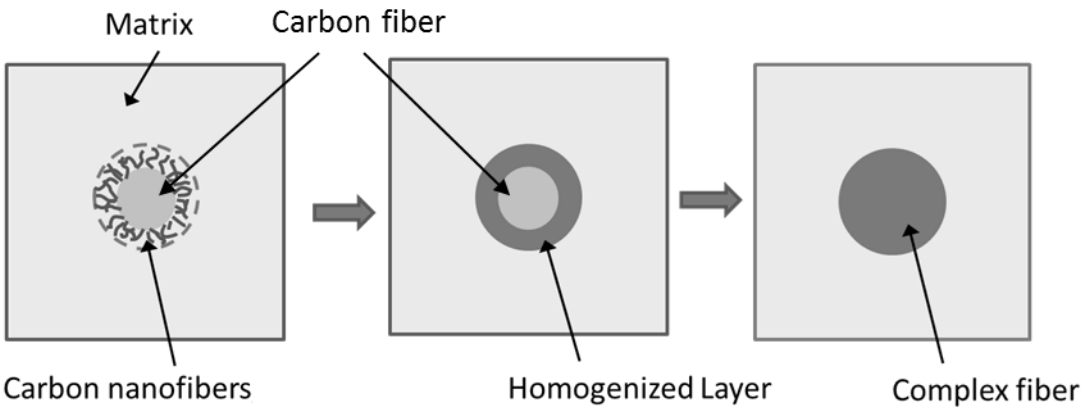

(a) (b) (c)

Figure 60 Development of model for hierarchical unidirectional carbon composites. (a) Schematic diagram of unit shell of hierarchical unidirectional carbon composites (b) homogenize growth as a well-blended layer, and (c) further homogenize the hierarchical fiber as complex fiber.

Now considering the complex fiber model with the carbon fiber "core" and the homogenized layer "shell" (Figure 61), the governing equation under a temperature gradient H_0 in cylindrical coordinate system is in the form of:

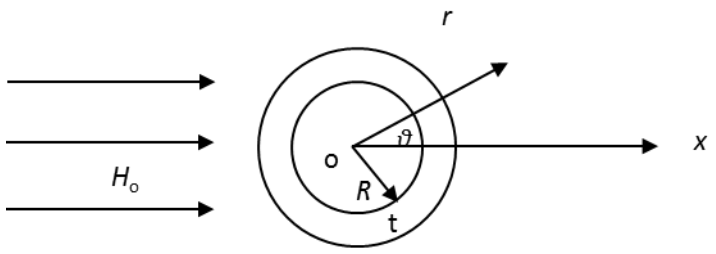

Figure 61 The model of complex carbon fiber in a temperature gradient field.

$$\nabla^2 T = \frac{\partial}{\partial r}\left(r^2 \frac{\partial T}{\partial r}\right) + \frac{1}{r^2}\left(\frac{\partial^2 T}{\partial \theta^2}\right) \tag{5.14}$$

$$T_1|_{r=0} = Constant, T_3|_{r=\infty} = -H_0 r cos\theta \tag{5.15}$$

$$T_1|_{r=R} = T_2|_{r=R}, T_2|_{r=R+t} = T_3|_{r=R+t} \tag{5.16}$$

$$k_{ft} \left.\frac{\partial T_1}{\partial r}\right|_{r=R} = k_g \left.\frac{\partial T_2}{\partial r}\right|_{r=R} , \; k_g \left.\frac{\partial T_2}{\partial r}\right|_{r=R+t} = k_g \left.\frac{\partial T_3}{\partial r}\right|_{r=R+t} \tag{5.17}$$

where T is temperature and the indices 1 to 3 respectively represent the carbon fiber, the homogenized layer and the matrix. k_{ft} and k_g are respectively the transverse thermal conductivities of an individual fiber and the homogenized layer. R and t are respectively the radius of the fiber and the thickness of the homogenized layer. By the solution of the equation (5.14), we get the temperature distribution function,

$$T_1 = \mathrm{A}r\cos\theta, \quad r < R, \tag{5.18}$$

$$T_2 = \left(\mathrm{B}r + \mathrm{C}r^{-1}\right)\cos\theta, \quad R < r < R + t\,. \tag{5.19}$$

where

$$\mathrm{A} = \frac{-4k_3k_2}{K}H_0, \tag{5.20}$$

$$\mathrm{B} = \frac{-2k_3(2k_2+k_1)}{K}H_0, \tag{5.21}$$

$$\mathrm{C} = \frac{2k_3(k_1-k_2)R^3}{K}H_0, \tag{5.22}$$

$$\mathrm{K} = (k_1+k_2)(k_2+k_3)-\alpha(k_2-k_3)(k_2-k_1), \tag{5.23}$$

$$\alpha = \left(\frac{R}{(R+t)}\right)^2 \tag{5.24}$$

Hence we can obtain the temperature gradient H

$$\vec{H}_1 = A\vec{e}_x, \tag{5.25}$$

$$\vec{H}_2 = B\vec{e}_x + r^{-2}\vec{e}_x - 2C_x r^{-3}\vec{e}_r, \tag{5.26}$$

Due to r>R, approximately we have

$$\vec{H}_2 = B\vec{e}_x, \tag{5.27}$$

Based on Fourier's law, we can introduce the effective thermal conductivity of the complex carbon fiber as:

$$\langle \vec{q} \rangle = k_c \left\langle \vec{H} \right\rangle, \tag{5.28}$$

where $\langle \vec{q} \rangle$ and $\left\langle \vec{H} \right\rangle$ are the special average of the heat flux and the temperature gradient, i.e.

$$\langle \vec{q} \rangle = \frac{1}{V} \int_V \vec{q} \mathrm{d}V, \tag{5.29}$$

$$\left\langle \vec{H} \right\rangle = \frac{1}{V}\int_V \vec{H}\mathbf{d}V, \tag{5.30}$$

Substitute (5.27) and (5.28) into (5.29) and (5.30), and using the following relation

$$\left\langle \vec{q}_i \right\rangle = k_c \left\langle \vec{H}_i \right\rangle, \text{i=1, 2} \tag{5.31}$$

We can obtain

$$\left\langle \vec{H} \right\rangle = \left[A\alpha + B(1-\alpha) \right] \vec{e}_x, \tag{5.32}$$

$$\left\langle \vec{q} \right\rangle = \left[A\alpha k_1 + B(1-\alpha) k_2 \right] \vec{e}_x, \tag{5.33}$$

Based on (5.28), we get the effective thermal conductivity of the complex fiber

$$k_c = \frac{\langle \vec{q} \rangle}{\langle \vec{H} \rangle} = \frac{A\alpha k_1 + B(1-\alpha)k_2}{A\alpha + B(1-\alpha)} = k_2 \frac{k_1 + k_2 + \alpha(k_1 - k_2)}{k_1 + k_2 - \alpha(k_1 - k_2)}, \quad (5.34)$$

Note that when α equals to 1, i.e. t=0, equation (5.34) reduces to $k_c = k_1$, which represents the case of neat micron fiber. Using the thermal conductivity k_c gained from equation (5.34) to replace k_{ft} in equation (5.4), the RVE model then represents the transverse thermal conductivity of hierarchical laminated CFRCs. The required variables to be known are the transverse thermal conductivity of carbon fiber, thermal conductivity of CNF-matrix homogenized layer, the thermal conductivity of matrix, thickness of the homogenized layer, and volume fraction of complex fiber.

5.3 Numerical Results

5.3.1 Selection of Parameters and Validation

Numerical results are presented for the effective transverse thermal conductivity of plain-weave CFRCs to demonstrate the effect of thickness and density of growth of carbon fiber. The fixed parameters used for the CFRCs model are respectively listed in Table 10. Without loss of generality, the volume fractions for both are fixed at 0.6. The parameters of material properties are based on value of typical PAN-based carbon fiber (Figure 55) while the geometric parameters are selected for typical carbon fiber composites with 0.6 volume fraction and calculated based on method in [87].

Table 10 Parameters for hierarchical plain-weave laminated model

Parameter	Value
k_m ($W/m^{-1}K^{-1}$)	0.2
k_{fa} ($W/m^{-1}K^{-1}$)	14 [88]
k_{ft} ($W/m^{-1}K^{-1}$)	2
v_f	0.59
v_{fy}	0.8
g/a	0.1 [87]
(a+g) (mm)	1.5
h_w (mm)	0.13
θ_1 (°)	7
θ_2 (°)	4

5.3.2 Effective Thermal Conductivity Using the Present Model

Two parameters are used for investigation of the effect of CNFs growth on the transverse thermal conductivity of CFRCs in this study. The first parameter is the thickness of the growth of carbon CNFs on the carbon fabric. Figure 62 and Figure 63, respectively shows the improvement of transverse thermal conductivities of CFRCs with surface growth and full growth respectively as the thickness of growth increases, assuming that the carbon fiber volume fraction does not change. As can be seen in Figure 62, transverse thermal conductivity of the laminated CFRC with surface growth is predicted to continuously improve as the thickness of the growth increases. With 20μm thick growth, there is an about 23% increment of transverse thermal conductivity. This is because the growth is assumed to be only on the surface of the lamina and is relatively thin compared to the thickness of the lamina (in hundred micron scale). Also, the growth

on the surface of the lamina does not have effect on the inner part of the tow, which remains as a resin-rich zone, insulating the heat conduction across the whole composite. As the thickness of the growth continues increasing, the enhancement of transverse thermal conductivity becomes nonlinear demonstrating a seemingly divisive increase. However, the maximum thickness of the growth is limited by the thickness of resin-rich zone h_m, the thickness of growth beyond which should be considered as artifact and hence was not plotted in Figure 62. In contract to the surface growth, transverse thermal conductivity of hierarchical composites with full growth demonstrates sharp increase following by evident asymptotes as the thickness of the growth increase. It should be noticed that equation (5.34) is based on the assumption that fibers are not closed to each other. In actual situation, as the CNFs growth becomes thicker, fibers will be connected by the nano-networks instead of expand unlimitedly [89]. Therefore in high thickness, the model fails to reflect the morphology of the composites anymore. However, at low thickness it is still valid and shows the promising improvement of thermal conductivity of hierarchical CFRCs.

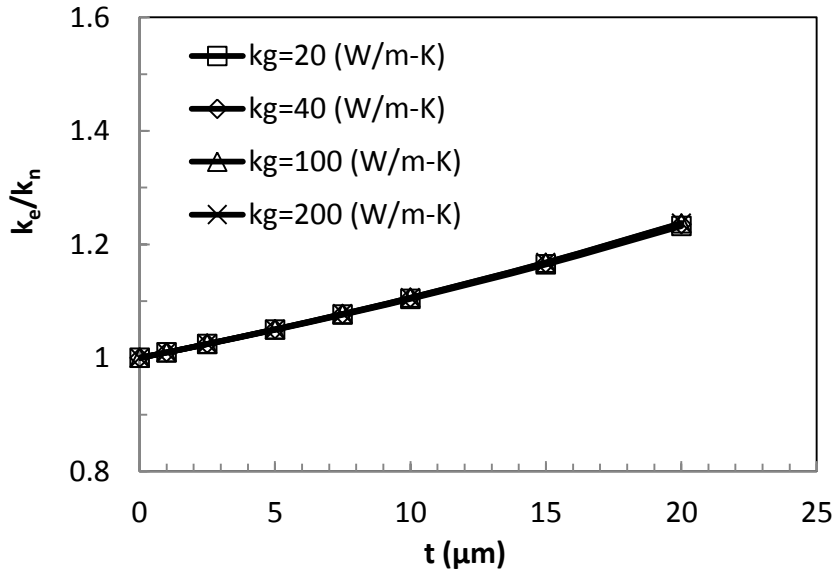

Figure 62 Through-thickness normalized thermal conductivity of hierarchical laminated CFRCs with surface growth of CNFs.

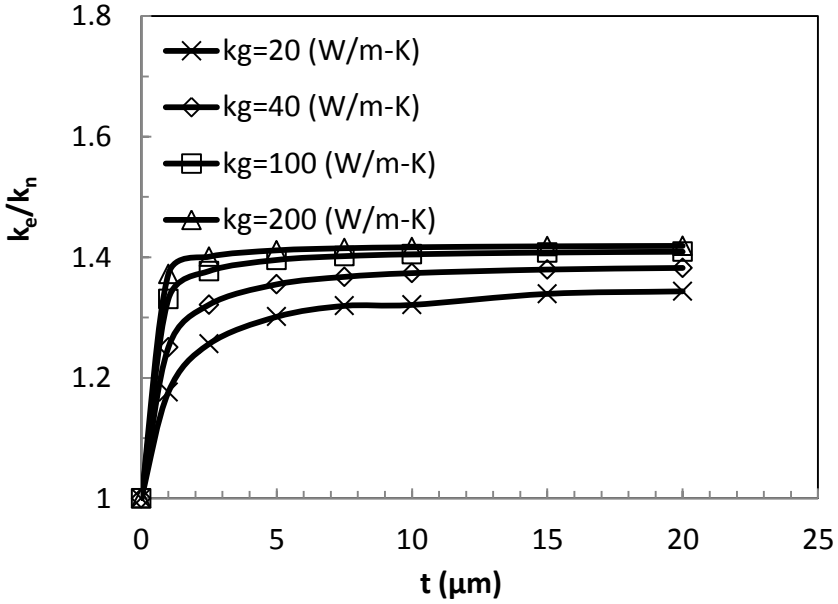

Figure 63 Through-thickness normalized thermal conductivity of hierarchical laminated CFRCs with full growth of CNFs.

Figure 64 and Figure 65 show the investigated transverse thermal conductivity of the homogenized layer as another parameter. The value of k_g is selected ranging from 5 W/m-K to 500 W/m-K, which is thermal conductivity of carbon nanofiber composites ranging from 0.3% to 50% based on rule of mixture (assuming thermal conductivity of CNF is 1000 W/m-K). The results from both models reach asymptote of the improvement of thermal conductivities as k_g increases. This is especially obvious for laminated CRFCs with surface growth, the increment of k_g almost does not affect the transverse thermal conductivity of composites any more after it reaches about 10 W/m-K, which indicates that density of growth is relatively insignificant comparing to the thickness of growth. Unlike hierarchical CRFCs with surface growth, hierarchical composites with full growth reach the point of asymptote at much higher k_g. Their transverse thermal conductivity enhancement is more sensitive to the k_g up to 500 W/m-K. This study of parameters shows that the two types of growth morphology of CNFs exhibit very different in enhancing transverse thermal conductivity of CFRCs as respective to density of the growth and the thickness of the growth. With the same range of parameter selection, hierarchical CFRCs with full growth demonstrate higher enhancement of transvers thermal conductivity. We will further compare these two models with the help of experimental data.

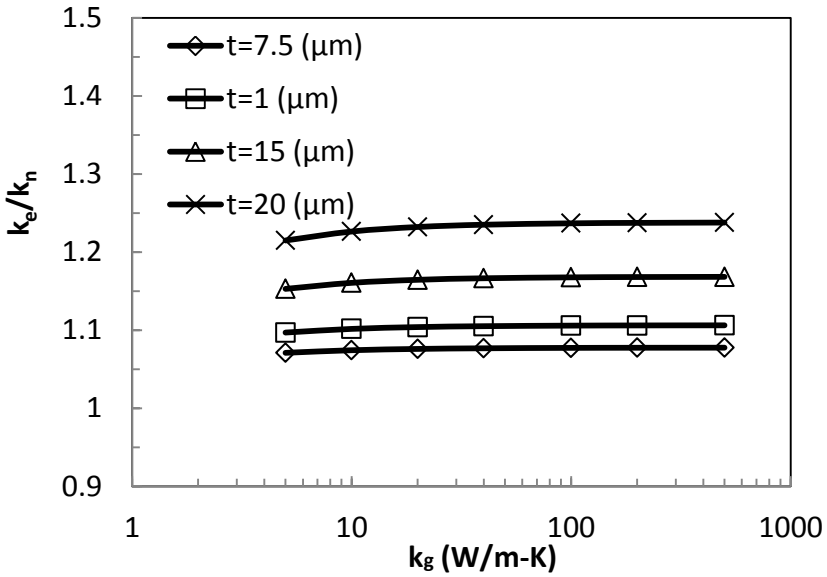

Figure 64 Through-thickness normalized thermal conductivities of hierarchical laminated CFRCs with surface growth.

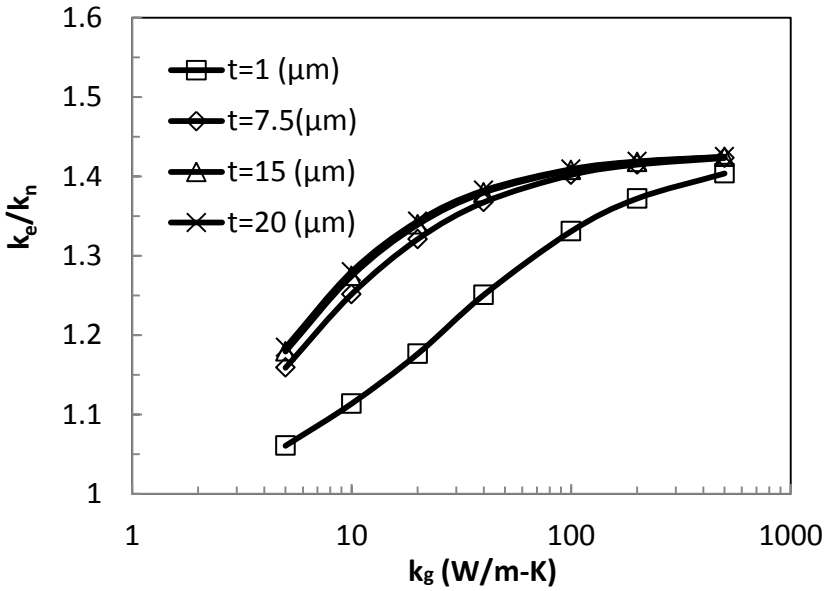

Figure 65 Through-thickness normalized thermal conductivities of hierarchical laminated CFRCs with full growth.

5.3.3 Comparison between Surface Growth and Full Growth of CNFs

The comparison of transverse thermal conductivities between surface growth and full growth of CNFs for hierarchical CFRCs can be seen in Figure 66. As has been discussed in the previous section, asymptote of enhancement of transverse thermal conductivity due to k_g appears much faster for surface growth model than full growth model (See Figure 64 and Figure 65). For illustration purpose we plotted the normalized transverse thermal conductivities of hierarchical CFRCs in these two morphologies at their asymptotic threshold k_g respectively. In order to further compare to experimental results in abscissa the thickness of growth was also replaced by weight percent of growth respective to the composites. Given the assumption that the density of the homogenized layer of CNFs growth is the same as the carbon fiber, the weight of growth is the same as the volume of growth. It can be seen that, at low weight percent of growth, hierarchical CFRCs with full growth gives a higher enhancement of transverse thermal conductivity, but the enhancement quickly reaches the maximum value, about 50%. As weight percent increases, growing CNFs on the surface of the fabric demonstrates more improvement for the transverse thermal conductivities of the hierarchical CRFCs, and this improvement is divisively up to 150%. For equal amount of CNFs growth, surface growth morphology will provide higher enhancement to the transverse thermal conductivities of the hierarchical CFRCs than full growth morphology. To sum up, it is promising to greatly enhance the transverse thermal conductivities of CFRCs with the help of growing CNFs on the carbon fiber if the growth can be controlled concentrating on the surface of the fabric.

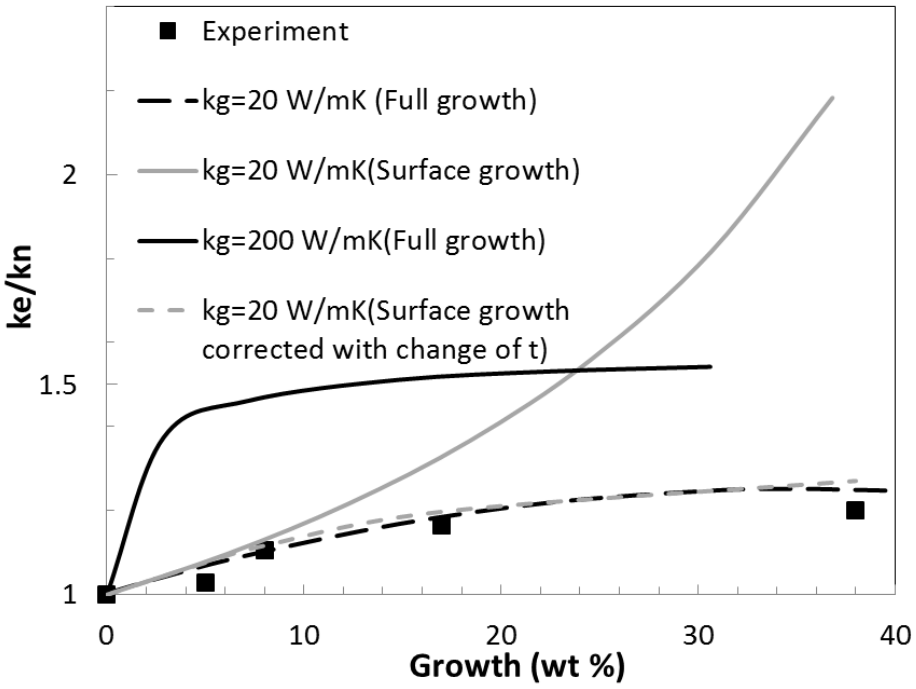

Figure 66 Comparison of normalized thermal conductivities of hierarchical CFRCs between present predictions and experimental results.

5.3.4 Comparison to Experimental Result

In order to validate the model, experimental results of thermal conductivity of hierarchical CFRCs presented in Chapter 4 are used to compare with the model prediction. The experimental results are shown in Figure 66. By letting k_g=20 W/mK, using the model of full growth, excellent agreement has been achieved between the experimental results and the model results. However, when the model of surface growth is directly used, we are unable to find such a k_g to obtain similar agreement. The results from the surface growth model are always higher than the experimental ones at high weight percent of growth. The reason is that, as the weight percent of growth increase the

thickness of the hierarchical CFRCs is also increase. Discrepancy is thus generated as the REV model is based on an unchanged total thickness of the lamina unit. A correction is thus done by replacing the fixed original lamina thickness with the actual measured laminate thickness of the hierarchical CFRCs (See Figure 67) corresponding to data point in Figure 66. The results are shown in Figure 67 labeled as "surface growth corrected with change of t". The surface growth model corrected with the thickness of lamina exhibits a good agreement with the experimental results. Although at this stage, it is impossible to determine the percentage between surface growth and the full growth of the CNFs, this comparison to some extend validate the models that can shed some light on the design of the hierarchical CFRCs. In term of the value of the prediction, a comparison can be also made by comparing the upper bound of the improvement of the thermal conductivity through growth of CNFs. Veedu *at el*. observed a 51% enhancement of through-thickness thermal conductivity on CNT forest modified laminated CFRC [90], which agrees with the upper bound of our prediction from full growth model (Figure 67). This is because their CNTs are aligned perpendicular to the micron fiber and the growth is three dimensional. To conclude, the present model agrees well with existed experimental results.

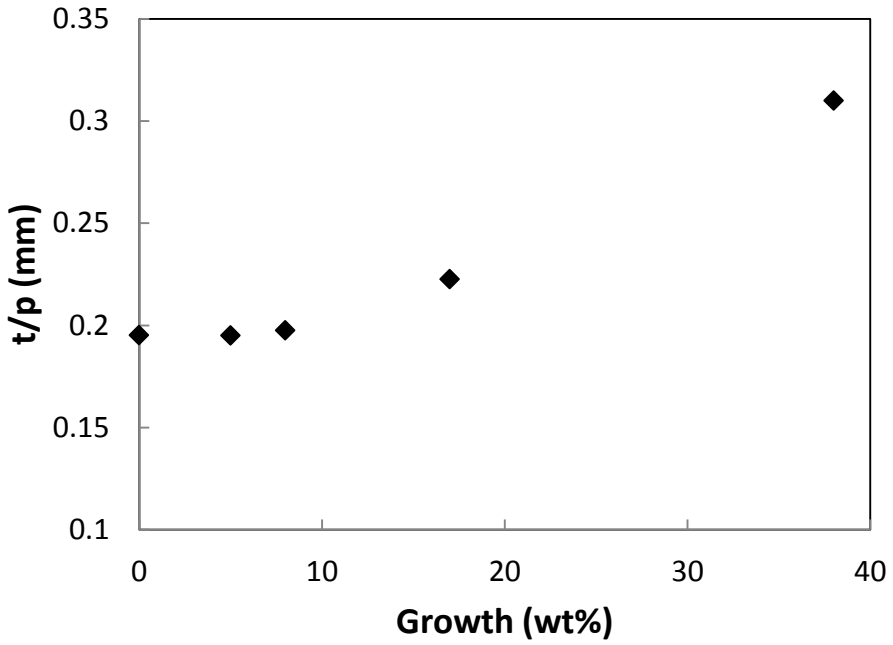

Figure 67 Average ply thickness of hierarchical CFRCs with respect to growth of CNFs.

5.4 Conclusion

Analytical models for plain-weave hierarchical CRFCs with CNFs modified carbon fibers were developed. The models represented two types of extreme growth morphology of CNFs, which are surface growth and full growth respectively. Prediction of improvement of transverse thermal conductivity is presented by parameters study. It is found that the thickness of growth is a critical factor for the improvement while the density is relatively insignificant for surface growth. A contrary phenomenon was found for full growth morphology. It is also found that CNFs grown on the surface of the fabric will provide more enhancement of transverse thermal conductivity for the hierarchical CFRCs above 25% weight percent of growth. These finding will be guide line for the design of hierarchical CFRCs.

Chapter 6 Summary

6.1 Conclusion

Both experimental measurement and theoretical modeling were used to study the thermal conductivities of CNF modified carbon fibers and their epoxy composites

In this study, a so called wire-based 3ω method was used for experimental measurement. In this method, the lithographic pattern is replaced with commercial metal wire. Without compromising the accuracy of the measurement technique, wire-based 3ω method greatly reduces the expense from $2000 to less than $5 [30] and equipment-wise complexity to prepare the sample for 3ω method.

To further reduce the complexity of the sample preparation for the measurement of thermal conductivities of CFRCs, an apparatus to mount the wire on the surface of the sample has been design. The mechanism is simple: a z direction translation stage was used to adjust the height of the sample to the level of the metal wire a, and a x direction translation stage was used to stretch the loosen wire to tightly attach to the surface of the sample. To solve the issue of electrical leakage, a coating technique was introduced to insulate the surface of the sample before mounting the wire on the surface of the sample. The effect brought in by the thin coating was compensated by using low frequency measurement range. A study was made to determine the frequency range that gives the same results with the thin coating.

For individual carbon fiber measurement, taking advantage of the fact that carbon fibers are semiconductive material, the original metal wire in the wire-based 3ω technique was replaced with the carbon fiber specimen. A one dimensional heat diffusion

equation was solved using Lu's proposed solution. In this way, thermal conductivities of individual carbons fibers in longitudinal were measured.

For the transverse thermal conductivities of carbon fibers, measurement technique has been developed by modifying the wire-based 3ω for longitudinal thermal conductivity measurement. By submerging the carbon fiber in deionized water, transverse thermal conductivities of the carbon fibers were measured with the help of solving the corresponding two-phase heat conduction problem. As a completely new technique, validation has been done with metal wire and polymer coated-metal wire. Analysis of the uncertainty and the error has been presented.

Consequently, the established 3ω techniques, experimental setups and protocols were used to characterize the thermal conductivities of CNFs modified T650 carbon fiber and its CFRCs.

The base CFRC selected for study is carbon laminated-epoxy composite. In this study, VARTM was used as the approach to fabricate the CFRCs. Two ways of incorporating CNFs have been tried to enhance the thermal conductivities. The first way was to blend the epoxy matrix with CNFs then used in the VARTM. The first method has been investigated with only up to 0.1% weight of CNFs due to the fact that inducing large amount of CNFs in the matrix can lead to unsolvable processing problems. The dramatic increase of viscosity of the matrix stemming from the nanofiller will bring in filtration during the fabrication process. By investigating up to 0.1% weight percent of CNFs applied on CFRCs, a trivial enhancement of thermal conductivity has been seen in the composites. As for comparison, oxidation also has been tried as a treatment on CNFs to

enhance thermal conductivity of hybrid CFRCs. However, oxidation on CNFs tends to decrease the thermal conductivity of hybrid CFRCs. When 0.1% oxidized CNFs were applied, diminishment of thermal conductivity can be so significant that it is 6.6 % lower than neat CFRCs.

The second way to use CNFs to modified CFRCs was directly growing CNFs on the surface of the carbon fabric. In this configuration, enhancement of the through-thickness thermal conductivities has been seen to some extent. A systematic study has been done on the hierarchical CFRCs with CNFs growth on the carbon fabric. Different amount of catalyst contents have been tried and a continue increase of through-thickness thermal conductivity was observed as the CNF growth increases. However, plateau of enhancement of transverse thermal conductivity appears rapidly while CNF growth reaches 38% weight. The general enhancement is not as high as expected. It is assumed that the issue stems from the complexity of the composites system. Voids and imperfect interface between the fabric and the matrix can lead to significant diminishment of the performance of the final composites product. Therefore, study has been scaled down to raw material level: thermal conductivities of the individual carbon fibers.

Before studying the hierarchical CNFs, the effect of heat treatment on the carbon fiber was investigated. It is found that, heat treatment does not have significant effect on thermal conductivity in longitudinal direction, but it does moderately decrease the transverse thermal conductivity of the carbon fiber. This can be due to the dislocating and the enlargement of the spacing between the basal layers of the carbon fiber after heat treatment.

After the heat treatment study, thermal conductivities of hierarchical carbon fiber were investigated with various amount of CNFs growth in both longitudinal direction and transverse direction. It is found that the growth of CNFs significant improve the transverse thermal conductivity of carbon fiber. With 38.1% of CNFs on the carbon fiber, a 71% of enhancement of transverse thermal conductivity has been observed, which is more than three folds of the enhancement for through-thickness thermal conductivity of hierarchical CFRCs (which is about 25.6%). This means that other factors in the hierarchical CFRC such as void and CNF-epoxy thermal interfacial resistance do reduce the final thermal conductivity of the composite although the hierarchical carbon fiber has superior thermal conductivity.

Growth of CNFs on the surface of the carbon fiber is also found to improve the thermal conductivity in longitudinal direction. With 38.1 % weight CNF growth, a 24% enhancement of longitudinal thermal conductivity was observed. In SEM, it is shown that curviness of the growth induces some horizontal aligned carbon nanofiber/nanotube, and this is the source where the enhancement of longitudinal thermal conductivity comes from.

The last section of this dissertation is some additional work on modeling the hierarchical laminated composites. An analytical model for plain-weave hierarchical CRFCs with CNFs modified carbon fibers were developed based on analogy between Fourier' s Law and Ohm's law. Numerical simulation has been implemented on two types of growth configuration which are surface growth and full growth of CNFs. Investigation has been done on the effect of growth thickness and growth density on the transverse thermal conductivities of hierarchical CFRCs. It is found that surface growth is

more sensitive growth thickness while full growth is more sensitive to growth density. By comparing the two configurations of growth in term of weight of CNFs applied, it has found that surface growth gives more enhancement of thermal conductivity for the through-thickness direction. The model was also compare with the experimental results of hierarchical CFRCs measured with 3ω method. A good agreement has been seen. This study shed some light on the further design of composites system with hierarchical carbon fibers.

6.2 Future Work

The following are recommendations for future work

1. Further Work is needed to improve the simplicity the 3ω measurement method. Although some improvement has be achieved by replacing photolithography pattern with commercial fine wire and building up a wire-mounting stage for assisting the sample preparation, the effort and skill to run a 3ω thermal conductivity measurement is still too demanding. It will be helpful if the heater is assembled into a probe and certain mechanism is designed to ensure the contact between the probe and the sample. Of course, a corresponding theory needed to be developed.

2. For measuring the transverse thermal conductivities of individual fibers, the temperature range that the measurement can run in is limited by the boiling temperature of the deionized water. Liquid with higher temperature point such as olive oil might be used; however, the low thermal conductivity of olive oil also compromises the accuracy of the measurement. New medium needs to be found if

high temperature measurement of transverse thermal conductivities of individual fibers is performed.

3. For bulk material measurement, the thermal boundary resistance between the heater and the sample is neglected and for transverse thermal conductivity of individual fiber measurement, the boundary resistance between the sample and the medium is neglected. More experimental and theoretical work may be carried on to study its effect on the amplitude and phase of the average temperature rise of the heater or the sample.

4. In this work, only one type of carbon fiber T650 is the focused for studying the thermal conductivity. Thermal conductivities of more commercial carbon fibers need to be measured since not many existed thermal conductivities for individual carbon fibers. In fact, in the future, work may need to be shifted from PAN-based carbon fiber to pitch-based carbon fiber because they have relative higher thermal conductivities.

5. CNT is another type of carbon filler with high thermal conductivity. In the future work, similar study can be rendered on CNTs filled CFRCs or CFRCs with CNTs growth on the surface of carbon fiber. In fact, some work has been accomplished by the author, but the results are not included in this dissertation.

5. If facility allows, work can be carried out in a more controlled situation. For example, instead of growing large amount of CNF on the surface of carbon fiber, a single CNF grown on the surface of carbon fiber may be achieved. There is significant meaning if the in-situ heat transfer from carbon fiber to the other end of CNF can be measured. Meanwhile, technique needs to develop to grow CNF on a single fiber directly instead

of fiber tows, which will give more representative specimen for measurement. Lastly, single fiber –epoxy system may be fabricated and transverse thermal conductivity of the fiber in epoxy can be measured. This will give more understanding on the heat transfer between the carbon fiber reinforcement and the matrix.

6. The model in this work is still in a premature stage, a more complicated model need to be developed. The future model may include other factors such as the distribution of the CNFs, the size of the CNFs, and the waviness of the CNFs. Instead of theoretical models, simulation such as FEM or MD may also be used.

References

[1] C. Silva, E. Marotta, M. Schuller, L. Peel, and M. O'Neill, "In-plane thermal conductivity in thin carbon fiber composites," *Journal of Thermophysics and Heat Transfer,* vol. 21, pp. 460-467, Jul-Sep 2007.

[2] "Today industries, Inc, Market Research Report: Strategic Business Expansion of Carbon Fiber, Torayca," 2005.

[3] H. B. Shim, M. K. Seo, and S. J. Park, "Thermal conductivity and mechanical properties of various cross-section types carbon fiber-reinforced composites," *Journal of Materials Science,* vol. 37, pp. 1881-1885, May 1 2002.

[4] S. Hind and F. Robitaille, "Measurement, Modeling, and Variability of Thermal Conductivity for Structural Polymer Composites," *Polymer Composites,* vol. 31, pp. 847-857, May 2010.

[5] K. Sharp, A. E. Bogdanovich, W. Tang, D. Heider, S. Advani, and M. Glowiana, "High Through-Thickness Thermal Conductivity Composites Based on Three-Dimensional Woven Fiber Architectures," *AIAA Journal,* vol. 46, pp. 2944-2954, Nov 2008.

[6] J. H. Kim, A. Feldman, and D. Novotny, "Application of the three omega thermal conductivity measurement method to a film on a substrate of finite thickness," *Journal of Applied Physics,* vol. 86, pp. 3959-3963, Oct 1 1999.

[7] S. Berber, Y. K. Kwon, and D. Tomanek, "Unusually high thermal conductivity of carbon nanotubes," *Physical Review Letters,* vol. 84, pp. 4613-4616, May 15 2000.

[8] M. J. Biercuk, M. C. Llaguno, M. Radosavljevic, J. K. Hyun, A. T. Johnson, and J. E. Fischer, "Carbon nanotube composites for thermal management," *Applied Physics Letters,* vol. 80, pp. 2767-2769, Apr 15 2002.

[9] T. Koyama and M. T. Endo, "Structure and Growth Process of Vapor-Grown Carbon Fibers," *Oyobuturi,* vol. 42, pp. 690-696, 1973.

[10] S. Iijima, "Helical Microtubules of Graphitic Carbon," *Nature,* vol. 354, pp. 56-58, Nov 7 1991.

[11] S. Ghose, K. A. Watson, D. C. Working, J. W. Connell, J. G. Smith, and Y. P. Sun, "Thermal conductivity of ethylene vinyl acetate copolymer/nanofiller blends," *Composites Science and Technology,* vol. 68, pp. 1843-1853, Jun 2008.

[12] S. Ghose, D. C. Working, J. W. Connell, J. G. Smith, K. A. Watson, D. M. Delozier, Y. P. Sun, and Y. Lin, "Thermal conductivity of Ultem (TM)/carbon nanofiller blends," *High Performance Polymers,* vol. 18, pp. 961-977, Dec 2006.

[13] M. Wang, Q. J. Kang, and N. Pan, "Thermal conductivity enhancement of carbon fiber composites," *Applied Thermal Engineering,* vol. 29, pp. 418-421, Feb 2009.

[14] F. H. Gojny, J. Nastalczyk, Z. Roslaniec, and K. Schulte, "Surface modified multi-walled carbon nanotubes in CNT/epoxy-composites," *Chemical Physics Letters,* vol. 370, pp. 820-824, Mar 21 2003.

[15] H. Fukushima, L. T Drzal, B. P. Rook, and M. J. Rich, "Thermal conductivity of exfoliated graphite nanocomposites," *Journal of Thermal Analysis and Calorimetry,* vol. 85, pp. 235-238, 2006.

[16] F. H. Gojny, M. H. G. Wichmann, B. Fiedler, W. Bauhofer, and K. Schulte, "Influence of nano-modification on the mechanical and electrical properties of conventional fibre-reinforced composites," *Composites Part a-Applied Science and Manufacturing,* vol. 36, pp. 1525-1535, 2005.

[17] A. K. Roy, B. L. Farmer, S. Sihn, V. Varshney, S. Patnaik, and S. Ganguli, "Thermal interface tailoring in composite materials," *Diamond and Related Materials,* vol. 19, pp. 268-272, Feb-Mar 2010.

[18] W. B. Downs and R. T. K. Baker, "Novel Carbon Fiber-Carbon Filament Structures," *Carbon,* vol. 29, pp. 1173-1179, 1991.

[19] E. T. Thostenson, W. Z. Li, D. Z. Wang, Z. F. Ren, and T. W. Chou, "Carbon nanotube/carbon fiber hybrid multiscale composites," *Journal of Applied Physics,* vol. 91, pp. 6034-6037, May 1 2002.

[20] K. H. Hung, W. S. Kuo, T. H. Ko, S. S. Tzeng, and C. F. Yan, "Processing and tensile characterization of composites composed of carbon nanotube-grown carbon fibers," *Composites Part a-Applied Science and Manufacturing,* vol. 40, pp. 1299-1304, Aug 2009.

[21] R. J. Sager, P. J. Klein, D. C. Lagoudas, Q. Zhang, J. Liu, L. Dai, and J. W. Baur, "Effect of carbon nanotubes on the interfacial shear strength of T650 carbon fiber in an epoxy matrix," *Composites Science and Technology,* vol. 69, pp. 898-904, Jun 2009.

[22] Q. H. Zhang, J. W. Liu, R. Sager, L. M. Dai, and J. Baur, "Hierarchical composites of carbon nanotubes on carbon fiber: influence of growth condition on fiber tensile properties," *Composites Science and Technology,* vol. 69, pp. 594-601, Apr 2009.

[23] Z. G. Zhao, L. J. Ci, H. M. Cheng, and J. B. Bai, "The growth of multi-walled carbon nanotubes with different morphologies on carbon fibers," *Carbon,* vol. 43, pp. 663-665, 2005.

[24] J. D. Farmer and E. E. Covert, "Thermal conductivity of a thermosetting advanced composite during its cure," *Journal of Thermophysics and Heat Transfer,* vol. 10, pp. 467-475, Jul-Sep 1996.

[25] D. D. Joseph and L. Preziosi, "Heat Waves," *Reviews of Modern Physics,* vol. 61, pp. 41-73, Jan 1989.

[26] Y. A. Cengel, *Heat Transfer: A Practical Approach*: McGraw-Hill, 1998.

[27] B. Stalhane and S. Pyk, "New Method for determining the coefficients of thermal conductivity," *Tek. Tidskr.,* vol. 61, pp. 389-393, 1931.

[28] D. G. Cahill, "Thermal-Conductivity Measurement from 30-K to 750-K - the 3-Omega Method," *Review of Scientific Instruments,* vol. 61, pp. 802-808, Feb 1990.

[29] D. G. Cahill and R. O. Pohl, "Thermal-Conductivity of Amorphous Solids above the Plateau," *Physical Review B,* vol. 35, pp. 4067-4073, Mar 15 1987.

[30] C. Garikapati, "Development of Low Cost Sample Preparation Technique for Applying Three Omega Method," M.S. Thesis, Mechanical Engineering, University of Oklahoma, Norman, 2006.

[31] L. Lu, W. Yi, and D. L. Zhang, "3 omega method for specific heat and thermal conductivity measurements," *Review of Scientific Instruments,* vol. 72, pp. 2996-3003, Jul 2001.

[32] Z. L. Wang, D. W. Tang, and W. G. Zhang, "Simultaneous measurements of the thermal conductivity, thermal capacity and thermal diffusivity of an individual carbon fibre," *Journal of Physics D-Applied Physics,* vol. 40, pp. 4686-4690, Aug 7 2007.

[33] O. M. Corbino, "Thermal oscillations in lamps of thin fibers with alternating current flowing through them and the resulting effect on the rectifier as a result of the presence of even-numbered harmonics," *Physikalische Zeitschrift,* vol. 11, pp. 413-417, 1910.

[34] O. M. Corbino, "Periodic resistance changes of fine metal threads, which are brought together by alternating streams as well as deduction of their thermo characteristics at high temperatures.," *Physikalische Zeitschrift,* vol. 12, pp. 292-295, 1911.

[35] E. Korostoff, "Relaxation Method for Studying Vacancies in Solids," *Journal of Applied Physics,* vol. 33, pp. 2078-&, 1962.

[36] L. Rosenthal, "Thermal Response of Bridgewires Used in Electroexplosive Devices," *Review of Scientific Instruments,* vol. 32, pp. 1033-&, 1961.

[37] G. C. Lowenthal, "The Specific Heat of Metals Between 1200oK and 2400oK," *Journal of Physics* vol. 16, 1962.

[38] L. R. Holland, "Physical Properties of Titanium .3. Specific Heat," *Journal of Applied Physics,* vol. 34, pp. 2350-&, 1963.

[39] D. Gerlich, B. Abeles, and R. E. Miller, "High-Temperature Specific Heats of Ge Si and Ge-Si Alloys," *Journal of Applied Physics,* vol. 36, pp. 76-&, 1965.

[40] N. O. Birge, "Specific-Heat Spectroscopy of Glycerol and Propylene-Glycol near the Glass-Transition," *Physical Review B,* vol. 34, pp. 1631-1642, Aug 1 1986.

[41] N. O. Birge and S. R. Nagel, "Wide-Frequency Specific-Heat Spectrometer," *Review of Scientific Instruments,* vol. 58, pp. 1464-1470, Aug 1987.

[42] D. G. Cahill, H. E. Fischer, T. Klitsner, E. T. Swartz, and R. O. Pohl, "Thermal-Conductivity of Thin-Films - Measurements and Understanding," *Journal of Vacuum Science & Technology a-Vacuum Surfaces and Films,* vol. 7, pp. 1259-1266, May-Jun 1989.

[43] T. Borca-Tasciuc, A. R. Kumar, and G. Chen, "Data reduction in 3 omega method for thin-film thermal conductivity determination," *Review of Scientific Instruments,* vol. 72, pp. 2139-2147, Apr 2001.

[44] B. W. Olson, S. Graham, and K. Chen, "A practical extension of the 3 omega method to multilayer structures," *Review of Scientific Instruments,* vol. 76, May 2005.

[45] W. Yi, L. Lu, D. L. Zhang, Z. W. Pan, and S. S. Xie, "Linear specific heat of carbon nanotubes," *Physical Review B,* vol. 59, pp. R9015-R9018, Apr 1 1999.

[46] T. Y. Choi, D. Poulikakos, J. Tharian, and U. Sennhauser, "Measurement of thermal conductivity of individual multiwalled carbon nanotubes by the 3-omega method," *Applied Physics Letters,* vol. 87, Jul 4 2005.

[47] O. Bourgeois, T. Fournier, and J. Chaussy, "Measurement of the thermal conductance of silicon nanowires at low temperature," *Journal of Applied Physics,* vol. 101, Jan 1 2007.

[48] J. B. Hou, X. W. Wang, P. Vellelacheruvu, J. Q. Guo, C. Liu, and H. M. Cheng, "Thermal characterization of single-wall carbon nanotube bundles using the self-heating 3 omega technique," *Journal of Applied Physics,* vol. 100, Dec 15 2006.

[49] T. Nozawa, Y. Katoh, L. L. Snead, T. Hinoki, and A. Kohyama, "Tensile and Thermal Properties of Chemically Vapor-Infiltrated Silicon Carbide Composites of Various High-Modulus Fiber Reincements," *Ceramic Engineering and Science Proceedings,* vol. 26, pp. 311-318, 2008.

[50] M. Abramowitz and I. A. Stegun, *Handbook of Mathematical Functions with Formulus, Graphs and Mathematical Tables* vol. 55: U.S. Department of Commerce, 1964.

[51] H. S. Carslaw and J. C. Jaeger, *Conduction of Heat in Solids,* 2 ed. Oxfrd: Oxford University, 1959.

[52] J. P. Holman, *Experimental Methods for Engineers*. New York: McGraw-Hill, 1978.

[53] J. L. Wang, M. Gu, X. Zhang, and Y. Song, "Thermal conductivity measurement of an individual fibre using a T type probe method," *Journal of Physics D-Applied Physics,* vol. 42, May 21 2009.

[54] H. D. Young, *University Physics,* 7 ed., Addison-Wesley Pub. Co., 1992.

[55] R. M. Pashley, M. Rzechowicz, L. R. Pashley, and M. J. Francis, "De-gassed water is a better cleaning agent," *Journal of Physical Chemistry B,* vol. 109, pp. 1231-1238, Jan 27 2005.

[56] T. F. Coleman and Y. Y. Li, "An interior trust region approach for nonlinear minimization subject to bounds," *Siam Journal on Optimization,* vol. 6, pp. 418-445, May 1996.

[57] T. F. Coleman and Y. Li, "On the Convergence of Reflective Newton Methods for Large-Scale Nonlinear Minimization Subject to Bounds," *Mathematical Programming,* vol. 67, pp. 189-224, 1994.

[58] M. J. Assael, K. Gialou, K. Kakosimos, and I. Metaxa, "Thermal conductivity of reference solid materials," *International Journal of Thermophysics,* vol. 25, pp. 397-408, Mar 2004.

[59] L. C. Hulstrom, "Interlaboratory Testing of Reference Materials for a Comparative Thermal Conductivity Measurement Apparatus," R. H. operations, Ed., ed: Dynatech R/D Co., 1985.

[60] K. Lafdi, W. Fox, M. Matzek, and E. Yildiz, "Effect of carbon nanofiber-matrix adhesion on polymeric nanocomposite properties - Part II," *Journal of Nanomaterials,* 2008.

[61] P. V. Lakshminarayanan, H. Toghiani, and C. U. Pittman, "Nitric acid oxidation of vapor grown carbon nanofibers," *Carbon,* vol. 42, pp. 2433-2442, 2004.

[62] B. Lively, S. Kumar, L. Tian, B. Li, and W. H. Zhong, "Mechanical, Thermal and Morphological Characterization of Polycarbonate/Oxidized Carbon Nanofiber

Composites Produced with a Lean 2-Step Manufacturing Process," *Journal of Nanoscience and Nanotechnology*, vol. 11, pp. 3929-3937, May 2011.

[63] A. Loiseau, P. Launois-Bernede, P. Petit, S. Roche, and J. P. Salvetat, *Understanding Carbon Nanotubes: From Basics to Application*: Springer, 2006.

[64] Y. Kinemuchi, H. Nakano, M. Mikami, K. Kobayashi, K. Watari, and Y. Hotta, "Enhanced Boundary-Scattering of Electrons and Phonons in Nanograined Zinc Oxide," *Journal of Applied Physics*, vol. 108, 2010.

[65] E. T. Swartz and R. O. Pohl, "Thermal-Boundary Resistance," *Reviews of Modern Physics*, vol. 61, pp. 605-668, Jul 1989.

[66] M. R. Kulkarni and R. P. Brady, "A model of global thermal conductivity in laminated carbon/carbon composites," *Composites Science and Technology*, vol. 57, pp. 277-285, 1997.

[67] R. A. Serway, *Principles of Physics*, 2nd ed. Fort Worth, Texas: London: Saunders College Pub, 1998.

[68] A. Goldsmith, T. E. Waterman, and H. J. Hirschhorn, *Handbook of Thermophysical Properties of Solid Materials*, 1st ed. vol. 1. New York: The Macmillan Company, 1961.

[69] *HexTow AS4 Carbon fiber Product data*. Available: http://www.hexcel.com/resources/datasheets/carbon-fiber-data-sheets/as4.pdf.

[70] *HexTow IM10 Carbon Fiber Product Data*. Available: http://www.hexcel.com/resources/datasheets/carbon-fiber-data-sheets/im10.pdf

[71] Q. Xue and W. M. Xu, "A model of thermal conductivity of nanofluids with interfacial shells," *Materials Chemistry and Physics*, vol. 90, pp. 298-301, Apr 15 2005.

[72] C. W. Nan, G. Liu, Y. H. Lin, and M. Li, "Interface effect on thermal conductivity of carbon nanotube composites," *Applied Physics Letters*, vol. 85, pp. 3549-3551, Oct 18 2004.

[73] E. Savitsky and V. Polyakov, *Physical Metallurgy of Platinum Metals*: Mir, 1978.

[74] *Thermal Conductivity of Platinum*. Available: http://www.efunda.com/materials/elements/TC_Table.cfm?Element_ID=Pt

[75] *Thermal Conductivity of Tunsten*. Available: http://www.efunda.com/materials/elements/TC_Table.cfm?Element_ID=W

[76] D. E. Soule and C. W. Nezbeda, "Direct Basal-Plane Shear in Single-Crystal Graphite," *Journal of Applied Physics,* vol. 39, pp. 5122-&, 1968.

[77] R. J. Diefendorf and E. Tokarsky, "High-Performance Carbon-Fibers," *Polymer Engineering and Science,* vol. 15, pp. 150-159, 1975.

[78] F. Seitz, H. Ehrenreich, and D. Turnbull, *Solid State Physics: Advances in Research and Applications*. New York: Academic Press, 1979.

[79] A. R. Bunsell, *Fibre Reinforcements for Composite Material* vol. 2. New York: Elsevier, 1988.

[80] F. I. Afzal, "Effect of Carbon Nanotube and POSS Coating on Mechanical Properties of Carbon Fiber Epoxy Composites " M.S. Thesis, University of Oklahoma, 2013.

[81] J. L. Abot, G. Bardin, C. Spriegel, Y. Song, V. Raghavan, and N. Govindaraju, "Thermal Conductivity of Carbon Nanotube Array Laminated Composite Materials," *Journal of Composite Materials,* vol. 45, pp. 321-340, Feb 2011.

[82] B. H. Seo, Y. J. Cho, J. R. Youn, K. Chung, T. J. Kang, and J. K. Park, "Model for thermal conductivities in spun yarn carbon fabric composites," *Polymer Composites,* vol. 26, pp. 791-798, Dec 2005.

[83] Q. G. Ning and T. W. Chou, "Closed-Form Solutions of the Inplane Effective Thermal-Conductivities of Woven-Fabric Composites," *Composites Science and Technology,* vol. 55, pp. 41-48, 1995.

[84] Q. G. Ning and T. W. Chou, "Closed-form solution of the transverse effective thermal conductivity of woven fabric composites," *Journal of Composite Materials,* vol. 29, pp. 2280-2294, 1995.

[85] W. A. Clayton, "Constituent and Composite Thermal Conductivities of Phenolic-carbon and Phenolicgraphite Ablators," in *AIAA/ASME 12th Structures, Structural Dynamics and Materials Conference*, Anaheim, CA, 1971, pp. 380-397.

[86] G. S. Springer and S. W. Tsai, "Thermal Conductivities of Unidirectional Materials," *Journal of Composite Materials,* vol. 1, pp. 166-173, 1967.

[87] A. Dasgupta and R. K. Agarwal, "Orthotropic Thermal-Conductivity of Plain-Weave Fabric Composites Using a Homogenization Technique," *Journal of Composite Materials,* vol. 26, pp. 2736-2758, 1992.

[88] *Cytec Engineered Materials* Available: http://www.cytec.com/engineered-materials/products/cfThornelT-65035CPAN.htm

[89] Y. A. Kim, S. Kamio, T. Tajiri, T. Hayashi, S. M. Song, M. Endo, M. Terrones, and M. S. Dresselhaus, "Enhanced thermal conductivity of carbon fiber/phenolic resin composites by the introduction of carbon nanotubes," *Applied Physics Letters,* vol. 90, Feb 26 2007.

[90] V. P. Veedu, A. Y. Cao, X. S. Li, K. G. Ma, C. Soldano, S. Kar, P. M. Ajayan, and M. N. Ghasemi-Nejhad, "Multifunctional composites using reinforced laminae with carbon-nanotube forests," *Nature Materials,* vol. 5, pp. 457-462, Jun 2006.